

1982

Measurement of surface roughness by a fiber-optic transducer.

Anil K. Agarwal
University of Windsor

Follow this and additional works at: <http://scholar.uwindsor.ca/etd>

Recommended Citation

Agarwal, Anil K., "Measurement of surface roughness by a fiber-optic transducer." (1982). *Electronic Theses and Dissertations*. Paper 2684.

This online database contains the full-text of PhD dissertations and Masters' theses of University of Windsor students from 1954 forward. These documents are made available for personal study and research purposes only, in accordance with the Canadian Copyright Act and the Creative Commons license—CC BY-NC-ND (Attribution, Non-Commercial, No Derivative Works). Under this license, works must always be attributed to the copyright holder (original author), cannot be used for any commercial purposes, and may not be altered. Any other use would require the permission of the copyright holder. Students may inquire about withdrawing their dissertation and/or thesis from this database. For additional inquiries, please contact the repository administrator via email (scholarship@uwindsor.ca) or by telephone at 519-253-3000ext. 3208.

CANADIAN THESES ON MICROFICHE

I.S.B.N.

THESES CANADIENNES SUR MICROFICHE



National Library of Canada
Collections Development Branch

Canadian Theses on
Microfiche Service

Ottawa, Canada
K1A 0N4

Bibliothèque nationale du Canada
Direction du développement des collections

Service des thèses canadiennes
sur microfiche

NOTICE

The quality of this microfiche is heavily dependent upon the quality of the original thesis submitted for microfilming. Every effort has been made to ensure the highest quality of reproduction possible.

If pages are missing, contact the university which granted the degree.

Some pages may have indistinct print, especially if the original pages were typed with a poor typewriter ribbon or if the university sent us a poor photocopy.

Previously copyrighted materials (journal articles, published tests, etc.) are not filmed.

Reproduction in full or in part of this film is governed by the Canadian Copyright Act, R.S.C. 1970, c. C-30. Please read the authorization forms which accompany this thesis.

THIS DISSERTATION
HAS BEEN MICROFILMED
EXACTLY AS RECEIVED

AVIS

La qualité de cette microfiche dépend grandement de la qualité de la thèse soumise au microfilmage. Nous avons tout fait pour assurer une qualité supérieure de reproduction.

S'il manque des pages, veuillez communiquer avec l'université qui a conféré le grade.

La qualité d'impression de certaines pages peut laisser à désirer, surtout si les pages originales ont été dactylographiées à l'aide d'un ruban usé ou si l'université nous a fait parvenir une photocopie de mauvaise qualité.

Les documents qui font déjà l'objet d'un droit d'auteur (articles de revue, examens publiés, etc.) ne sont pas microfilmés.

La reproduction, même partielle, de ce microfilm est soumise à la Loi canadienne sur le droit d'auteur, SRC 1970, c. C-30. Veuillez prendre connaissance des formules d'autorisation qui accompagnent cette thèse.

LA THÈSE A ÉTÉ
MICROFILMÉE TELLE QUE
NOUS L'AVONS REÇUE

MEASUREMENT OF SURFACE ROUGHNESS BY A FIBER-OPTIC TRANSDUCER

A Thesis
Submitted to the Faculty of Graduate Studies through the
Department of Mechanical Engineering in Partial Fulfillment
of the Requirements for the Degree of
Master of Applied Science
at the
University of Windsor

by


© Anil K. Agarwal

Windsor, Ontario
1982

©

Anil K. Agarwal

774628



ABSTRACT

The purpose of this research work was to develop a technique for the measurement of surface roughness of "ground" surfaces using a fiber-optic transducer. The reflection characteristic of a machined surface which is simplistically modelled as a triangular wave profile was first analyzed theoretically. Based on this theoretical prediction and subsequent experimental verifications, it has been shown that the ratio of reflected light, measured by a pair of fiber-optic transducers of similar specifications at 0° and 35° detection angles, can be effectively used to characterize the roughness of "ground" surfaces of upto 40 micro inches average roughness. This output ratio has been found to correlate to the calibrated surface roughness by a general equation of following form:

$$Ra = A.X^{-B}$$

Where, Ra is the calibrated average roughness,

X is the output ratio V_0/V_{35} , and;

A and B are constants.

The results of the experimental investigation also indicated that this procedure is practically feasible and the roughness measurements can be carried out accurately and repeatably. This can also be done at very high speed

compared to a stylus instrument and can be built into a package compact enough to be used in a typical automotive crankshaft production line.

It has also been found that a coaxial fiber-optic transducer is best suited for the purpose of roughness measurement.

ACKNOWLEDGEMENTS

The author wishes to express his sincere gratitude to Dr. W.P.T. North for his supervision and encouragement throughout the course of this study.

The author is grateful to Mr. Werner Beck and Mr. Robert Tattersall for their technical assistance in this project.

Special thanks are due to Mr. Krishna Reddy for typing and Miss Kim Hooper for proof-reading this manuscript.

Acknowledgement is made to the National Science and Engineering Research Council of Canada (NSERC grant no. A3360) for providing the financial support for this study.

CONTENTS

ABSTRACT	ii
ACKNOWLEDGEMENTS	iv
LIST OF FIGURES	vii
LIST OF TABLES	x
NOMENCLATURE	xi

<u>Chapter</u>	<u>page</u>
I. INTRODUCTION	1
Concept of Surface Roughness	4
Surface Roughness Parameters	5
Average Roughness - Ra	6
Maximum Peak to Valley Roughness Height - Rt	6
Ten Point Height - Rz	7
Bearing Length Ratio - tp	7
Existing Methods of Surface Finish Measurement	8
Stylus Instrument	9
Optical Instruments	12
Optical Sectioning	13
Interferometric Methods	13
Electron Microscopy	14
II. LITERATURE SURVEY	21
Interaction of Light with Rough Surfaces	22
Measurement of Surface Roughness by Light Scattering Methods	23
Objective of the Present Research	29
III. THEORY	35
Fiber-Optic Fundamentals	35
Output Response Characteristic of a Fiber	38
Theoretical Reflection Model	40
IV. EXPERIMENTAL APPARATUS & PROCEDURE	52
The Apparatus	52
Experimental Procedure	59
Response Characteristic	59

Transducer Output Vs. Surface Roughness	60
Ratio of Transducer Outputs Vs. Surface Roughness	60
V. RESULTS AND DISCUSSION	72
Individual Response Curves	72
Effect of Roughness and Detection Angle on Transducer Output	74
Normalized Fiber-Optic Roughness Measurement	76
Mean Surface Roughness by a Scan of the Surface	79
Stability and Repeatability of Measurement	81
Effect of Surface Positioning Errors	82
VI. CONCLUSIONS	107
VII. RECOMMENDATIONS	113
LIST OF REFERENCES	117
<u>Appendix</u>	<u>page</u>
A. LINEARITY RESPONSE CURVES FOR THE PHOTODETECTORS	120
B. CALIBRATION CURVES FOR THE OPERATIONAL AMPLIFIER	123
C. PROFILOMETRIC AND OPTICAL MEASUREMENT READINGS FOR LAB. SPECIMENS	127
VITA AUCTORIS	133

LIST OF FIGURES

<u>Figure</u>	<u>page</u>
1.1. Pictorial Display of Surface Characteristics . . .	16
1.2. Average Roughness	17
1.3. Section of a Surface Profile Divided in Increments	17
1.4. Maximum Peak to Valley Roughness	18
1.5. Ten- Point Height	18
1.6. Bearing Length Ratio	18
1.7. Principle of Roughness Measurement by the Stylus Instrument	19
1.8. Principle of Schmaltz Microscope	20
2.1. Possible Modes of Light Reflection from a Surface	32
2.2. Possible Fiber Orientations in a Bifurcated Transducer	33
2.3. Schematic of the Experimental Setup of Spurgeon & Slatter	34
2.4. Schematic of the Experimental Setup of Lin, Shea & Hoang	34
3.1. An Optical Fiber	46
3.2. Response Characteristic of an Optical Fiber	47
3.3. Response Characteristic of a Random Fiber Optic Transducer	48
3.4. Vertical Shift of the Response Peak with Variation in Roughness	48

3.5.	Theoretical Reflection Model	49
3.6.	Specific Reflection Output ρ Vs. Facet Angle α at Different Detection Angles	50
3.7.	Facet Angle α Vs. Ratio of Reflection Outputs $\frac{R_0}{R\phi}$	51
4.1.	Schematic of the Operational Amplifier	63
4.2.	Fiber-Optic Transducers	64
4.3.	Pictorial Display of the Initial Experimental Setup	65
4.4.	Schematic of the Initial Setup	66
4.5.	Possible Positions of the Fiber-Optic Transducer Relative to the Work Surface.	67
4.6.	Pictorial Display of the Final Experimental Setup	68
4.7.	Schematic of the Final Setup	69
4.8.	Pictorial Display of Transducers Position Relative to the Surface	70
5.1.	Effect of Surface Roughness on Transducer Response Characteristic	83
5.2.	Response Characteristic Curve for EC824	84
5.3.	Response Characteristic Curve for EK3012, ET824, ED824 & EC824	85
5.4.	Response Characteristic Curves for EC424	86
5.5.	Transducer (ET824) Output Vs. Roughness for Different Detecting Angles.	87
5.6.	Transducer (ED824) Output Vs. Roughness for Different Detecting Angles	88
5.7.	Transducer (EC824) Output Vs. Roughness fo Different Detecting Angles.	89
5.8.	Transducer (EC424) Output Vs. Roughness for Different Detecting Angles.	90
5.9.	Output Ratio V_0/V_{30} Vs. Roughness for EC424, EC824, ET824 & ED824	91

5.10.	Output Ratio V_0/V_{35} Vs. Roughness for EC424, EC824, ET824 & ED824	92
5.11.	Relation Between Surface Roughness and the Transducer Output Ratio V_0/V_{30} for EC424 & EC824	93
5.12.	Logarithmic Relation Between Surface Roughness and the Transducer Output Ratio V_0/V_{30} for EC424 & EC824	94
5.13.	Relation Between Surface Roughness and the Transducer Output Ratio V_0/V_{35} for EC424 & EC824	95
5.14.	Logarithmic Relation Between Surface Roughness and the Transducer Output Ratio V_0/V_{35} for EC424 & EC824	96
5.15.	Output Ratio V_0/V_{35} from a Scan of Surfaces by Transducer EC424	97
5.16.	Output Ratio V_0/V_{35} from a Scan of Surfaces by Transducer EC824	98
5.17.	Variations in Output Ratio V_0/V_{35} with Time, for Transducer EC824	99
5.18.	Variations in Output Ratio V_0/V_{35} with Time, for Transducer EC424	100
5.19.	Effect of Positive or Negative Rotation About Z-Axis, on V_0/V_{35}	101
5.20.	Effect of Positive or Negative Rotation about X-Axis, on V_0/V_{35}	101
5.21.	Effect of Positive Rotation About Y-Axis on V_0/V_{35}	102
5.22.	Effect of Negative Rotation About Y-Axis on V_0/V_{35}	102
6.1.	A Typical Position of the Fiber-Optic Transducers to Measure Roughness of a Crankshaft Journal	112
A.1.	Linearity Response Curve for Photodetector No.1	121
A.2.	Linearity Response Curve for Photodetector No.2	122
B.1.	Calibration Curve for the Amplifier Channel A	124
B.2.	Calibration Curve for the Amplifier Channel B	125
B.3.	Calibration Curve for the Analog Divider	126

LIST OF TABLES

<u>Table</u>	<u>page</u>
4.1. Specifications of the Fiber-Optic Transducers . . .	71
5.1. Working Range of the Transducers	103
5.2. Correlation Equations for Transducers EC424 & EC824	104
5.3. Comparison Between Roughness Measured by Profilometer and EC824	105
5.4. Comparison Between Roughness Measured by Profilometer and EC424	106
C.1. Stylus Calibrated (Mitutoyo Surf-test III) Surface Roughness of Laboratory Machined Specimens . .	128
C.2. Output Ratio V_0/V_{30} for Transducer EC-824	129
C.3. Output Ratio V_0/V_{35} for Transducer EC-824	130
C.4. Output Ratio V_0/V_{30} for Transducer EC-424	131
C.5. Output Ratio V_0/V_{35} for Transducer EC-424	132

NOMENCLATURE

B	-	Reflection Distribution Function
f	-	Feed Rate of Machining
I _i	-	Incident Intensity
l	-	Length of the Profile Facet
L	-	Length of the Light Source
L'	-	Illuminated Surface Length
LL	-	Sampling Length
m	-	RMS Surface Slope
n	-	Number of Increments
N ₁	-	Index of Refraction of the Air
N ₂	-	Index of Refraction of the Fiber Core
N ₃	-	Index of Refraction of the Fiber Cladding
R	-	Reflection Output from a Rough Surface
R _o	-	Reflection Output from a Perfectly Smooth Surface
R _a	-	Average Roughness
R _t	-	Max. Peak to Valley Roughness Height
R _z	-	Ten-Point Height
S	-	Length Subtended on the Profile by a Line Drawn Parallel and at a Preselected Distance from the Center Line
tp	-	Bearing Length Ratio
V	-	Output from the Fiber Optic Transducer
Y	-	Ordinate of the Surface Profile

Greek Letters

- α - Facet Angle of the Triangular Profile
- γ - Angle of Refraction
- θ - Angle of Incidence
- ϕ - Detection Angle
(Transducer Inclination Angle measured from
a normal to the surface)
- ρ - Specific Reflection Output
- σ - RMS Deviation of Surface Heights
- λ - Wavelength of the Illumination

Chapter I

INTRODUCTION

In recent years surface finish is starting to emerge as an important manufacturing specification for machined parts. Just a few years ago the character of the surface was regarded as a problem primarily for gage-blocks, gyros, jet-engine components, precision bearings and similar specialized products.

Today, surface finish is of concern in a much larger portion of the metal-working industry. It has become a standard manufacturing specification for pumps, valves, pistons, rotors, machine spindles and slides, most types of bearing surfaces and numerous other types of parts. The expanding interest in surface measurement reflects the trend to upgrade quality levels in many product lines. This also reflects the increasing realization that control of surface quality is cost effective.

Close control over surface finish has traditionally been associated with close dimensional tolerances on parts that are ground, honed or lapped to size. Finish and size do, of course, go hand in hand in precision applications, but even when dimensional tolerances are not particularly tight, there are sound economic reasons for monitoring

surface finish. For example, superior surface finish of automotive sheet steel improves paintability and drawability. Better surface finish increases motor shaft life and reduces oil leakage, improves adhesion and uniformity in plating and painting operations and provides various advantages in hundreds of other applications.

The determination of the relationship between the proper finish of a surface and its function can, therefore, save untold dollars in industries where surfaces either fail to meet the requirement or are overspecified because they have been improperly characterized.

The increasing importance of surface characterization has resulted in the development of several types of roughness measuring instruments. The only instrument commonly used today is a profilometer where the measurement of surface finish is carried out by drawing a fine stylus, attached to an electrical transducer, across the surface to be tested and observing the resulting electrical signal. Light section microscope, interferometer and electron microscopes are some of the other instruments also used for estimating the surface quality.

Presently used instruments, however, have several drawbacks. These instruments can not be used "on line" and are essentially laboratory instruments requiring considerable time to set up and use and rely heavily upon subjective operator's skills and experience.

These instruments are particularly unsuitable for the purpose of quality control in the production lines where surface finish is a critical factor and where production with unsatisfactory finish needs to be removed from the line. For example, during a conversation Mr. Malconian, who is the quality control manager at the Chrysler Engine plant in Windsor, indicated the necessity of inspecting each journal surface of every crankshaft in order to ensure the required surface quality. In this present case each crankshaft has 12 bearing surfaces and the inspection period by a profilometer is approximately 30 seconds for every surface. Since the profilometer takes many minutes per crankshaft it is obviously impossible to gage the surface quality of each crankshaft using existing technology to determine whether the surface roughness falls within the acceptable range of ≤ 15 micro in. Ra. As a result the current procedure is to take one crankshaft per shift into the inspection room for gaging and to train an inspector on the production floor to "visually" look for errors beyond the 15 micro in. range. Since the human eye can not be calibrated, this inspection is qualitative at best. Mr. Malconian, therefore, stressed the requirement for an instrument which could be used on the production floor at production rates to test the surface roughness.

For many years attempts have been made to develop alternative techniques with a view to overcome the drawbacks

of present methods. As surface roughness modifies the light reflecting properties of a surface, many optical methods for the measurement of surface roughness, by measuring the reflected light intensities, have been proposed. However, none of these optical methods has yet been developed to a reliable instrument for production floor measurements.

1.1 CONCEPT OF SURFACE ROUGHNESS [1,2]

Regardless of how it is machined or finished, no surface can be perfect. It varies from the nominal surface by many types of irregularities. Each machining process, and each individual machine, in fact, produces a distinctive surface texture. Surface texture includes roughness, waviness, lay and flaws. Fig. 1.1 shows an expanded view of a unidirectional lay surface.

a) Roughness: Roughness consists of finer irregularities of surface texture usually resulting from the inherent action of the production process. These are considered to include traverse feed marks and other fine irregularities within the limits of the surface roughness sampling length.

b) Waviness: Waviness is the more widely spaced component of the surface texture. It includes all irregularities whose spacing is greater than the roughness sampling length. Waviness may result from such factors as machine or work deflections,

Numbers appearing in the square brackets designate references at the end of the thesis.

vibration, chatter, heat treatment or warping strains. Roughness may be considered superimposed on a 'wavy' surface.

- c) Lay: Lay is the direction of predominant surface pattern, ordinarily determined by the production method used.
- d) Flaws: Flaws are unintentional irregularities which occur in one place or at relatively infrequent or widely varying intervals on the surface. Flaws include such defects as pits, cracks, blow holes, inclusions, ridges, scratches etc.

1:2 SURFACE ROUGHNESS PARAMETERS [1-3]

The most commonly used and universally recognized parameter for roughness characterization is the 'Average or Arithmetic Roughness' usually denoted by Ra. For most engineering applications the average roughness provides adequate information about the surface quality, but in cases where a more precise surface characterization is required the average roughness measurement alone has not been found adequate. In recent years, however, several more parameters have been developed which can provide further knowledge about the surface quality for specific applications. Some of the more important parameters are described herein.

1.2.1 Average Roughness - Ra

This is the arithmetic average of the absolute values of the measured profile height deviations, taken within a sampling length and measured from a graphical centerline. The centerline is such that the total areas of profile lying above and below the line are equal (Fig. 1.2). Mathematically the average roughness can be represented as;

$$Ra = \frac{1}{LL} \int Y \cdot dx \quad \text{-----(1.1)}$$

Where, Y is the ordinate of the profile curve, and;
LL is the sampling length.

An approximation of Ra may be obtained by adding the 'Y' increments, shown in Fig. 1.3, regardless of their sign and dividing the sum by the number of increments taken;

$$Ra = \frac{Y_1 + Y_2 + Y_3 + \dots + Y_n}{n} \quad \text{-----(1.2)}$$

Where, Y₁, Y₂, - -, Y_n are the ordinates, and;
n is the number of increments.

The Average Roughness can also be denoted by AA (Arithmetic Average) and is specified in micro inches (μ in.) or micrometers (μm.).

1.2.2 Maximum Peak to Valley Roughness Height - Rt

This is the distance between two lines parallel to the mean line which contact the extreme outer and inner points on the profile within a sampling length (Fig. 1.4). Because this

value can be greatly affected by a spurious scratch or a dust particle, it is more usual to use the average (R_{tm}) of five consecutive sampling lengths;

$$R_{tm} = \frac{R_{t1}+R_{t2}+R_{t3}+R_{t4}+R_{t5}}{5} \text{ -----(1.3)}$$

1.2.3 Ten Point Height - R_z

This is the average distance between the five highest peaks and the five deepest valleys within the sampling length and measured perpendicular to it (Fig 1.5). R_z is given by;

$$R_z = \frac{(Y_1+Y_3+Y_5+Y_7+Y_9)-(Y_2+Y_4+Y_6+Y_8+Y_{10})}{5} \text{ -----(1.4)}$$

Where, Y₁, Y₃, Y₅, Y₇ & Y₉ are the ordinates of highest peaks, and;
Y₂, Y₄, Y₆, Y₈ & Y₁₀ are the ordinates of lowest valleys.

1.2.4 Bearing Length Ratio - t_p

A reference line is drawn parallel to the centerline and at a preselected distance from it to intersect the profile in one or more subtended lengths. The bearing length ratio is the ratio of the sum of these subtended lengths to the sampling length (Fig. 1.6).

$$t_p = \frac{S_1+S_2+S_3+\dots +S_n}{LL} \text{ -----(1.5)}$$

Where, S₁, S₂, S₃ ... are the subtended lengths on the profile, and;

LL is the sampling length.

Besides these, there are several more parameters used for surface characterization. For a detailed description of these and other parameters the reader is urged to see references 1 to 3 .

1.3 EXISTING METHODS OF SURFACE FINISH MEASUREMENT [1,4]

With increased understanding of the influence of surface roughness on how a part performs its function, there has been a definite trend towards specifying surface roughness more closely in order to ensure a certain type or level of functioning. A few years ago it was not possible for many manufacturers to measure the surface finish with any degree of accuracy, but today, because of the recent developments in surface roughness measurements, a variety of different instruments are available. These instruments consist mainly of the following elements:

- a) A measuring transducer to transform the surface topography into some type of image for processing. The most common image in use today is an electrical voltage signal obtained as the transducer is scanned across the specimen surface. However, the image could equally well be an interferogram, a micrograph or a light scattering pattern.
- b) Analyzing equipment for processing the image of the surface in order to characterize the topography or for displaying the topography in a convenient manner.

c) A data display system which could be a simple analog meter, a chart recorder, an oscilloscope or a complete graphic computer terminal.

Surface measuring instruments can be broadly classified into two types: Stylus type and Optical. Of the two, the stylus instrument is most commonly used but optical instruments offer unique advantages.

1.3.1 Stylus Instrument

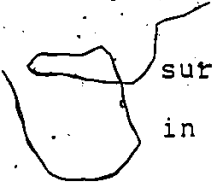
The only instrument that has achieved general use and widespread acceptance for surface roughness measurement is the stylus instrument commonly known as a 'Profilometer'. The measurement of the surface finish is carried out by lightly tracing a fine diamond stylus across the surface contour, as shown in Fig. 1.7. The radius of the stylus is normally between 400 to 500 micro inches (10 to 12 μm). The vertical movements of the stylus are transmitted to a coil inside the tracer body. The coil moves in the field of a permanent magnet and this produces a small fluctuating voltage whose magnitude is directly proportional to the height of the surface contour.

The tracer may be moved either manually or mechanically over the work surface. Manual operations make for convenience and time saving setups. Mechanical movements, however, give a more consistent and dependable roughness measurement.

The profilometer has the advantage that it yields an absolute measurement and the resulting electrical signal can be processed conveniently by conventional electronic techniques to provide either the average surface roughness (Ra) or a trace on a strip chart that represents, in highly magnified terms, the surface profile. In addition, all national and international standards are defined in terms of measurements made by the profilometer. This instrument, therefore, is in almost universal use. The profilometer performs fairly well for its intended purpose, however, it suffers from the following disadvantages:

- a) Production Capability: The main disadvantage of the profilometer is the mechanical frequency limitations to affect the measurement which renders it inadequate for production line measurements. In many processes where surface finish is critical, the requirement of this technique that the part be taken off the production line for roughness measurement, frequently means that only a very small sample of the production can be measured. This can result in substantial scrap if the surface finishing process deteriorates without being detected. This is particularly true with the increased use of automation in the industry where tool wear may not be detected until many defective parts have been produced.

- b) Repeatability of Measurement on Smooth Surfaces: Another deficiency of the stylus instrument is the lack of repeatability of measurement on surfaces with less than 10 micro inches average roughness. This is due to relatively large stylus tip radius when compared with the topography of the surface. This lack of repeatability can be critical as most roughness specifications, where roughness determines the functional characteristic as in journals, bearings, cylinders etc., are in the range of ≤ 20 micro in. Ra.
- c) Correlation with Other Instruments: Another problem with the stylus instrument is its lack of correlation with a similar instrument made by another manufacturer. This makes it difficult to maintain the uniformity of measurement if the instrument needs to be replaced. In addition, it is difficult to ensure the reliability and the accuracy of measurement offered by a given instrument.
- d) Surface Deformation: The last major fault of the stylus instrument is the inherent deformation or damage to the work surface caused because of excessive stylus pressure. This problem is obvious on soft materials but can be significant even on hard materials since the stylus pressure may approach 50,000 psi or more. On the other hand, a very hard



surface may also cause damage to the stylus resulting in measurement errors.

1.3.2 Optical Instruments

In addition to the profilometer there are several optical instruments available for the measurement of surface finish. These instruments have some distinct advantages as well as limitations for evaluating surface quality. They are particularly useful for fine finish and probably the most practical approach for finding random pits and flaws and for measuring the depth of scratches too fine for a stylus instrument. Their main advantage over the profilometer is that they inspect an area of a surface, rather than just the profile of a line traced by the stylus, thus providing a three dimensional view of the surface texture. Also since they make little or no contact with the work surface, they avoid the problem of marring the surface finish and deforming soft materials. However, these instruments are primarily inspection instruments and are not suitable for shop use because of the time and skill needed to set up and interpret their results.

Optical instruments can be broadly classified into three categories: Optical sectioning, Interferometric methods and Electron microscopy.

1.3.2.1 Optical Sectioning

This method was first developed by Schmaltz of Germany in 1931 and has since been refined and modified by a number of designers. The method is based on the fact that when a surface is illuminated with an oblique thin sheet of light, the projected line image provides a cross-sectional view of the specimen surface from which it is possible to obtain information regarding surface roughness and contour heights. The Schmaltz microscope, as shown in Fig. 1.8, uses two objective lenses at 45 degrees to the surface. One lens casts a thin sheet of light and other lens observes the profile that is produced.

1.3.2.2 Interferometric Methods

The interferometric methods have the widest application, among all the available optical methods, for surface texture analysis. In these methods, interference fringes are used for measuring the height of surface irregularities. Basically the instruments used for these methods are interferometers with microscope optics to enlarge the fringe patterns.

The fringe pattern appears as a series of parallel dark bands each separated by a light band. This fringe pattern is produced when parallel rays of monochromatic light reflected off of two surfaces rejoin 180 degrees out of phase. If the measured surface is perfectly flat in

relation to the reference surface, the dark fringes will be straight. But any discrepancy in the elevation, such as a high spot or a pit will cause a distortion in the fringe pattern.

The fringes are separated by a known distance of half the wavelength of illumination. This spacing provides a grid against which the surface height irregularities can be measured. The interferometric techniques work best for highly finished and flat surfaces. Following are the various interferometric techniques used for roughness measurement: double beam interferometry, multiple beam interferometry and differential interferometry.

1.3.2.3 Electron Microscopy

Electron microscopy is by far the most sophisticated technique for the analysis of surface topographical features. The two types of electron microscopes used for this purpose are the 'Transmission Electron Microscope' and the 'Scanning Electron Microscope'.

The Transmission Electron Microscope (TEM) employs transmitted electrons to form an image of the specimen surface. The low penetrating power of the electrons requires that the specimen and the entire electron path be in a high vacuum region with absolute pressures of 10^{-6} in. of Mercury or less. To study the surface topography, a suitable replica whose thickness is less than 4 μ in. (100

nm.) must be made of the test specimen's surface. The quantitative information about the topography may then be obtained with the aid of a measuring stereoscope and two micrographs of the surface taken at different angles.

In contrast to the TEM, the Scanning Electron Microscope (SEM) employs a beam of electrons focused to as small a spot as possible on the specimen surface. An image of the specimen surface is produced on a cathode ray tube face with a signal derived from specimen radiation. The requirement for a high vacuum, discussed for the TEM, also holds true for the SEM. Since the SEM depends primarily upon reflected or emitted radiations, there are no stringent requirements on specimen thickness. However, the extraction of quantitative information about surface topography from the output of the SEM is much more difficult and complex than from the TEM.

The main advantage of an electron microscope is its very high magnification of the order of 5×10^5 at a horizontal resolution of about $0.4 \mu\text{in.}$ (10 nm.) However, the high costs, inspection time and complexity involved in relating the output to the functional aspect of the surface, limit the use of this technique for only special applications.

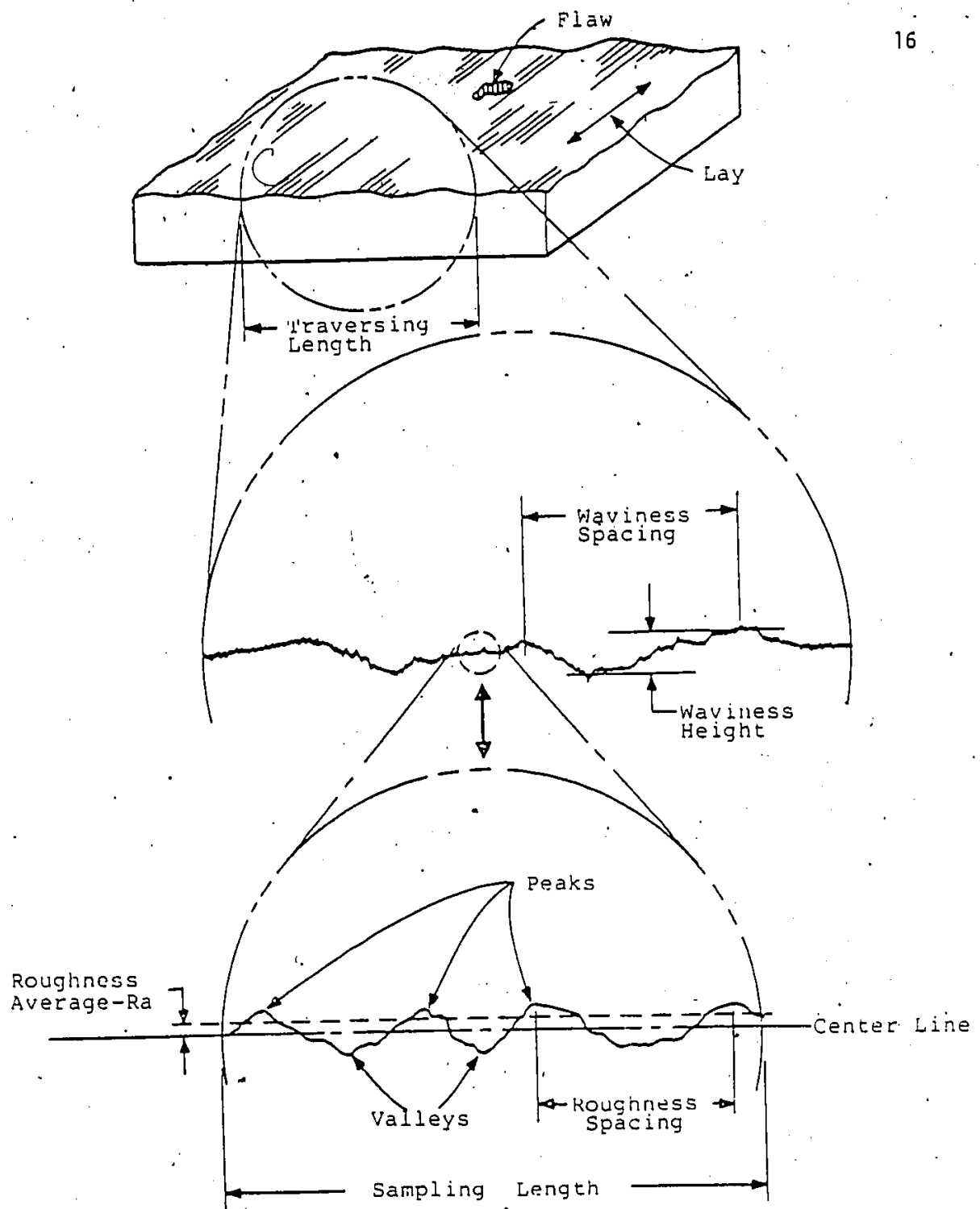


Figure 1.1: PICTORIAL DISPLAY OF SURFACE CHARACTERISTICS

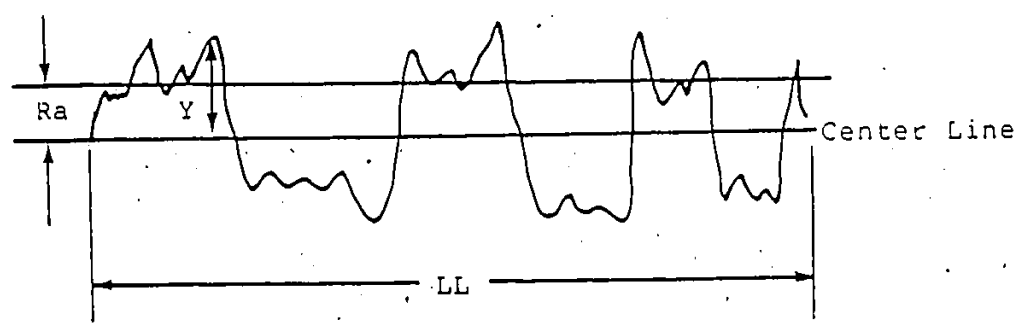


Figure 1.2: AVERAGE ROUGHNESS

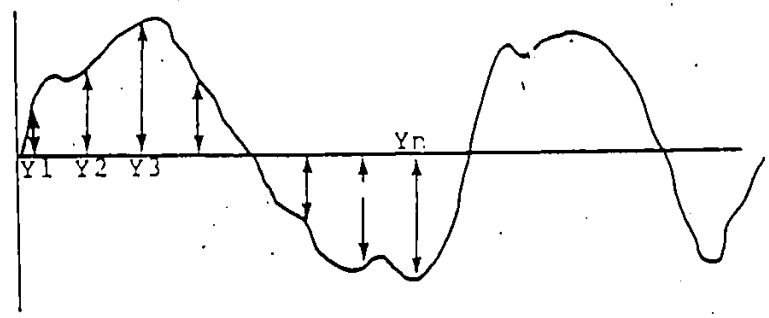


Figure 1.3: SECTION OF A SURFACE PROFILE DIVIDED IN INCREMENTS

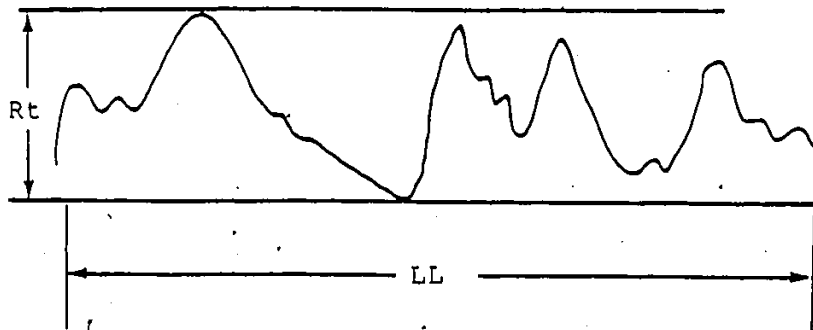


Figure 1.4: MAXIMUM PEAK TO VALLEY ROUGHNESS

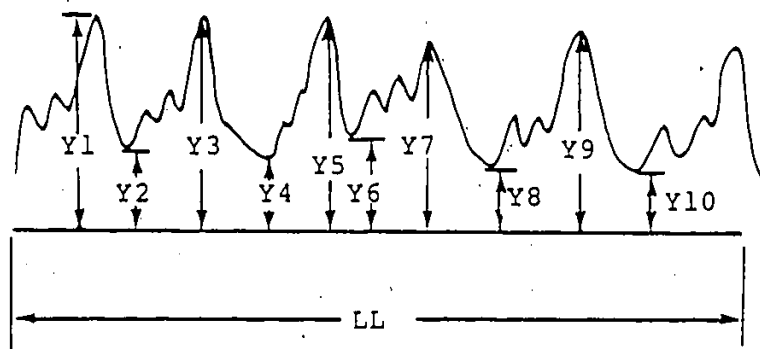


Figure 1.5: TEN- POINT HEIGHT

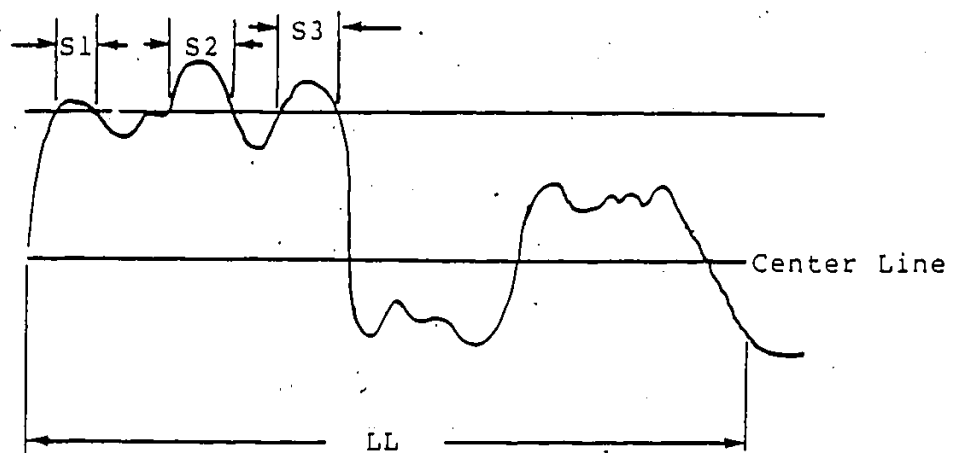


Figure 1.6: BEARING LENGTH RATIO

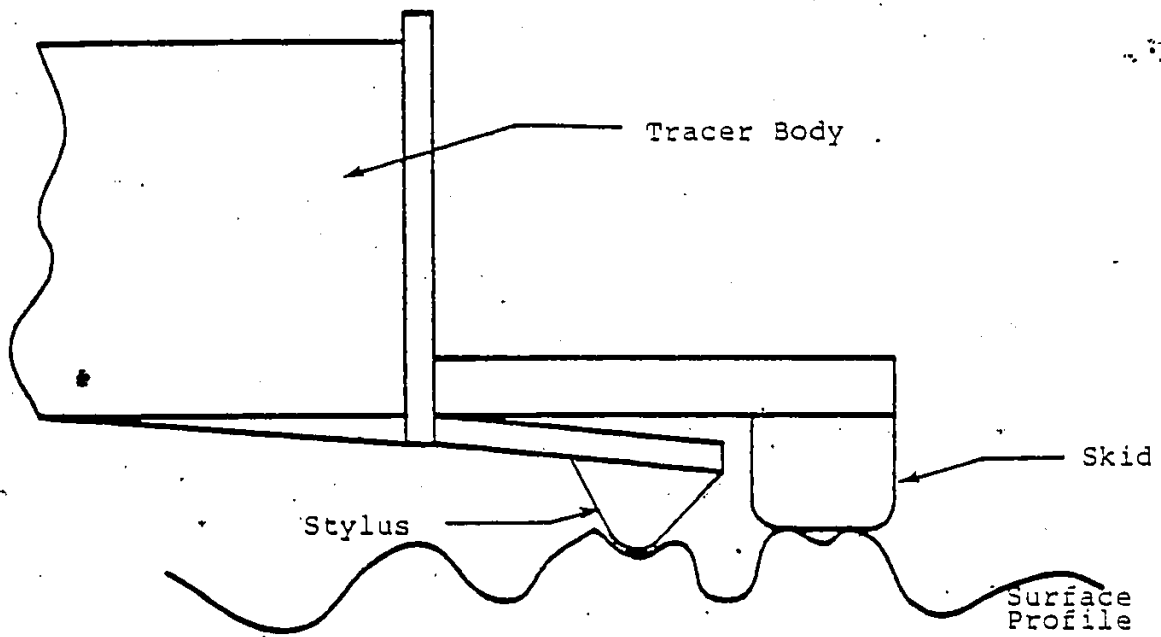


Figure 1.7: PRINCIPLE OF ROUGHNESS MEASUREMENT BY THE
STYLUS INSTRUMENT

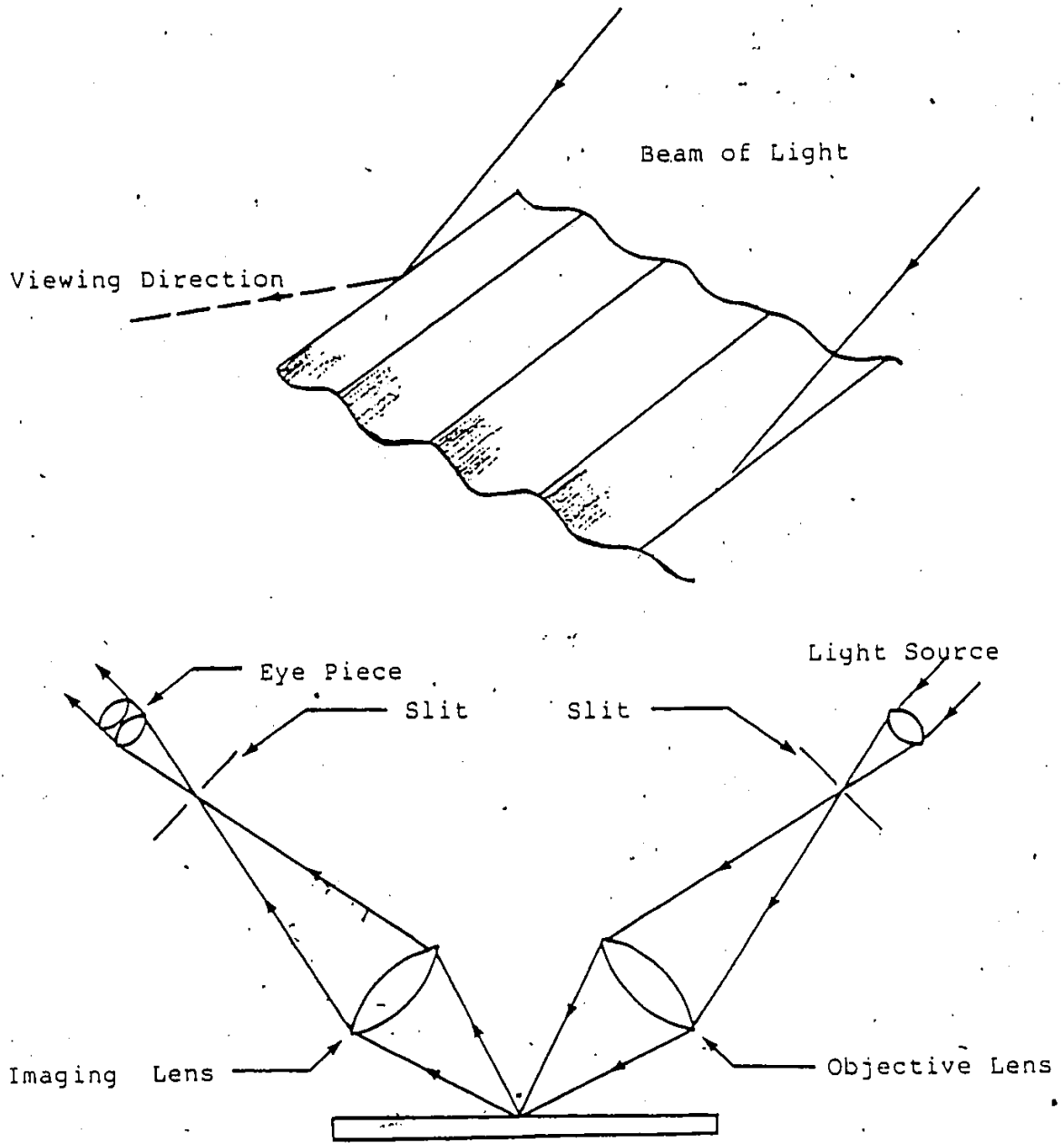


Figure 1.8: PRINCIPLE OF SCHMALTZ MICROSCOPE

Chapter II.

LITERATURE SURVEY

In order to overcome the drawbacks of the profilometer and limitations of existing optical instruments, extensive efforts have been made to develop an alternate optical method which could measure the surface finish rapidly, over large areas and in shop environments. The optical technique was considered an attractive method because of the following basic advantages:

- a) Non contact: The optical method is inherently non contact which not only avoids the problem of marring surface finish but also makes production line operation easier since it can operate at some distance from the work surface. Moreover there is no wearout which can change the calibration equation.
- b) Probe Size: The optical system has an effective probe size which is the order of a wavelength of the light used. For available light sources this can be about 20 micro inches which is much smaller than stylus tips commonly used.
- c) Area Averaging: The area averaging properties of a light beam helps to ensure better repeatability.

d) High Speed: An optical system can perform at high speed subject only to electronic rather than mechanical band width limitations.

The ability to quantify the surface roughness optically could also be of value in the in-process estimation of surface roughness, with the purpose of controlling the finishing process during machining or as a diagnostic aid to evaluate the tool wear.

Recently developed optical techniques are mostly based on the property of rough surfaces which causes an incident light beam to scatter in various directions.

2.1 INTERACTION OF LIGHT WITH ROUGH SURFACES [5]

When an electromagnetic wave is incident on a plane surface, it is reflected according to well known law: the reflected field depends on the wavelength, the angle of incidence and the electrical properties of the medium.

If the surface is absolutely smooth the incident wave gets reflected specularly in a single direction obeying Snell's law, i.e. angle of incidence is equal to angle of reflection (Fig. 2.1a). If, however, the surface is rough the incident energy gets scattered into various directions, though certain directions may receive more energy than others (Fig. 2.1b). This phenomenon of reflection can be used to define a rough surface.

According to this description, the same surface may be rough for some wavelengths of electromagnetic radiation and smooth for others, or for the same wavelength it may be either rough or smooth depending on the angle of incidence. The proportion of diffuse to specular reflection, therefore, depends on surface roughness, wavelength and angle of incidence of incident radiation.

The general theory of the scattering of electromagnetic radiation, from rough surfaces has been developed by several authors [5,6], for applications to both periodic and random rough surfaces. The most comprehensive development of this work is given by Beckmann [5] who formulated the theory of specular and diffused reflection to obtain the angular distribution of intensities in specular and other directions.

2.2 MEASUREMENT OF SURFACE ROUGHNESS BY LIGHT SCATTERING METHODS

The work of Davies [6] and Beckmann [5] on the scattering of electromagnetic waves from rough surfaces provided a theoretical basis for optical methods of estimating surface roughness, from the measurement of scattered light intensities. Beckmann's theory gives the average intensity scattered in and away from the specular direction; broadly speaking, the light reflected into the specular direction gives information about the variance of surface height, while that scattered away from the specular direction depends, in addition, on the surface slopes.

The use of specular reflection measurement for determination of the surface roughness was first successfully investigated by Bennett & Porteus[7], based on the relation between reflectance and root mean square (RMS) roughness obtained from the statistical treatment of the reflection of electromagnetic radiation from rough surfaces derived by Davies. The expression for the reflectance measured normal to the surface, for illumination at normal incidence, is given by:

$$R = R_0 \cdot \text{Exp} \left[- \left(\frac{4\pi\sigma}{\lambda} \right)^2 \right] + \frac{R_0 \cdot 2^5 \cdot \pi^4}{m^2} \cdot \left(\frac{\sigma}{\lambda} \right)^4 \cdot (\Delta\theta)^2 \quad \dots(2.1)$$

Where, R_0 is the reflectance from a perfectly smooth surface of the same material,

σ is the RMS deviation of the surface heights,

λ is the wavelength of the illumination,

m is the RMS surface slope, and;

$\Delta\theta$ is the instrument's acceptance angle.

The first term in equation 2.1 is the specular component of reflected light while the second term is the diffused light component. If the wavelength of the incident light is much longer than the RMS deviation of surface height σ , the equation 2.1 reduces to;

$$R = R_0 \cdot \text{Exp} \left[- \left(\frac{4\pi\sigma}{\lambda} \right)^2 \right] \quad \text{-----}(2.2)$$

by neglecting the diffused reflectance component.

Equation 2.2 may then be written as,

$$\text{Ln} \left(\frac{R_0}{R} \right) = \left(\frac{4\pi\sigma}{\lambda} \right)^2 \quad \text{-----}(2.3)$$

Thus, if R_o/R is plotted on a semilog paper Vs. $1/\lambda^2$, a straight line through the origin with a slope which is directly proportional to σ^2 is obtained. It is possible, therefore, to measure the RMS roughness by measuring the surface reflectance at normal incidence with illumination of various wavelengths.

This method was experimentally verified by Bennett and Porteus on ground glass and steel surfaces. They found a good agreement between optically measured roughness and that measured by a profilometer.

The same method was subsequently verified by other authors like K.E. Torrance[8], C.A. Depew & R.D. Weir[9] and R.C. Birkebak[10], using different types of surfaces. Their results are summarized by R.C. Birkebak[11]. These results all show a significant correlation between specular reflection measurement at normal incidence, with surface roughness as measured with a profilometer. However, this method was found suitable only for surfaces having roughness values of 20 μ in. or less and where surface height distribution was approximately Gaussian in nature.

More recently the results obtained by D.H. Hensler[12] from his light scattering experiments on fused polycrystalline aluminum oxide surfaces have shown good agreement with the scattering theory developed by Beckmann. The equation for specular reflection, R_s , as given by Beckmann's theory is:

$$R_s = R_o \cdot \text{Exp} \left[- \left(\frac{4\pi \sigma \cos\theta}{\lambda} \right)^2 \right] \quad \text{-----} (2.4)$$

Where, R_o is the reflection intensity from a perfectly smooth surface of the same material, σ is a measure of average vertical roughness based on the assumption of Gaussian distribution of surface heights, λ is wavelength of illumination and θ is angle of incidence.

If the value of $\ln(R_s/R_o)$ is plotted Vs. $\cos^2\theta$, a straight line with a slope of $-\left(\frac{4\pi\sigma}{\lambda}\right)^2$ is obtained. Therefore by knowing the slope of the line, it is possible to estimate the value of σ .

By measuring the reflectance from a surface at various angles of incidence θ , and estimating the value of σ from the plot of $\ln(R_s/R_o)$ and $\cos^2\theta$, Hensler has shown that a good correlation exists between RMS roughness thus obtained and the surface roughness as determined by a profilometer. However, Hensler's results are also valid only for surfaces which could be approximated to have Gaussian height distribution and whose roughness is only a fraction of the wavelength of the illumination.

In yet another work, P.J. Chandley [13] using Beckmann's theory has estimated both variance and autocorrelation of height on ground glass surfaces by measurement in and away from the specular direction. Measurements of the variance of surface height obtained have been shown to agree closely with stylus measurements for each surface. Though Chandley's work has shown excellent results, his experimental procedures are too complex for it to be of any practical utility.

Investigations have also been made into measurements of the coherent power spectrum scattered by the rough surfaces. It has been found that the measurements taken from portions of the power spectrum curve do correlate with profilometric measurements but the correlation is not good enough for accurate measurement of surface roughness. The reason for this lack of correlation is that the power spectrum is more closely related to the slope of surface profile rather than its heights [14]. Measurements of the power spectrum, thus are different for surfaces of the same roughness but having different slopes.

B.J. Pernick [15] has demonstrated that the characteristic pattern in the optical Fourier transform distribution of the light scattered from a rough surface is also related to the surface roughness. He obtained an optical Fourier transform of the scattered light by using a transform and a cylindrical lens. By fitting an integrated

5

Gaussian curve to the experimentally observed Fourier transform pattern, Pernick has developed an empirical linear relation between a Gaussian width parameter and average surface roughness.

Although these works have all shown some degree of success in correlating the surface roughness with the scattered light measurements, they have primarily remained of theoretical interest only because of the complex experimental procedures which were not suitable for ordinary practical purposes.

A more practical approach, for estimating surface roughness from light scattering measurements, has been adapted by some workers using a bifurcated fiber-optic transducer. A bifurcated fiber-optic transducer consists of optical fibers bounded in a common leg at one end and divided into two legs at the other end. The fibers from the two legs can be grouped at the common end in several possible orientations, for example; random, concentric, hemispheric etc. (Fig. 2.2). The first successful attempt to use a fiber-optic transducer was made by D. Spurgeon and R.A.C. Slatter[16]. They used a randomized fiber-optic transducer where one half of the fibers were used to carry the light from an incandescent lamp to be incident on the work surface at normal incidence while the other half detected the light reflected from the surface and was measured using a photodetector (Fig. 2.3). The reflected

light output from the transducer was shown to be correlated for turned surfaces with the surface roughness by the following equation:

$$L \cdot Ra^{0.724} = 5.1 \quad \text{-----} (2.5)$$

Where, L is the Transducer output (mv.), and;

Ra is the Average Surface Roughness ($\mu\text{m.}$)

More recently G.C.I. Lin, T. Shea and K. Hoang [17] have also shown a strong relationship between average surface roughness and reflected light output from ground surfaces, using a similar randomized fiber-optic bundle and a He-Ne laser as a light source (Fig. 2.4). Mathematically, this relationship has been expressed by the authors as:

$$Y = A \cdot X^B \quad \text{-----} (2.6)$$

Where, Y is the Average Roughness ($\mu\text{in.}$)

X is the Transducer Output (mv.), and;

A & B are constants.

2.3 OBJECTIVE OF THE PRESENT RESEARCH

The main objective of this research work is to develop a technique for the measurement of surface roughness of 'ground' surfaces using a fiber-optic transducer.

Although a successful attempt has been made to use a fiber-optic transducer in both the works by Spurgeon &

Slatter[16] and Lin, Shea & Hoang[17], the main drawback with their method has been that the output from the transducer was not normalized before correlating it with the surface roughness. This is an important concern because the transducer output could be easily affected by variables other than surface roughness and lead into an erroneous measurement.

The small range of measurement is another limiting factor for their techniques to be of more general use. Although Lin, Shea & Hoang have shown that a linear relationship, between surface roughness and transducer output, exists up to about 70 micro inches, the most practical range of measurement by their method is not more than 20 micro inches.

Moreover, no effort has been made by any worker to study the affect of bundle size and fiber orientation on the proper choice of the transducer.

This research work, therefore, also pursues efforts:

1. To develop a technique where a normalized parameter is used to characterize the surface roughness and which could be used to measure the roughness over a range larger than that achieved by other techniques using optical methods.
2. To study the effect of transducer size and the geometry of fiber orientation on the selection of a transducer most suitable for the purpose of roughness measurement.

3. To bear in mind that the technique should be practically feasible.
4. To satisfy, if possible, the requirements of Mr. Malconian (Manager QCD at Chrysler's Engine Plant at Windsor) whose goal is to sample 100% of the pin and main journals on a crankshaft for roughness in the acceptable range of ≤ 15 micro inches Ra.

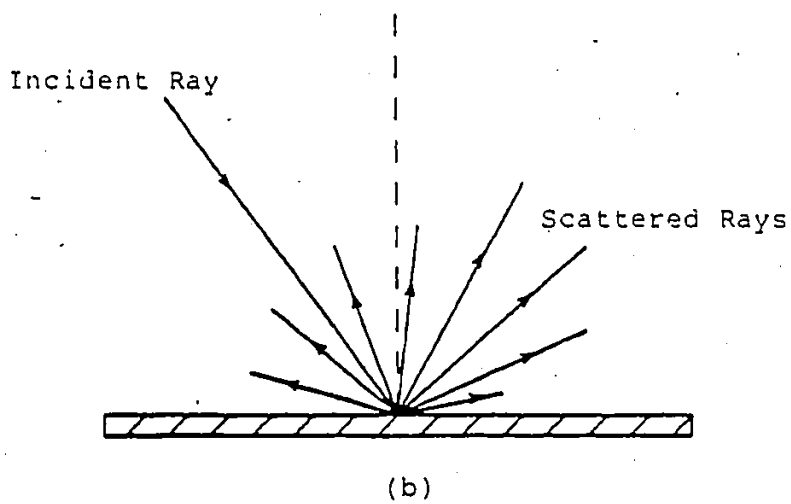
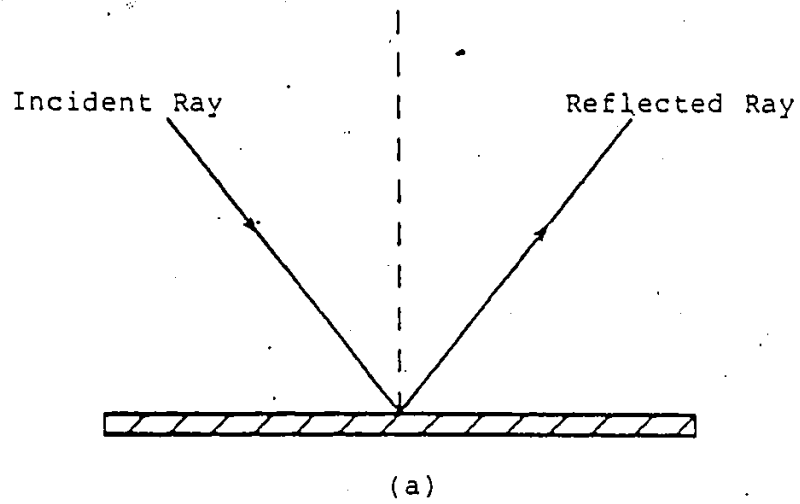
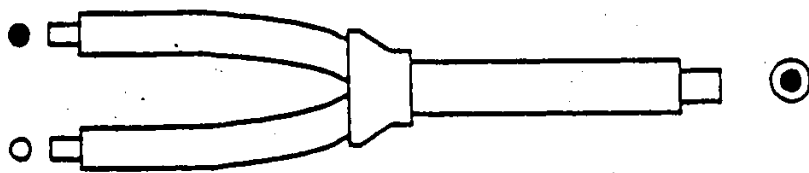
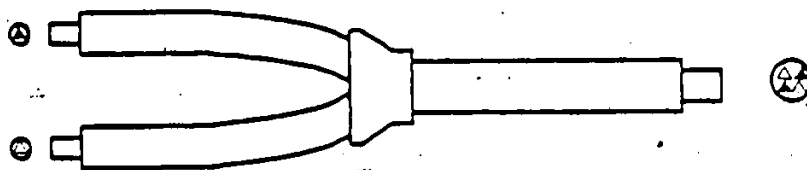


Figure 2.1: POSSIBLE MODES OF LIGHT REFLECTION FROM A SURFACE

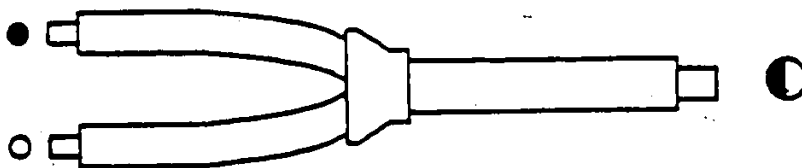
(a) Specular (b) Scattered



(a)



(b)



(c)

Figure 2.2: POSSIBLE FIBER ORIENTATIONS IN A BIFURCATED
TRANSDUCER

(a) Concentric (b) Random (c) Hemispheric

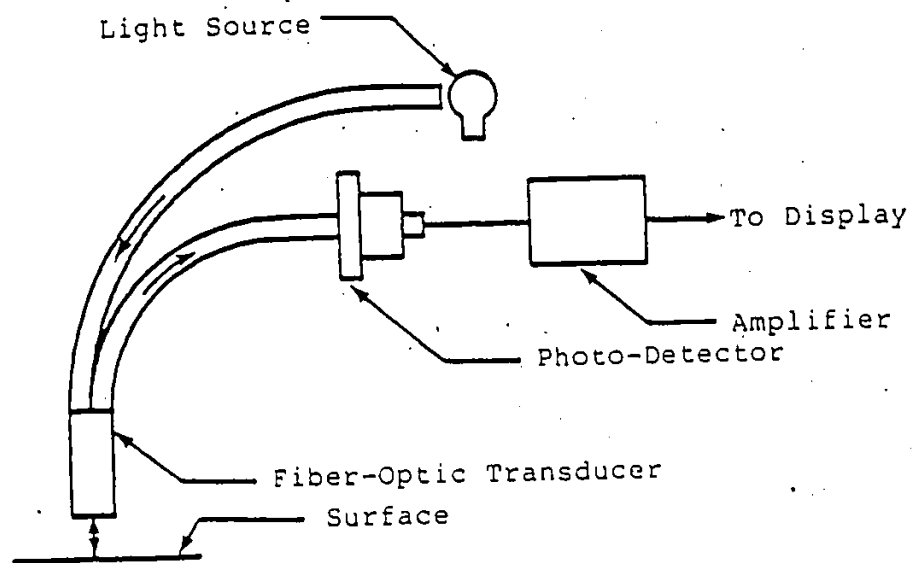


Figure 2.3: SCHEMATIC OF THE EXPERIMENTAL SETUP OF SPURGEON & SLATTER

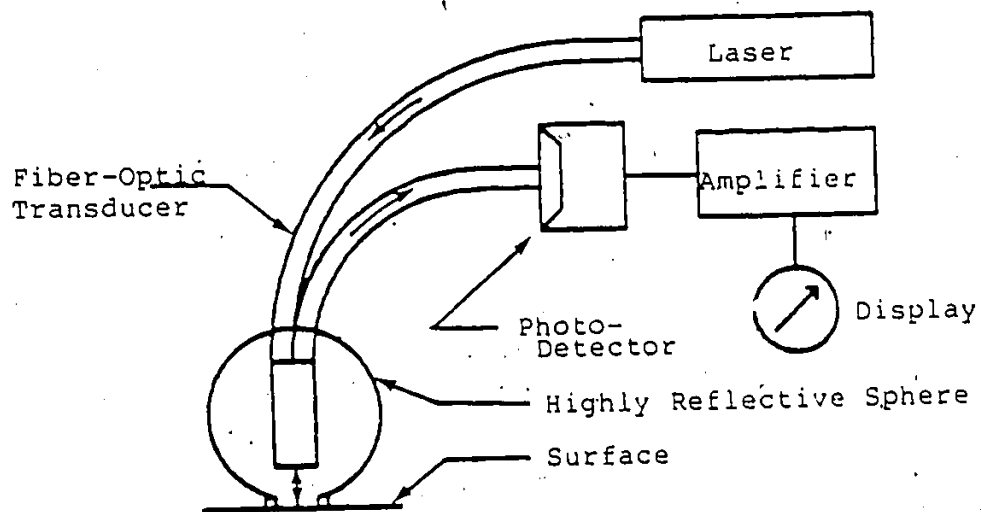


Figure 2.4: SCHEMATIC OF THE EXPERIMENTAL SETUP OF LIN, SHEA & HOANG

Chapter III

THEORY

3.1 FIBER-OPTIC FUNDAMENTALS [18]

The science of fiber-optics deals with the transmission or guidance of light along transparent fibers of glass or plastic by the process of total internal reflection.

A ray of light, incident upon the interface between two transparent optical materials having different indices of refraction, will be totally internally reflected if:

1. the ray is incident upon the interface from the direction of more dense material, and;
2. the angle made by the ray with the normal to the interface is greater than some critical angle which depends only on the indices of refraction of the media.

An optical fiber (Fig. 3.1) is made of a high refractive index material 'core', along which the light is propagated, and a low refractive index material 'cladding' which sheaths the fiber core and serves to provide optical insulation and protection to the total reflection interface. The fiber core is generally made of glass, plastic or certain polymers like polymethyl-methacrylate and could be coated with a low refractive index glass, plastic or a

polymer. Glass coated glass fibers are normally superior in quality than plastic or polymer fibers.

A ray of light traversing a fiber 0.002 in. in diameter may be reflected as many as 3000 times per foot of fiber length. The number of reflections increase in direct proportion to diameter decrease. In superior quality fibers this total internal reflection process results in a loss of 0.001 percent per reflection, thus a useful quantity of illumination can be transported from thin and even long fibers.

Light is transmitted down the length of a fiber at a constant angle with the fiber axis. Scattering from the true geometric path can occur, however, as a result of:

1. Imperfections in the bulk of the fiber,
2. Irregularities in the core/clad interface of the fiber and;
3. Surface scattering upon entry.

In the first two instances, light will be scattered in proportion to the fiber length, depending on the angle of incidence. To be functional, therefore, long fibers must have an optical quality superior to that of short fibers. Surface scattering occurs readily if the fiber ends are not polished properly to produce a surface that is perpendicular to the fiber axis.

The speed of light in matter is less than the speed of light in air, and the change in velocity that occurs when

light passes from one medium to another, results in refraction. It should be noted that a portion of the light incident on a boundary surface is not transmitted but is instead reflected back into air. That portion which is transmitted is totally reflected from the sides, assuming that the angle is less than the critical angle. The relationship between the angle of incidence θ and the angle of refraction γ (Fig. 3.1), is expressed by Snell's law as:

$$N_1 \sin \theta = N_2 \sin \gamma \quad \text{-----(3.1)}$$

Where, N_1 is the index of refraction of air and

N_2 is the index of refraction of the core.

Since $N_1=1$ for all practical purposes, the refractive index of the core becomes

$$N_2 = \sin \theta / \sin \gamma \quad \text{-----(3.2)}$$

Snell's law can also be used to calculate the maximum angle within which light will be accepted into and conducted through a fiber (Fig. 3.1):

$$N_1 \sin \theta_{\max} = (N_2^2 - N_3^2)^{1/2} \quad \text{-----(3.3)}$$

Where θ_{\max} is the maximum angle of incidence,

N_1 is refractive index of air ($N_1=1.0$),

N_2 is refractive index of the core and

N_3 is refractive index of the clad.

Substituting $N_1=1.0$, equation 3.3 can be written as:

$$\sin \theta_{\max} = (N_2^2 - N_3^2)^{1/2} \quad \text{-----(3.4)}$$

The quantity $\sin \theta_{\max}$ is more commonly known as 'Numerical Aperture' and is considered a basic descriptive characteristic of specific fibers.

3.2 OUTPUT RESPONSE CHARACTERISTIC OF A FIBER [18,19]

The general response characteristic between the reflected light output and the fiber distance from the surface, using an adjacent pair of transmitting and receiving fibers, is shown in Fig. 3.2.

When both transmitting and receiving fibers are in contact with the surface, no light is reflected to the receiving fiber and consequently there is no output from it. As the distance between the fibers and the surface increases the cone of light from the transmitting fiber illuminates an increasingly larger area on the work surface. This area becomes, in effect, the source of a secondary cone of reflected light, which in turn increasingly illuminates the receiving element.

The relationship between the surface displacement and receiver output remains essentially linear, until the entire surface of the receiving fiber is illuminated by the reflected light cone, at which point the curve reaches its peak (Fig.3.2). As the distance increases beyond this point, the output from the receiver decreases in approximately inverse proportion to the square of the distance.

In practice, however, a random bundle of transmitting and receiving fibers shows a response characteristic as depicted in Fig.3.3. It may be noticed that the curve has three distinct regions a-b, b-c and c-d. In the regions a-b

and c-d, the output from the fiber-bundle is dependent upon its position from the object surface. The third portion of the curve b-c, is the region adjacent to the peak which occurs at a particular value of displacement when all the receiving fibers in the bundle are illuminated by the reflected light. In this region (b-c) the output from the fibers remains relatively insensitive to the displacement. The output in this region is entirely a function of the reflectivity of the work surface, and any change in the output is the result only of a change in surface reflectivity.

This behavior of the response curves provides the possibility for estimating the surface roughness by measuring the output from the fiber-optic transducer, set at the peak distance. For any given transducer, the characteristic shape of the output Vs. displacement curve remains the same regardless of work surface reflectivity, and the curve will always attain its peak at the same distance (Fig. 3.4). The distance of the transducer from the work surface over which its output remains maximum can be termed as the working distance since the transducer has to be positioned here for the purpose of roughness measurement. The average working distance is therefore the transducer 'stand-off' and the displacement over which the output remains constant is its working range. It is obvious that a transducer with a longer stand-off and a larger range is rather desirable for this purpose.

3.3 THEORETICAL REFLECTION MODEL

From the behaviour of the fiber response characteristic curve it was observed that if the transducer is placed at a distance from the surface, so as to obtain a maximum output from its receiving fibers, the reflected light output from the surface can possibly be correlated with its roughness. In order to obtain a basic guideline for a technique to be suitable for roughness measurement, a theoretical relationship between the reflected light output and the surface roughness is developed here. A rough surface which is simplistically modelled as a triangular wave profile is used to develop this relationship.

Fig. 3.5 shows a machined surface with triangular wave profile whose individual facets are inclined at an angle α from the horizontal and have a length of l . This surface receives incident light over a length L from a source of length L and inclined at an angle θ from the vertical. 'ABC' represents one machined groove on this surface.

The reflection output, dR , from an elemental length dl of surface AB, in the direction of incident ray, is given by[20]:

$$dR = I_i \cdot B \cdot \cos\theta \cdot dl \quad \text{-----(3.5)}$$

Where, I_i is incident intensity,

θ is angle which the incident ray makes with normal to the surface AB and;

$$1 \text{ Ra} = f/8 \cdot \tan\alpha$$

B is the reflection distribution function.

The reflection distribution function represents the nature of intensity distribution in the scattered light. It is generally a complicated function of a number of variables, although it takes on simple forms in special cases. For finely lapped and ground surfaces this function has been estimated by some authors[21,22] to be approximately exponential with respect to angle of incidence and scatter. In this case this function has been assumed as:

$$B = ae^{-k|2\theta|} \quad \text{-----(3.6)}$$

Where a and k are constants depending upon the reflection coefficient of the surface and wavelength of illumination respectively.

The equation 3.5 can, therefore, be written as:

$$dR = I_i \cdot ae^{-k|2\theta|} \cdot \cos\theta \cdot d\ell \quad \text{-----(3.7)}$$

It can be noticed from Fig. 3.5, that,

$$\theta = \alpha - \phi \quad \text{if, } \phi < \alpha$$

The reflected light output from the entire surface AE is, thus, given by:

$$R_{AB} = \int dR = \int_0^{\ell} I_i \cdot ae^{-2k|\alpha-\phi|} \cdot \cos(\alpha-\phi) \cdot d\ell \quad \text{-----(3.8)}$$

Similarly the reflected light output from face BC is:

$$R_{BC} = \int_0^{\ell} I_i \cdot ae^{-2k|\alpha+\phi|} \cdot \cos(\alpha+\phi) \cdot d\ell \quad \text{-----(3.9)}$$

Adding equation 3.8 and 3.9, the output from a single groove ABC is obtained as:

$$R_{ABC} = a I_i \left[\int_0^{\ell} e^{-2k|\alpha-\phi|} \cdot \cos(\alpha-\phi) \cdot d\ell + \int_0^{\ell} e^{-2k|\alpha+\phi|} \cdot \cos(\alpha+\phi) \cdot d\ell \right] \quad \text{....(3.10)}$$

The total number of illuminated grooves N , on this surface, can be estimated as:

$$N = L'/f$$

Where, L' is illuminated surface length and;

$$f = 2\ell \cdot \cos\alpha, \text{ is machining feed rate.}$$

Assuming a parallel light flux from the source, it can be shown that:

$$L' = L/\cos\phi$$

$$\text{Therefore, } N = \frac{L}{2\ell \cos\alpha \cos\phi}$$

The total reflected output from the entire illuminated surface length is then:

$R_{\text{total}} = N \cdot \text{Output from one groove}$

$$R_{\text{total}} = \frac{a I_i L}{2\ell \cos\alpha \cos\phi} \left[\int_0^{\ell} e^{-2k|\alpha-\phi|} \cos(\alpha-\phi) \cdot d\ell + \int_0^{\ell} e^{-2k|\alpha+\phi|} \cos(\alpha+\phi) \cdot d\ell \right]$$

$$R_{\text{total}} = \frac{a I_i L}{2\cos\alpha \cos\phi} \cdot [e^{-2k|\alpha-\phi|} \cos(\alpha-\phi) + e^{-2k|\alpha+\phi|} \cos(\alpha+\phi)] \quad \dots(3.11)$$

$$\rho = \frac{R_{\text{total}}}{I_{\text{total}}} = \frac{a}{2\cos\alpha \cos\phi} [e^{-2k|\alpha-\phi|} \cos(\alpha-\phi) + e^{-2k|\alpha+\phi|} \cos(\alpha+\phi)] \quad \dots(3.12)$$

Where $I_{\text{total}} = I_i \cdot L$, is the total incident input, and;

ρ is the specific reflection output.

Similarly for case where $\alpha < \phi$, it can be shown that:

$$\rho = \frac{a}{2\cos\alpha \cos\phi} [e^{-2k|\phi-\alpha|} \cos(\phi-\alpha) + e^{-2k|\phi+\alpha|} \cos(\phi+\alpha)] \quad \dots(3.13)$$

Equations 3.12 and 3.13 are essentially similar equations which represent the necessary relationship between output to input ratio ρ surface slope α and transducer inclination angle ϕ

It should be noted that the relationship developed here is very approximate and is useful to the extent that it represents only the behavior of the transducer output with respect to surface roughness and its angle of inclination.

The ratio ρ as calculated from equation 3.12 is plotted, Vs., α for varying angles of transducer inclination ϕ and for an assumed value of $a=1$ and $k=1$. These plots are presented in Fig. 3.6. When the transducer is normal to the object surface ($\phi=0^\circ$), it is seen from this figure that ρ decreases monotonously as α increases or in other words the transducer output decreases as the roughness of object surface increases. This relationship between the reflected light output and surface roughness is similar to that obtained experimentally by Spurgeon and Slatter[16] and Lin, Shea & Hoang[17] in their works. It will, therefore, seem to indicate that this simplified theoretical relation fairly well represents the correlation between the transducer output and the surface roughness.

By increasing the inclination angle ϕ , the transducer output pattern changes and at $\phi=30^\circ$ it is noticed that the value of ρ increases monotonously as α increases, meaning that the transducer output now shows an increase with increasing roughness.

This pattern of transducer output at $\phi=30^\circ$ (or more) is completely opposite to that at $\phi=0^\circ$ and it suggests that a ratio of transducer output at two different detecting angles would be a normalized and a very sensitive parameter which could be correlated with the surface roughness.

The ratio of transducer output at two detecting angles ϕ_1 and ϕ_2 can be obtained from equation 3.11, as:

$$\frac{R_{\phi_1}}{R_{\phi_2}} = \frac{\cos\phi_2}{\cos\phi_1} \left[\frac{e^{-2k|\alpha-\phi_1|} \cos(\alpha-\phi_1) + e^{-2k|\alpha+\phi_1|} \cos(\alpha+\phi_1)}{e^{-2k|\alpha-\phi_2|} \cos(\alpha-\phi_2) + e^{-2k|\alpha+\phi_2|} \cos(\alpha+\phi_2)} \right] \dots (3.14)$$

Substituting $\phi_1=0$ and $\phi_2=\phi$

The output ratio at 0 and ϕ degrees is then;

$$\frac{R_0}{R_\phi} = \left[\frac{2e^{-2k\alpha} \cos\alpha \cos\phi}{e^{-2k|\alpha-\phi|} \cos(\alpha-\phi) + e^{-2k|\alpha+\phi|} \cos(\alpha+\phi)} \right] \dots (3.15)$$

This equation indicates that the output ratio depends only on surface roughness, transducer inclination angle and the wave length of illumination and is independent of the reflection coefficient of the surface.

Calculating the value of R_0/R_ϕ for various values of α , a simplified correlation equation has been obtained between α and R_0/R_ϕ . This correlation equation is approximately of the following form:

$$\alpha = A + BX^C \quad \text{-----} (3.16)$$

Where, X indicates the output ratio R_0/R_ϕ and;

A, B and C are constants.

This plot between α and R_0/R_0 is shown in Fig. 3.7 for $\phi=30^\circ$ and 35° .

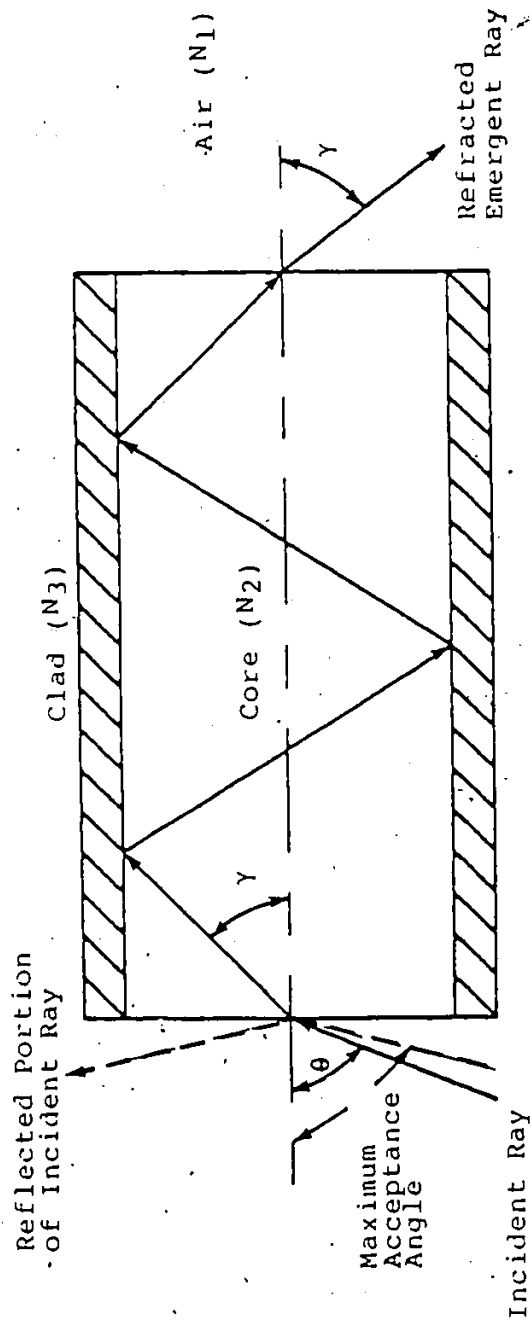


Figure 3.1: AN OPTICAL FIBER

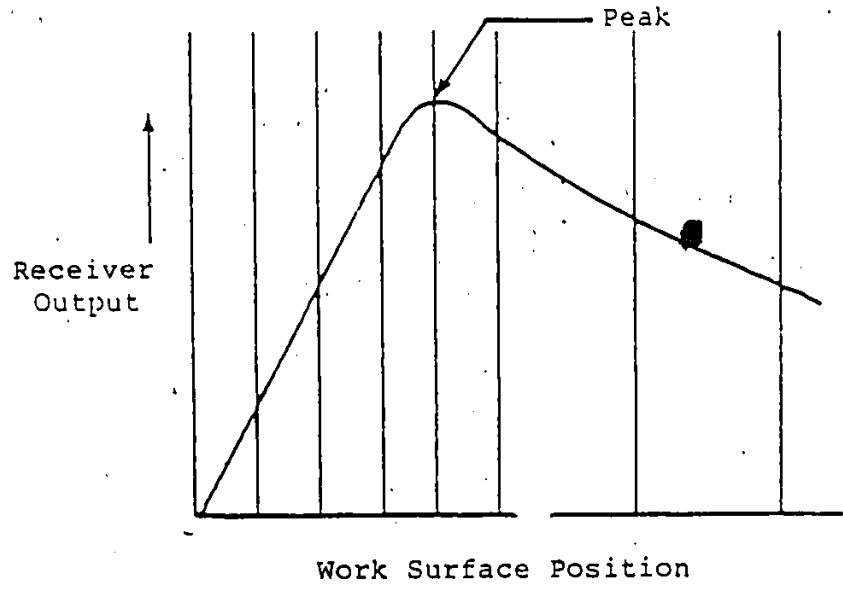
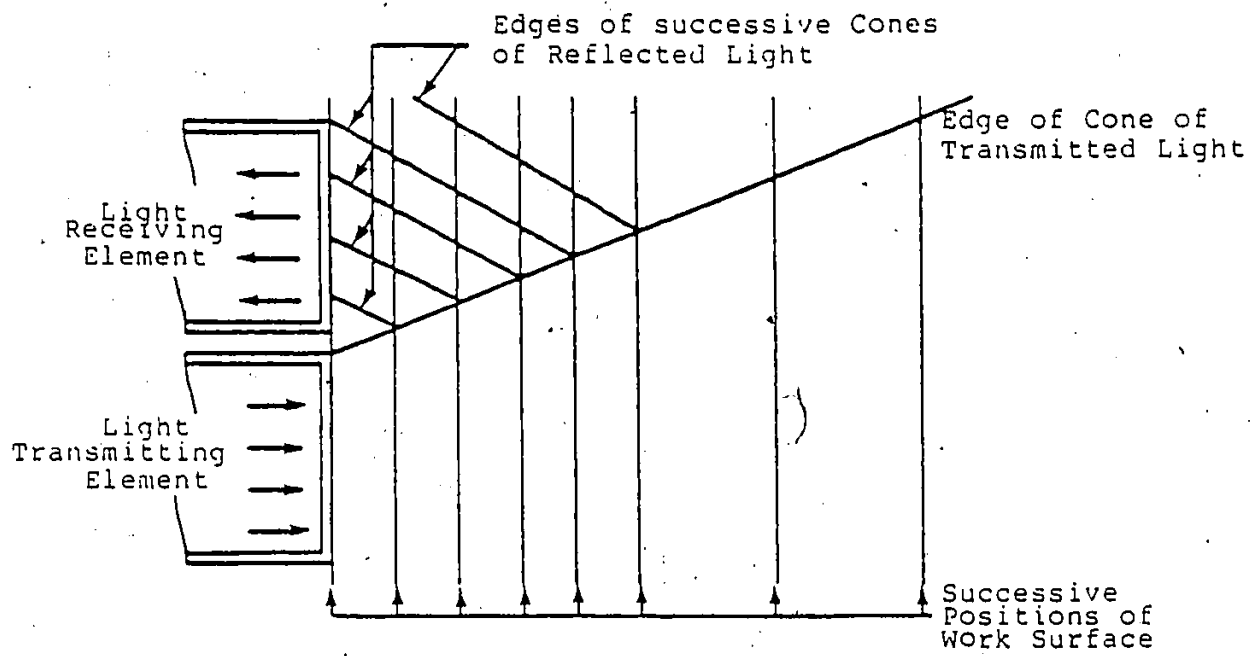


Figure 3.2: RESPONSE CHARACTERISTIC OF AN OPTICAL FIBER

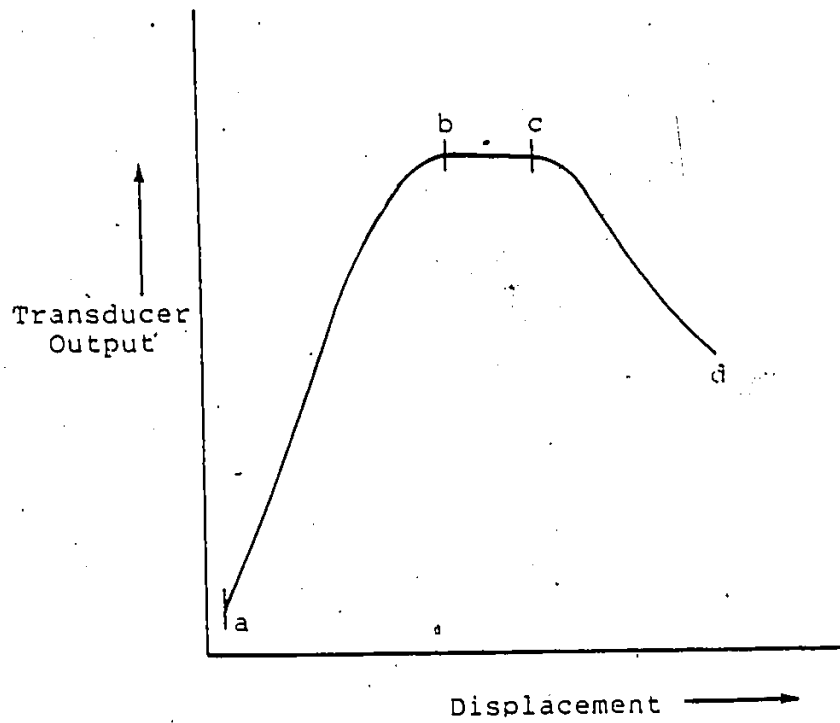


Figure 3.3: RESPONSE CHARACTERISTIC OF A RANDOM FIBER OPTIC TRANSDUCER

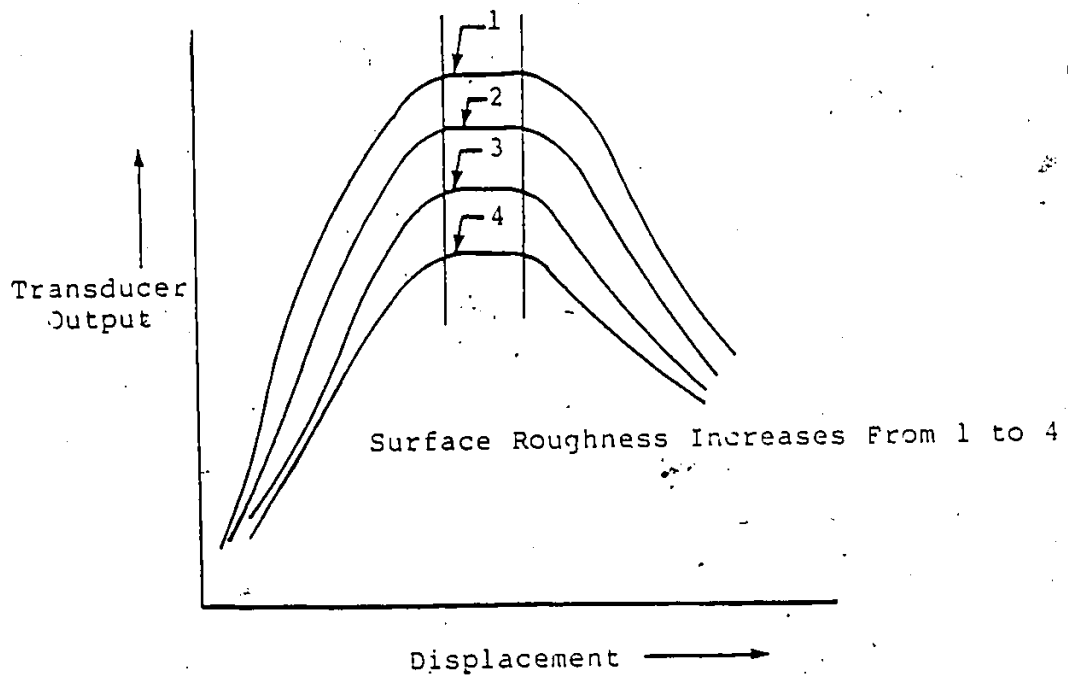


Figure 3.4: VERTICAL SHIFT OF THE RESPONSE PEAK WITH VARIATION IN ROUGHNESS

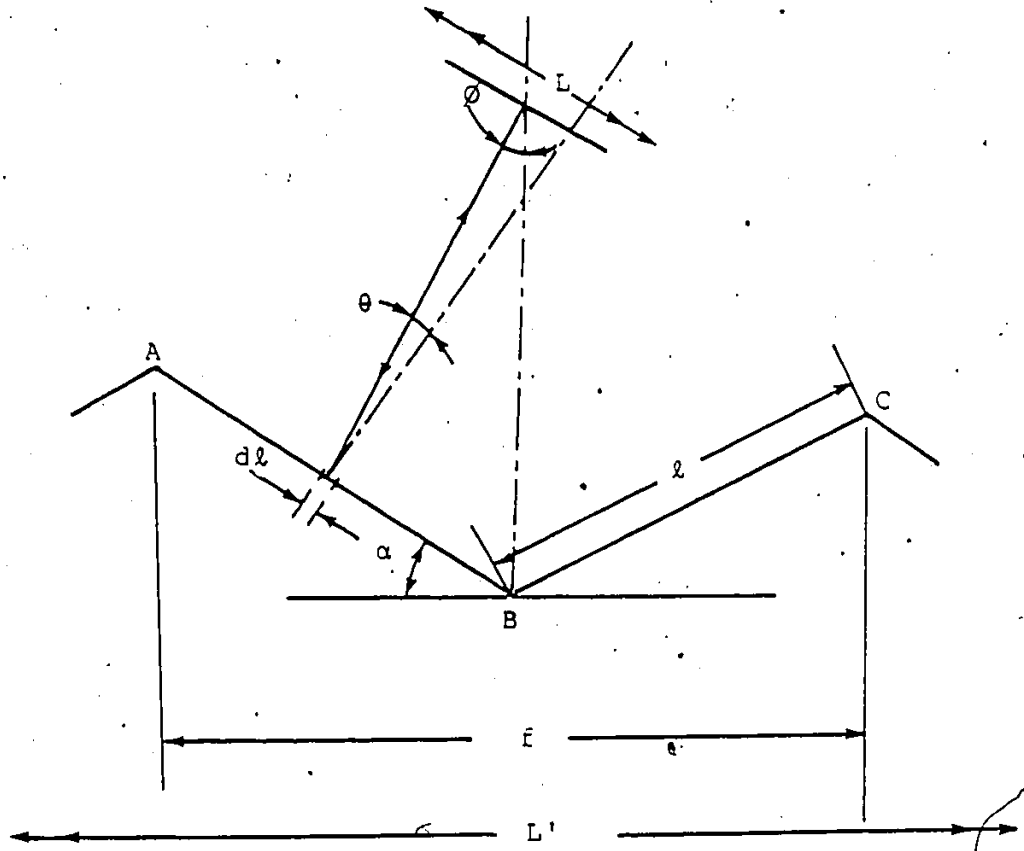


Figure 3.5: THEORETICAL REFLECTION MODEL

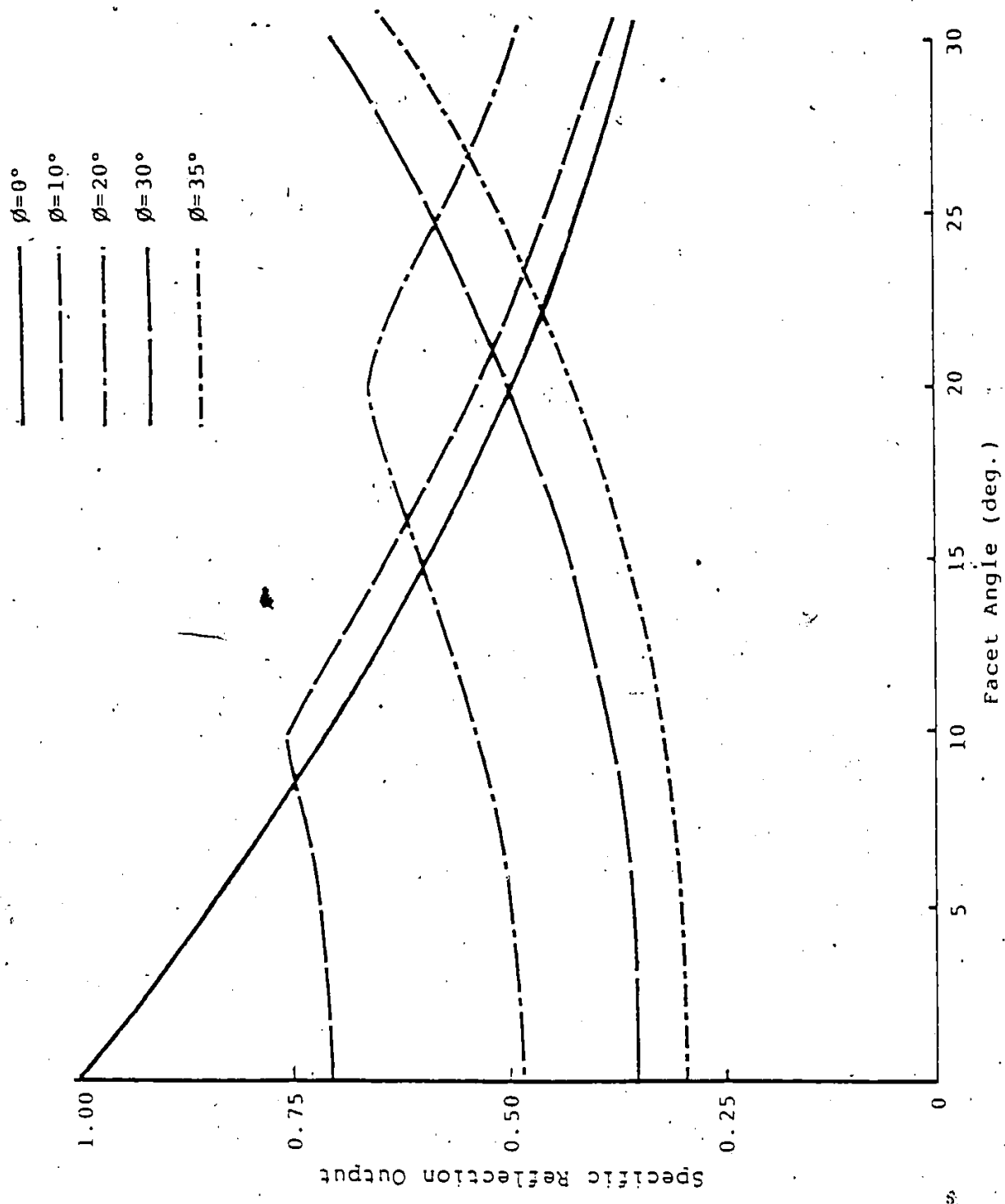


Figure 3.6: SPECIFIC REFLECTION OUTPUT ρ Vs. FACET ANGLE α AT

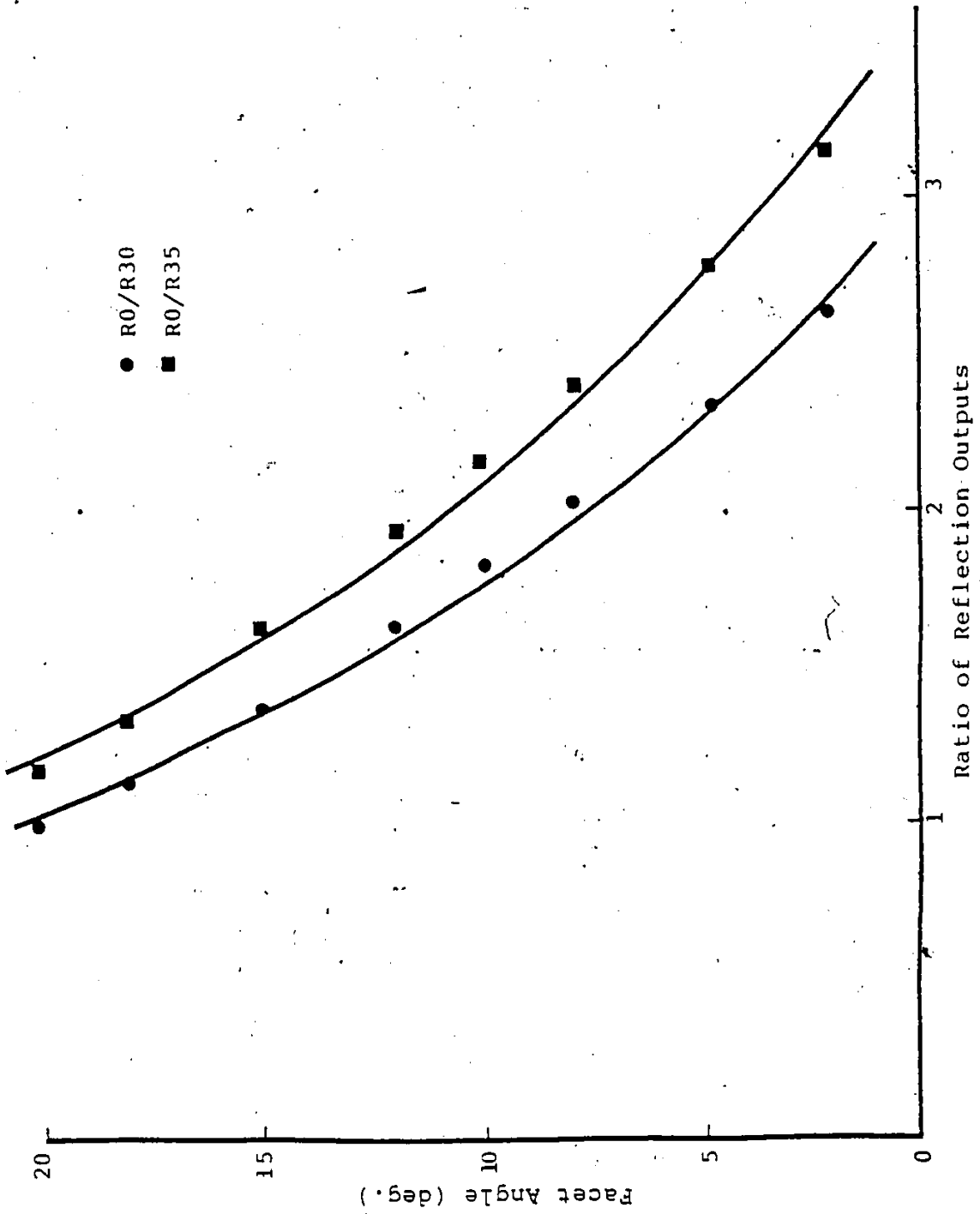


Figure 3.7: FACET ANGLE α Vs. RATIO OF REFLECTION OUTPUTS $R0/R\phi$

Chapter IV

EXPERIMENTAL APPARATUS & PROCEDURE

To verify the technical feasibility of the method suggested by the theoretical model, experiments were carried out to determine the relationship between surface roughness and fiber-optic output at various detecting angles. Five different transducers were used in these experiments to study the effect of transducer size and orientation of the fibers on this relationship.

4.1 THE APPARATUS

The experimental apparatus consists of the following main components:

- a) Light Source: A He-Ne laser is used as a light source. The use of a laser is desirable in this work as it provides an effective source of monochromatic and coherent light.

The laser used is a Spectra Physics model 120, Stablite Gas Laser[23] which provides a highly uniphase power output.

Specifications:

Output power: 5.0 mW at 25 μ in.
Operating temperature: 50-100 °F.

Long-term power drift: Less than 5%.
 Beam diameter: .025 in. at $1/e^2$ point.
 Beam divergence: 1.7 millirad. at $1/e^2$ point.
 Beam amplitude noise: Less than 3%.
 Cost: \$ 1500

b) Spatial filter: Spatial filtering of the laser beam eliminates any spatial noise and provides a clean fundamental laser mode. The spatial filter used is a Spectra Physics model 332 [24], which utilizes a precision pinhole to eliminate spatial noise producing a smooth Gaussian intensity profile.

Specifications:

Entrance beam dia. : Variable, 0.02-0.4 in.

Operating range: 18-26 μ in.

(Wavelength)

Exit beam dia. : Variable, depends on
input beam dia.

Aperture adjustments: Independent in X, Y and Z
axes

Cost: \$ 200

c) Photodetectors: The photodetectors are used to measure the reflected light intensity. These are United Detector Technology model PIN 10 DP detectors[25] which are optimized for an unbiased mode of operation.

Because of their high zero bias impedance, these detectors are ideally suited for coupling to an operational amplifier in the current mode, in which the DC light level changes of up to ten decades can be linearly detected and converted to an output voltage.

Specifications:

Active area:	0.155 in ² .
Incident light power:	Max. , 10 ⁻⁴ mW
Response time:	1 micro sec.
Responsivity:	0.35 A/W
Linearity:	D.C. light level changes of upto 10 decades.
Operating temperature:	32-160 °F
Cost:	\$ 100

Figures A.1 and A.2 (Appendix-A) show the linearity response curves of the two photodetectors used in the present work. The response curves were obtained by using a Photodyne model 66-XLA optical power meter with model 250 photodetectors.

d) Amplifier: The operational amplifier used is a high gain D.C. amplifier which is built using two Burr-Brown model 3622 Differential Input Instrument Amplifier [26] and a Burr-Brown model 4291 analog divider [27]. The amplifier can accept two input

voltages E_{ia} and E_{ib} to provide an output voltage E_{ca} , E_{cb} or a divided output in the ratio of $10 \cdot N/D$, where N and D are the numerator and denominator voltages respectively. Fig. 4.1 shows a schematic diagram of the amplifier.

Specifications (Amplifier) :

Gain:	1.01 to 1000
Nonlinearity (at $G=100$):	$\pm 0.1\%$, max.
Input voltage range:	± 8 Volts
Rated output:	± 10 Volts, ± 20 mA.
Input noise:	
10 Hz to 100 kHz	10 micro Volts, rms.
10 Hz to 10 kHz	2 micro Volts, rms.
Output noise:	
10 Hz to 10 kHz	100 micro Volts, rms.
Frequency response:	
for $\pm 1\%$ flatness, min.	100 kHz
for ± 3 dB flatness	2 MHz
Settling time:	5 micro sec.
(To within 0.01% of final value)	
Operating temperature:	32-160 °F
Cost:	\$ 75

Specifications (Analog Divider):

Rated input voltage N , $N \leq D$: ± 10 Volts.

Rated output voltage :	+10 Volts.
Accuracy, D>10mV :	0.1%.
Frequency response, D=10 V :	20 kHz.
Output noise, D>1 V :	500 microvolts.
Operating temperature :	32-160 °F
Cost :	\$ 50.

Figures B.1 to B.3 (Appendix-B) show the calibration curves for the amplifier model 3622 and the analog divider model 4291.

e) Signal Processor: This is an ORIEL model 7600, microprocessor based multifunctional signal processor[28], used to process the output signal from the photodetectors. The processor provides several functions but, only the 'running average' function is used in this experimental work.

The running average function provides an average value of a varying signal. The processor reads the input signal at about a 1 KHz rate. In the beginning, the average of the first 256 readings, which takes about 0.25 secs., is applied to the output system. Thereafter the average of every 256 readings is averaged with the previous output and then sent to the output system. The averaging process thus continues to provide an updated average signal at a rate of about four times per second. The output can be

conveniently read on a digital voltmeter or plotted on an X-Y plotter.

Specifications :

Analog input

impedance: 100 kOhms
 amplitude: 10 mV to 10 V

Analog output

impedance: 1000 Ohms
 amplitude: 0 to 10 V
 resolution: 10 mV

Digital resolution: A/D converter, 10 bits.
 D/A converter, 10 bits.
 Computation, 16 bits.

Frequency response: 100 Hz, max.

Sampling rate: 1 milli sec.
 (running avg. function)

Cost: \$ 1000

f) Fiber Optic Transducers: The following bifurcated fiber-optic transducers[29] from Dolan-Jenner Industries are used in the experiments.

EK3012, ET824, EC824, EC424 and ED824.

Each of these fiber-optics is made from high quality glass cladded flint glass fibers of 0.003 in. diameter. In EK3012 and ET824 the fibers from each leg are intermixed (randomized) to produce a uniform

dispersion within the entire cross-section of the common leg (Fig. 2.2a). In EC424 and EC824 the fibers from each leg are bound in two concentric circles (Fig. 2.2b) and in ED824 they are separated into two semicircles (Fig. 2.2c) at the common end.

These transducers are shown in Figure 4.2 and their specifications are given in Table 4.1.

g) Roughness Specimens: A surface roughness standard, manufactured by Rubert & Co. Ltd., England, having precision ground surfaces of 2.0, 4.0, 8.0, 16.0, 32.0 and 64.0 micro inches roughness along with several laboratory machined specimens of 7.86, 11.73, 15.08, 21.0, 26.5, 36.0, 43.2, 57.2 and 68.0 micro inches roughness were used in the experimental work.

The laboratory specimens were machined using different grades of grinding wheels and feed rates to produce various roughness. The surface roughness, measured by a Mitutoyo Surf-test III profilometer[30], is an average of six readings taken over the entire surface. These readings are tabulated in Table C.1 in Appendix-C.

In addition to these equipments, a Philips model no. 42423 digital voltmeter to read the photodetector output, a linear variable differential transducer (LVDT) to obtain signals corresponding to the position of the fiber-optic transducer with respect to the specimen, and a Hewlett Packard model no. 7001A X-Y plotter to plot the photodetector output signal were also used.

4.2 EXPERIMENTAL PROCEDURE

The experimental setup to determine the transducer response characteristic and to measure the transducer output for different surfaces at various detecting angles, is shown in Fig. 4.3. The schematic of the setup is shown in Fig. 4.4. The object surface was oriented in such a way so that its machining lay was always along Y-direction and the transducer is located in a plane which is perpendicular to both the surface and the direction of machining marks on it (X-Z plane). The transducer can be inclined in this plane at a desired angle ϕ from the surface normal (Fig. 4.5). The fixture itself was attached to a carriage to facilitate the positioning of the transducer with respect to the surface in either X or Z direction.

The light from the He-Ne laser was carried by half of the transducer fibers to be incident on the object surface. The reflected light from the surface was collected by the other half of the fibers and was measured by the photodetector whose output, through the operational amplifier, was displayed on a digital voltmeter.

4.2.1 Response Characteristic

The fixture was adjusted to make the transducer perpendicular ($\phi=0^\circ$) to a surface of the roughness standard specimen which was placed on a good flat support.

The transducer distance from the surface was varied and for each displacement the transducer output was recorded. The procedure was repeated for each of the five transducers.

For one of the transducers (EC824) three response curves were plotted using surfaces of different roughness values to ensure that the peak output always occurs at the same distance from the surface.

4.2.2 Transducer Output Vs. Surface Roughness

The transducer distance from the object surface was so adjusted as to obtain its peak output. The transducer was first kept perpendicular to the surface ($\phi=0^\circ$) and its output was recorded for each of the six surfaces of the roughness standard specimen. The procedure was repeated for each of the five transducers. Similarly, the output from each transducer was recorded for each surface at various other detecting angles as well.

4.2.3 Ratio of Transducer Outputs Vs. Surface Roughness

From the results of the previous experiments it was observed that either of the output ratios V_0/V_{30} or V_0/V_{35} ² can be correlated with surface roughness and the transducer with concentric fiber orientation is the most suitable one for the purpose. These results are discussed in detail in the next chapter. This investigation for directly measuring the

² V_0 , V_{30} and V_{35} are transducer outputs at $\phi=0^\circ$, 30° and 35° respectively.

output ratio was, therefore, limited only to concentric transducers EC424 and EC824.

The general experimental setup and the schematic diagram are shown in Figs. 4.6 and 4.7 respectively. A pair of similar transducers were mounted in a fixture such that both the transducers were located in X-Z plane (Fig. 4.5). One of the transducer was kept perpendicular to the surface while the other was inclined at an angle of 30° from the surface normal (Fig. 4.8). The distance of the transducers from the surface was adjusted to obtain their peak outputs. Also, the two transducers were so arranged that the incident illuminations on the surface did not interfere with each other.

The light from the laser, divided approximately in half by a beam splitter, was carried to the surface, by the transmitting fibers of the two transducers. The reflected light collected by the receiving fibers was measured by two photodetectors whose outputs were sent to two input channels of the operational amplifier to provide a divided output in the ratio of V_0/V_{30} . The output was recorded for each surface of roughness standard as well as for all the laboratory machined specimens. This output for the laboratory machined specimen, was an average of 10 measurements taken over the entire specimen surface. The procedure was repeated for the other set of transducers as well. Next, by setting the transducer inclination angle to

35, the output ratio V_0/V_{35} was similarly recorded for all the surfaces.

As is mentioned, in the previous experiment the output ratios V_0/V_{30} or V_0/V_{35} were taken as an average of 10 values measured over the specimen surface. This procedure is rather cumbersome from a practical viewpoint. Therefore, in another experiment, the specimen surface was scanned by moving the transducers at a speed of about 1 in./sec. The resulting output signal was processed by the running average function of the signal processor and was plotted on a X-Y plotter.

To test the repeatability of this procedure, the average output ratio V_0/V_{35} was obtained from a scan of the specimen surface once every day, over a period of eight days. The ratio V_0/V_{35} was measured for several specimen surfaces using both the transducers EC424 and EC624. Everyday, after the measurement for each specimen was taken, the amplifier and the signal processor were switched off while the rest of the experimental set up was left undisturbed.

To determine the transducer sensitivity with respect to the part location, the output ratio V_0/V_{35} was also measured by rotating the specimen surface along any of three axes independently, in increments of 2° , up to 8° .

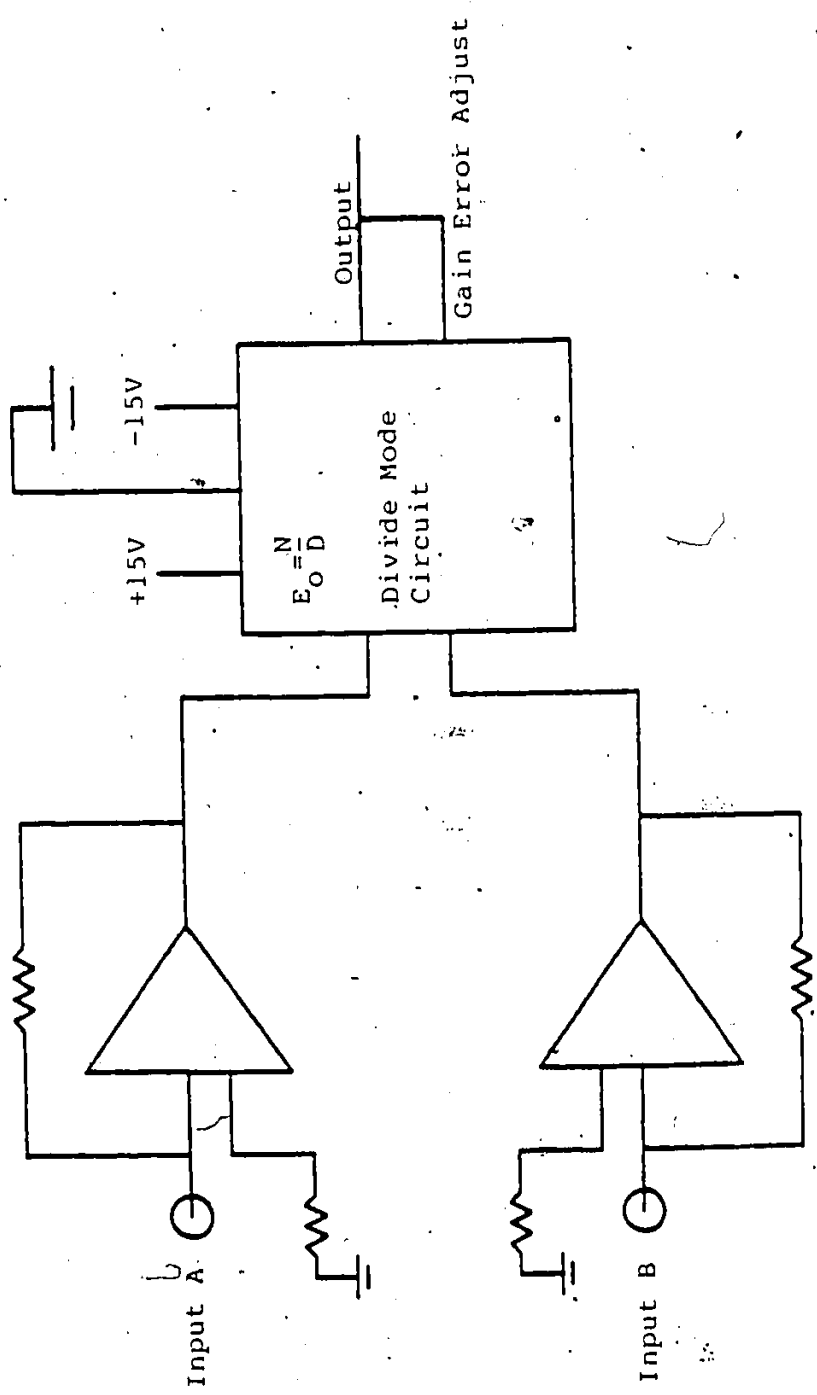


Figure 4.1: SCHEMATIC OF THE OPERATIONAL AMPLIFIER

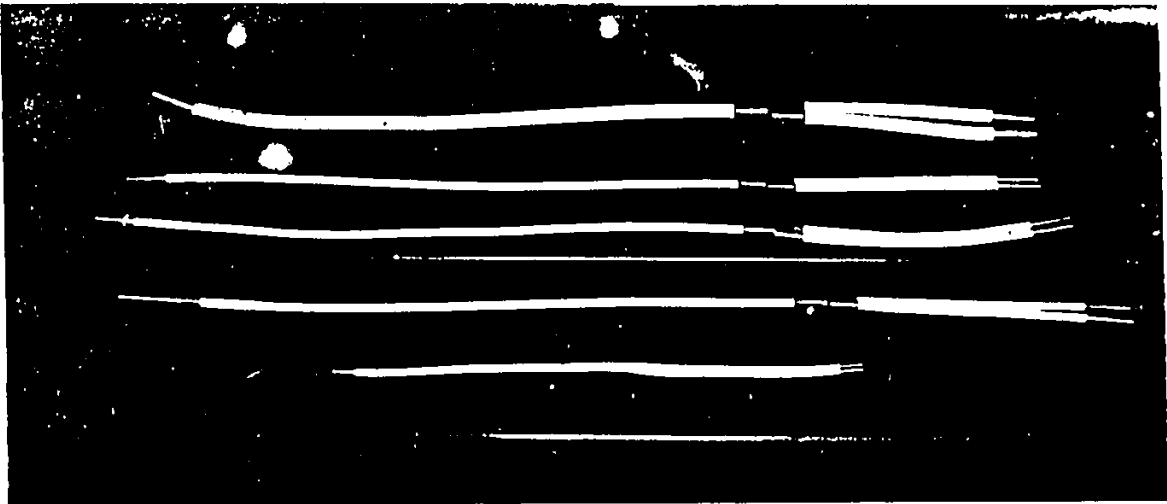


Figure 4.2: FIBER-OPTIC TRANSDUCERS

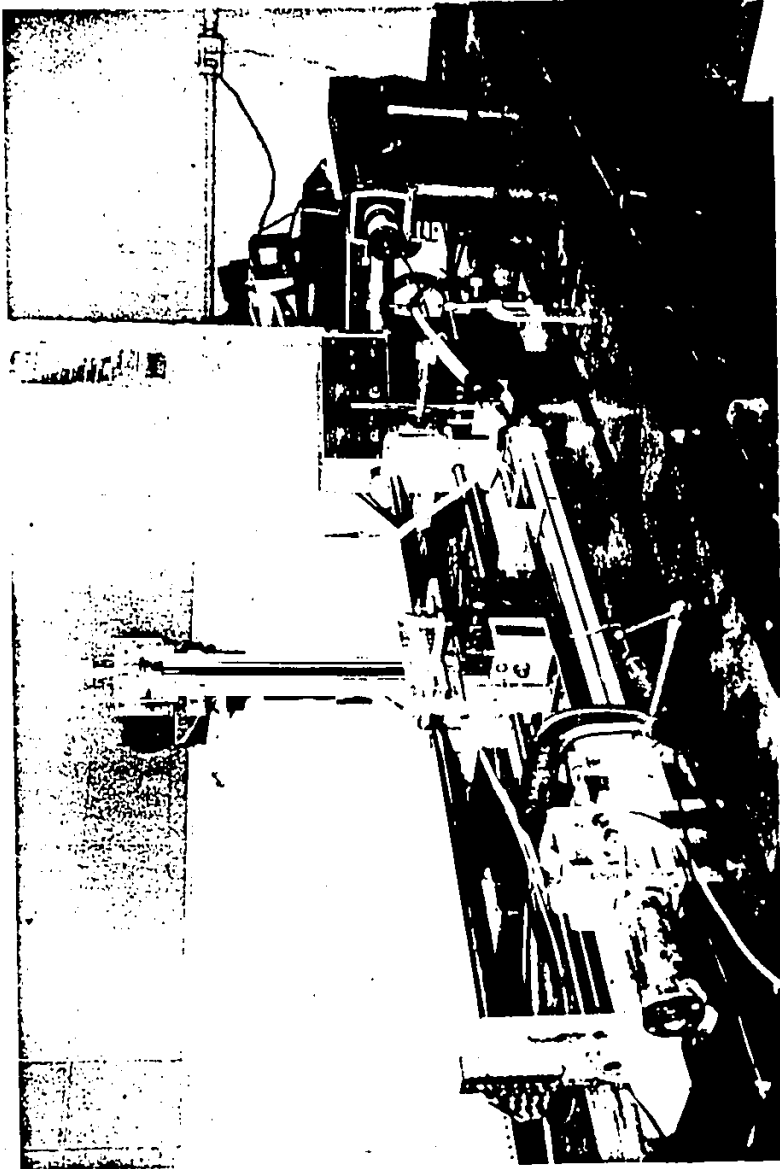


Figure 4.3: PICTORIAL DISPLAY OF THE INITIAL EXPERIMENTAL SETUP

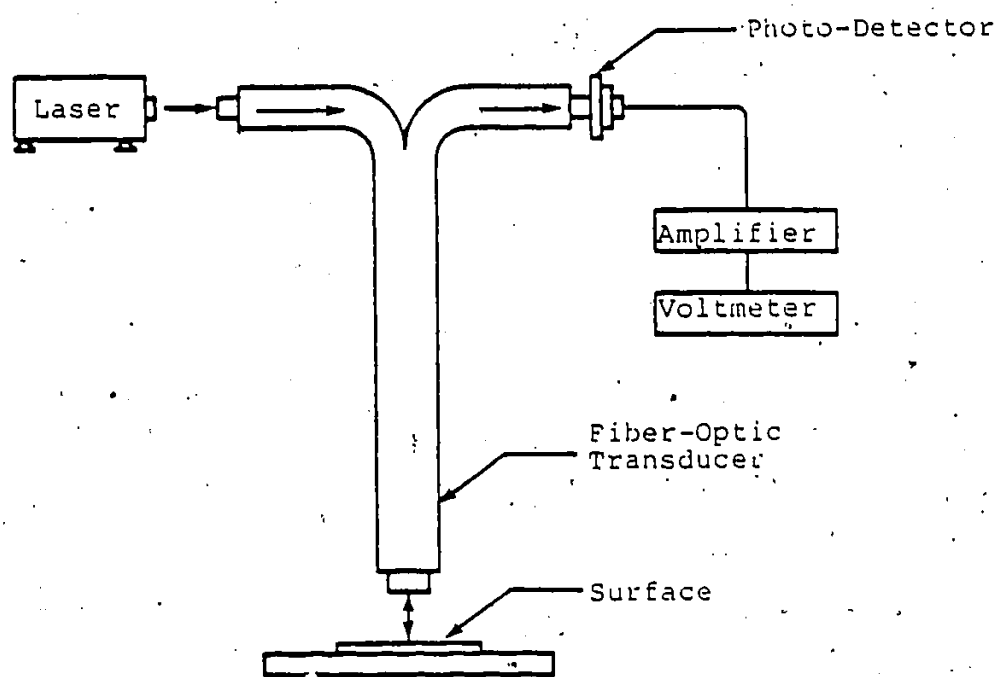


Figure 4.4: SCHEMATIC OF THE INITIAL SETUP

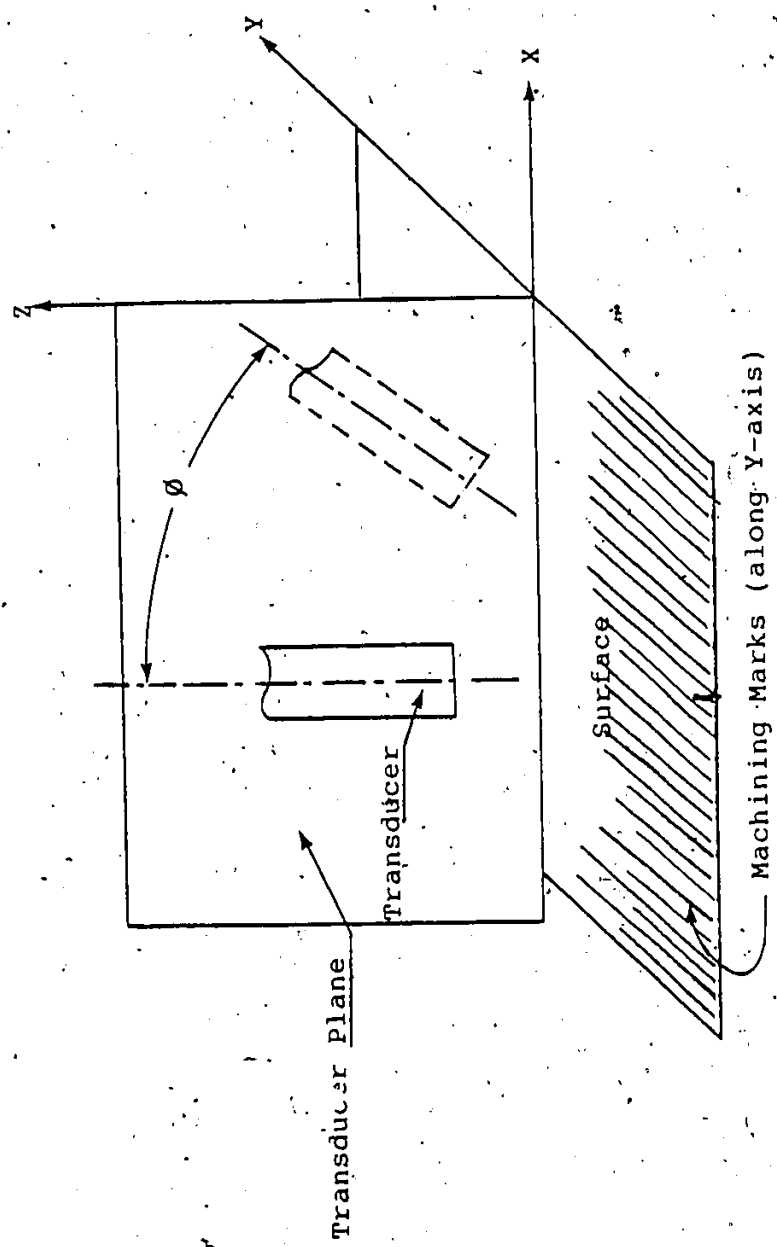


Figure 4.5: POSSIBLE POSITIONS OF THE FIBER-OPTIC TRANSDUCER RELATIVE TO THE WORK SURFACE

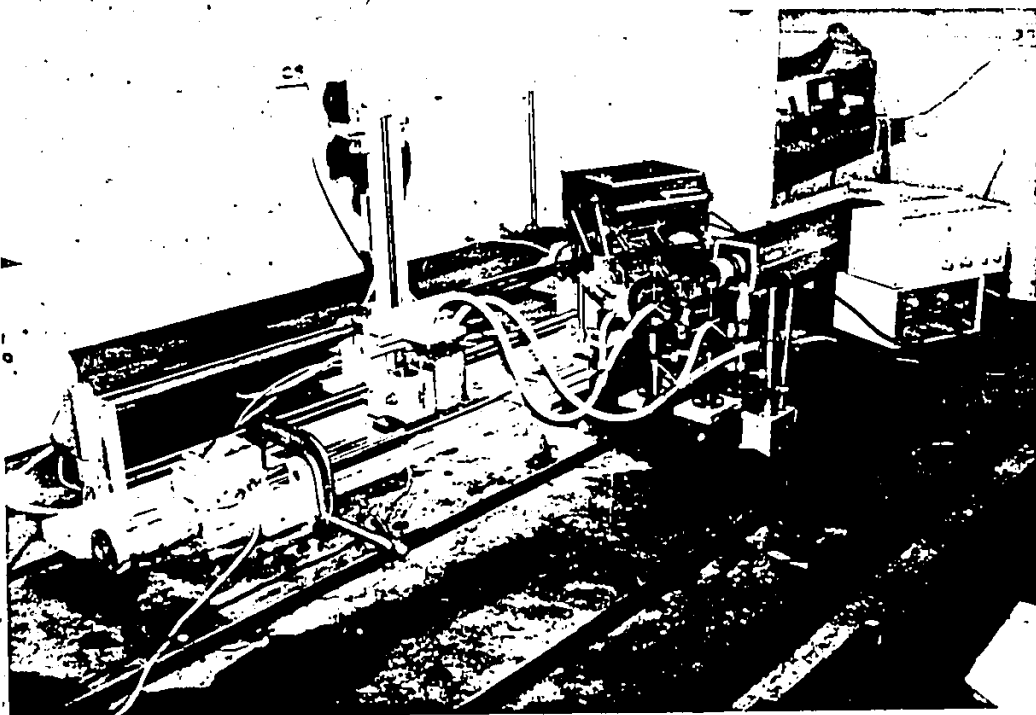


Figure 4.6: PICTORIAL DISPLAY OF THE FINAL EXPERIMENTAL
SETUP

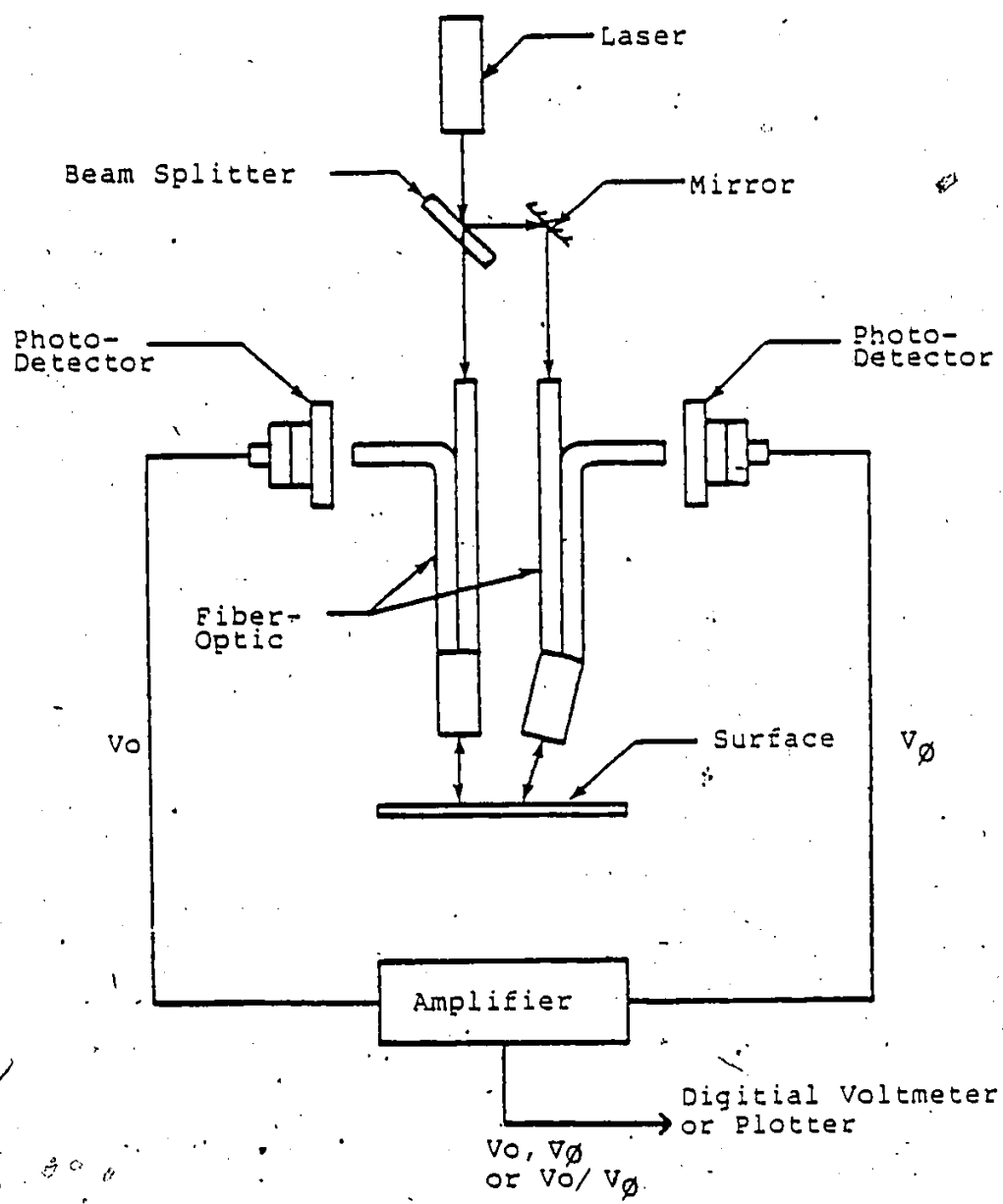


Figure 4.7: SCHEMATIC OF THE FINAL SETUP

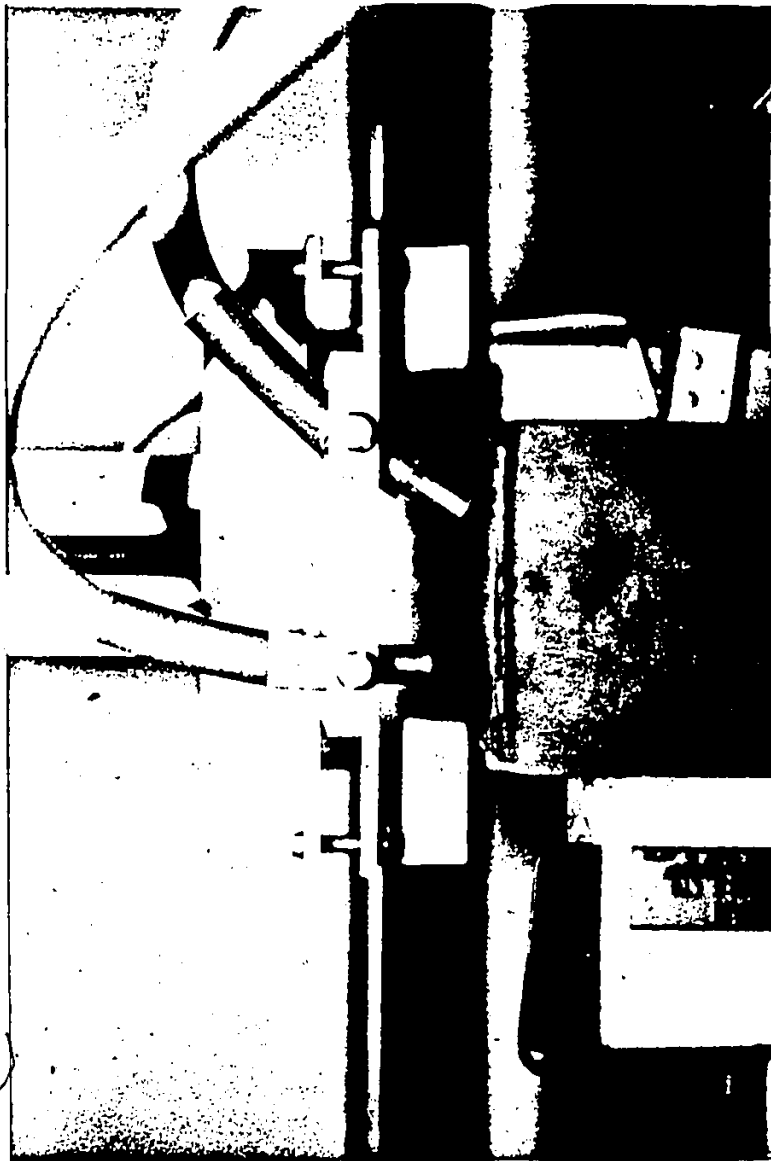
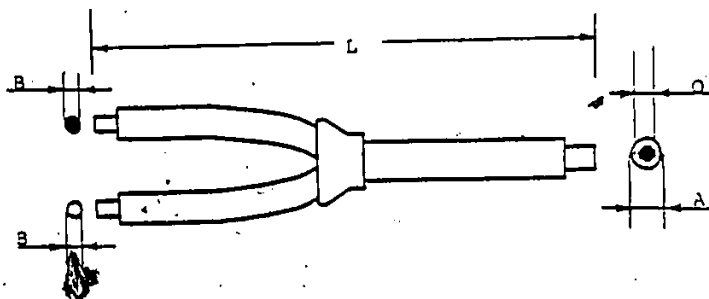


Figure 4.8: PICTORIAL DISPLAY OF TRANSDUCERS POSITION
RELATIVE TO THE SURFACE

TABLE 4.1

Specifications of the Fiber-Optic Transducers

Transducer Type	A (in.)	B (in.)	O (in.)	L (in.)	No. of Fibers in Each Leg	Fiber Orientation	Cost (\$)
EK3012	0.118	0.085	-	12	1650	RANDOM	40
ET824	0.125	0.089	-	24	1700	RANDOM	65
ED824	0.125	0.089	-	24	1700	DIVIDED	130
EC824	0.125	0.089	0.089	24	1700	COAXIAL	135
EC424	0.250	0.177	0.177	24	7000	COAXIAL	175



Chapter V

RESULTS AND DISCUSSION

5.1. INDIVIDUAL RESPONSE CURVES

Figure 5.1 shows the three response curves, as obtained by using surfaces of different roughness values, for transducer EC824. These curves are plotted for a case where the fibers in the outer circle are used as transmitting fibers while those in the inner circle act as receiving fibers.³ The ordinate in the figure represents the transducer output while the abscissa represents the transducer distance from the object surface. It can be observed from these curves that the peak transducer output always occurs and remains constant for the same distance from the surface, in all the three curves.

If the ordinate is changed to a non-dimensional parameter as percentage of maximum output, the three curves get converted to a single general response curve (Fig. 5.2), thereby showing that the response characteristic of a fiber-optic transducer remains the same regardless of the work surface roughness.

³ The shaded area in the concentric circles indicates the transmitting fibers, in the figures 5.1 to 5.8.

Similarly Figures 5.3 & 5.4 illustrate the response curves of the other transducers. It is quite evident from these curves that the response characteristics depend both on the transducer size as well as the orientation of the fibers in it. The stand-off and the working range for various transducers are shown in Table 5.1. It can be observed from this table, that:

1. The transducer stand-off distance increases with the increase in transducer size, for the same fiber orientation.
2. Among the same size, the transducer with concentric fiber orientation has the largest stand-off as well as the working range.
3. The concentric transducer reaches its peak output at about the same distance using either of the outer or the inner fibers as the transmitting or the receiving fibers. However, this transducer has a longer working range while using the inner and outer fibers as the transmitting and receiving fibers respectively.

As was noted in Chapter III, a transducer with the largest working range and the greatest stand-off will be the most desirable one for the purpose of roughness measurement. It is apparent from these results that EC824 and EC424, with a stand-off distance of 0.15 and 0.25 inches respectively, are the most suitable among all the transducers.

5.2 EFFECT OF ROUGHNESS AND DETECTION ANGLE ON TRANSDUCER OUTPUT

Figures 5.5 to 5.8 show the plots for the fiber-optic transducer output versus stylus calibrated surface roughness at three detecting angles of 0, 30 and 35 degrees. The ordinate in these figures represents the transducer output while the abscissa represents the stylus calibrated surface roughness. The plots for transducer EK3012 could not be obtained because of the physical limitation caused by its extremely short working distance. For the other transducers, measurements were also taken at several detecting angles between 0 and 30 degrees. However, the output pattern at these angles was not found to be continuously decreasing or increasing in nature. These results, therefore, were unsuitable to be used for roughness measurement and hence discarded. Also, for detecting angles beyond 35°, measurements could not be taken because of physical limitations of the transducer dimensions.

It can be observed from these figures that the output characteristic for each transducer is very similar in nature. The transducer output decreases at 0° while increases monotonously at 30 & 35 degrees, in each case. This trend is similar to that predicted by the theoretical derivations in Chapter III.

Another important point to be noted from these curves is, that the output levels for the three transducers of the same size (ET824, ED824 and EC824) are almost equal. It

seems to indicate that the transducer output level depends only on its size and not on fiber orientation.

The output level for EC424 is lower than the output levels of any other transducer at all three detecting angles. This is rather peculiar because a larger transducer is expected to provide higher outputs. However, since the output is lower at each detecting angle, it was most likely caused because of a drop in the laser power, which is normally a result of fluctuating line voltage, thermal distortion in the gas tube, etc.

For concentric transducers, as seen in figures 5.7 & 5.8, no appreciable difference occurs in output levels by using either inner or outer fibers as receivers.

From these curves, the ratio of transducer output at two detecting angles namely V_0/V_{30} and V_0/V_{35} are plotted, versus surface roughness. These plots are presented in Figures 5.9 & 5.10. The ordinates V_0/V_{30} and V_0/V_{35} represent the normalized output ratio while the abscissa represents the stylus calibrated surface roughness.

These figures further illustrate that the output ratio V_0/V_{30} , as well as V_0/V_{35} , is almost the same for each transducer of the same size but of different fiber orientation. The coaxial transducer EC424 provides maximum output ratio, showing that the ratio increases with the increase in transducer size. It could, therefore, be concluded from these results that the output level of a

fiber-optic transducer depends essentially upon its size and is rather independent of the fiber orientation.

As has been discussed earlier, the working distance of a transducer not only depends upon its size but also on the fiber orientation. The coaxial fiber-optic transducer because of its maximum stand-off distance would, therefore, be an obvious choice for the purpose of surface roughness measurement.

The surface roughness has a varied influence on the output ratio V_0/V_{30} or V_0/V_{35} . The ratio decreases rapidly as the roughness increases from 2 micro inches to 16 micro inches. But for any increase in the roughness beyond this point it decreases at a much slower rate. The influence of the roughness above 32 micro inches reduces significantly and the curves tend to become asymptotic beyond this point. However, there appears to be a definite correlation between the ratio of the outputs at two detecting angles and the surface roughness. It is also apparent from these figures that the ratio V_0/V_{35} will be a more sensitive discriminator than V_0/V_{30} , for the measurement of surface roughness.

5.3 NORMALIZED FIBER-OPTIC ROUGHNESS MEASUREMENT

Figures 5.11 to 5.14 show the plots between surface roughness and the output ratios V_0/V_{30} and V_0/V_{35} for transducers EC824 and EC424. The ratio is obtained by electrically dividing the outputs from the two similar

transducers set at different angles. Figures 5.11 & 5.13 are essentially the same as figures 5.12 & 5.14 respectively, except that logarithmic scales are used in the latter case. The ordinate in these figures represents the stylus calibrated surface roughness R_a , while the abscissa indicates the output ratio V_0/V_{30} or V_0/V_{35} . [This fiber-optic output ratio for the laboratory machined specimens is an average of ten values measured over the entire surface. These values are tabulated in Tables C.2 to C.5 in Appendix C.]

The equations of correlation between surface roughness and the output ratio were obtained for both transducers using the statistical method of linear regression. These correlation equations along with the standard error of estimate and coefficient of correlation are presented in Table 5.2.

The standard error of estimate is a measure of dispersion of actual data points about the fitted line while the coefficient of correlation determines the degree of relationship between the variables. The high value of coefficient of correlation in each case indicates a confidence level of better than 99% for the present regression analysis. This, in other words, means that the probability of drawing a wrong conclusion about the correlation is less than 1% [32].

It is further observed from the results of this analysis that:

1. The average surface roughness is correlated with either of the output ratios V_0/V_{30} or V_0/V_{35} by a general equation of the form;

$$Ra = A.X^{-B} \quad \text{-----(5.1)}$$

Where, X is the fiber-optic output ratio, and;

A and B are constants.

It is obvious from equation 5.1 and also evident from figures 5.12 & 5.14 and Table 5.2 that the roughness and output ratio have a strong log-log linear relationship.

2. For both the coaxial, fiber-optic transducers, the change in V_0/V_{35} is greater than the change in V_0/V_{30} for a corresponding change in the surface roughness value. Also, the equation of correlation between average roughness Ra and V_0/V_{35} is a better fit than the equation between Ra and V_0/V_{30} as indicated by the standard error of estimate and the coefficient of correlation (Table 5.2).

These results, therefore, indicate that the output ratio V_0/V_{35} is a more sensitive and accurate parameter for estimating the surface roughness.

3. The correlation equation between roughness and output ratio V_0/V_{35} is a better fit for transducer EC824 than for EC424. However, a similar change in the

surface roughness value causes a greater change in V_0/V_{35} for the transducer EC424 than EC824. This seems to indicate that a small coaxial transducer, though less sensitive, will provide a more accurate estimate of the surface roughness.

5.4 MEAN SURFACE ROUGHNESS BY A SCAN OF THE SURFACE

Figures 5.15 & 5.16 show the continuous plots of the output ratio V_0/V_{35} , for each laboratory machined specimen as obtained by scanning the specimen surface and processing the resulting signal through the signal processor, using transducers EC824 and EC424 respectively. The ordinate, in these plots, represents the output ratio V_0/V_{35} while the abscissa represents the length for which the specimen surface is scanned. The number over each plot indicates the average value of V_0/V_{35} . The surface roughness for each specimen, estimated from this average value of V_0/V_{35} , using the corresponding equations of correlation for the two transducers, is shown in Tables 5.3 & 5.4. A comparison between the roughness estimated from this optical method and the roughness obtained from stylus measurements indicates that the two values are within $\pm 5\%$ of each other, up to a roughness of about 40 micro inches, for both the optical transducers. It is also evident from these tables that the transducer EC824 gives the best roughness measurements.

It is postulated that a small coaxial transducer provides a more accurate measurement of surface roughness because it averages the reflected light output from a smaller illuminated surface area.

On one hand it is preferable to use a small coaxial fiber-optic transducer for an accurate measurement, but, on the other hand a large coaxial transducer because of its longer working distance, higher output and better resolution. It is, therefore, necessary to compromise in choosing a proper transducer. A more comprehensive study is further required to determine the optimum size of the transducer for the purpose of roughness measurement.

The plots in figures 5.15 & 5.16 were obtained by scanning the object surface at a rate of about 1 inch/sec. The speed at which the surface can be scanned, ultimately determines the time required to make a measurement by this method. Since the transducers are not in contact with the surface, the scanning speed essentially depends upon the dynamic response characteristics of the photodetectors, the amplifier, the analog divider and the signal processor used. For the present case the output signal from the fiber-optic transducers can be processed at a rate of about 1000 readings per second, as determined by the signal processor. The limiting scan speed would then be determined by the number of readings required in a given length. For example if the specifications were to require reading every 0.03"

then the maximum scan rate would be 30 inch/sec.⁴

For the same specifications, a stylus instrument typically scans a one inch length in 12 seconds.

5.5 STABILITY AND REPEATABILITY OF MEASUREMENT

Figures 5.17 & 5.18 show the variations in the fiber-optic output as measured over a period of eight days. The values of V_0/V_{35} shown are the average values obtained by scanning the specimen surface. The measurements were started about 30 minutes after the amplifier and the signal processor were turned on every day.

It can be observed from figures 5.17 & 5.18 that the maximum difference in the measured value of V_0/V_{35} is less than 1.8% for either of the transducers, which could cause a variation of about 5% in the roughness value estimated by this optical method. A variation of 10% in the roughness measurements by a stylus instrument is quite common. It is apparent, therefore, that the measurement of surface roughness by this optical method is stable with the time and repeatable within acceptable limits.

⁴ Maximum scan rate= 1000 readings/sec * 0.03
inch/reading=30 inch/sec.

5.6 EFFECT OF SURFACE POSITIONING ERRORS

Figures 5.19 to 5.22 show the effect of surface orientation on the output ratio V_0/V_{35} . These curves were obtained by rotating the calibrated surface about the three axes independently. It should be noted that the direction of lay on the surface is along Y-direction and the transducers are placed in X-Z plane such that one is normal to the surface while the other is inclined from the normal at 35 degrees ($\phi=35^\circ$) as shown in fig. 4.8.

It is apparent that transducer output is most sensitive to the surface rotation in the positive direction about the Y-axis, as indicated by fig. 5.21. Rotating the surface about the other axes has a varied effect on the output ratio. However, a small rotation of 2° about any of the three axes seems permissible without causing any appreciable variation in the output ratio V_0/V_{35} . The effect of transducer distance from the surface was previously demonstrated in figures 5.1 to 5.4 where it was shown that the permissible variation in the working distance is approximately 0.10" for EC424. It is, however, evident that proper surface orientation, particularly about the Y-axis, is most important for an accurate measurement of the ratio of the transducer outputs and consequently the surface roughness.

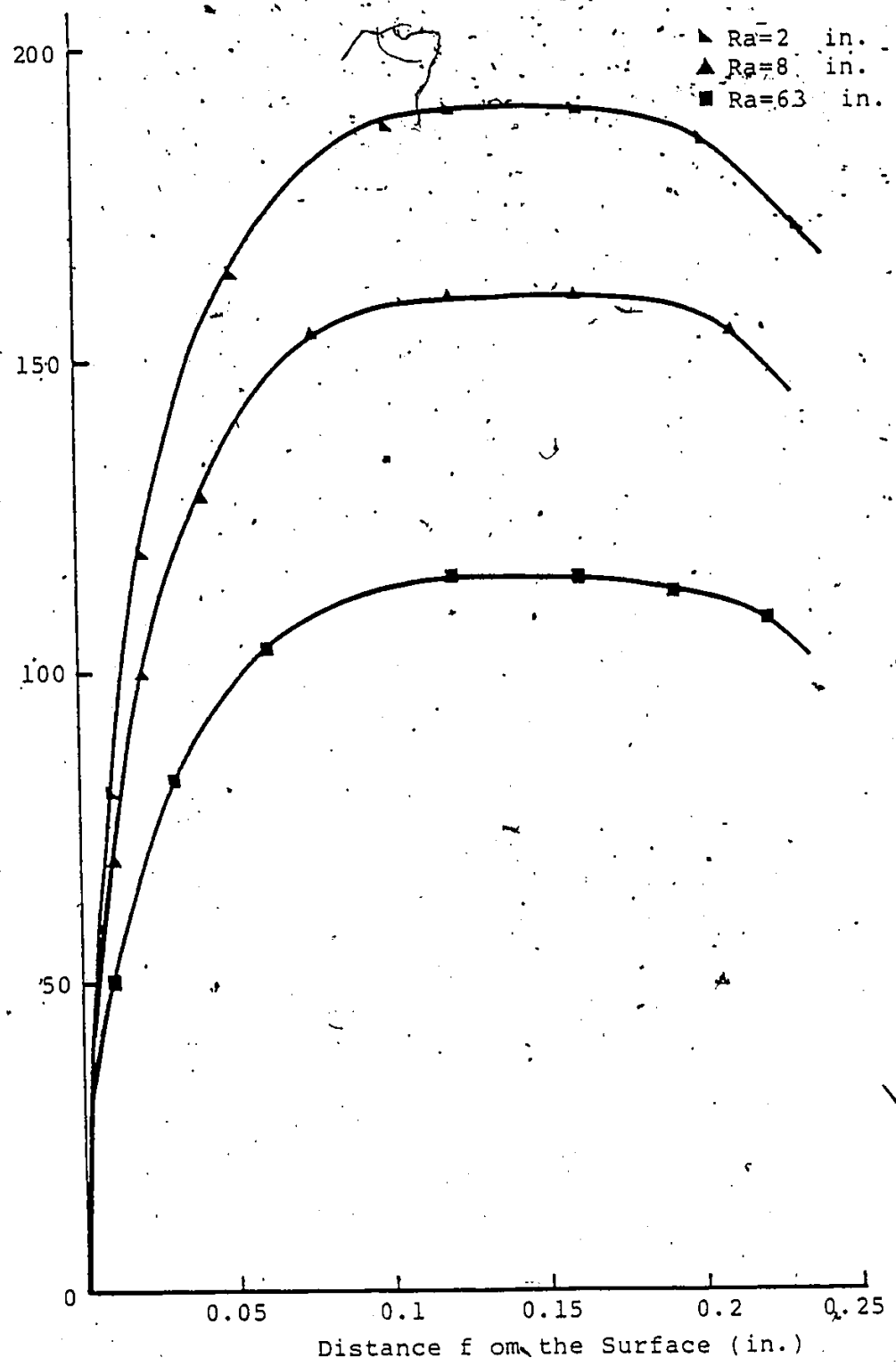


Figure 5.1: EFFECT OF SURFACE ROUGHNESS ON TRANSDUCER RESPONSE CHARACTERISTIC

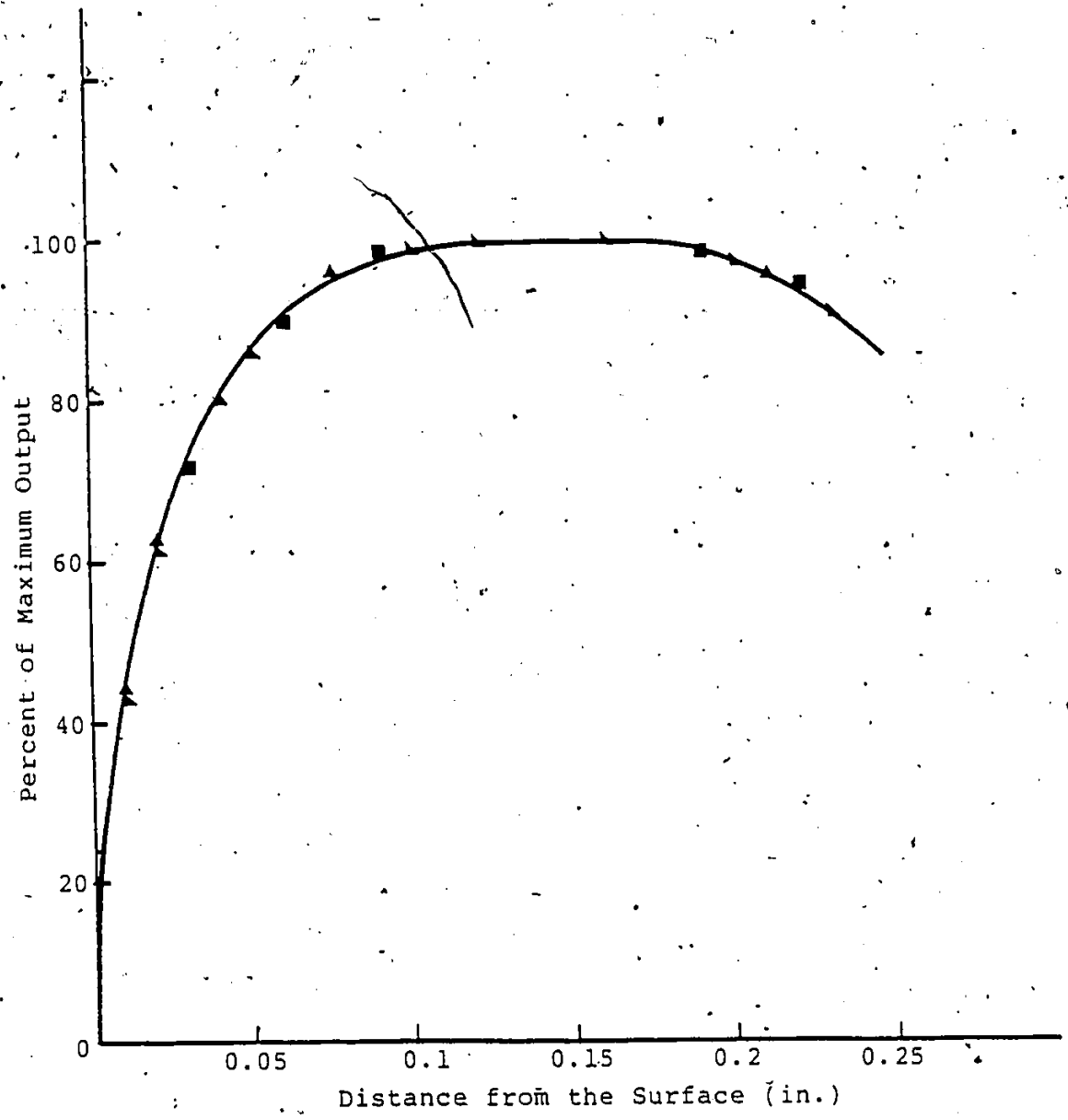


Figure 5.2: RESPONSE CHARACTERISTIC CURVE FOR EC8-24

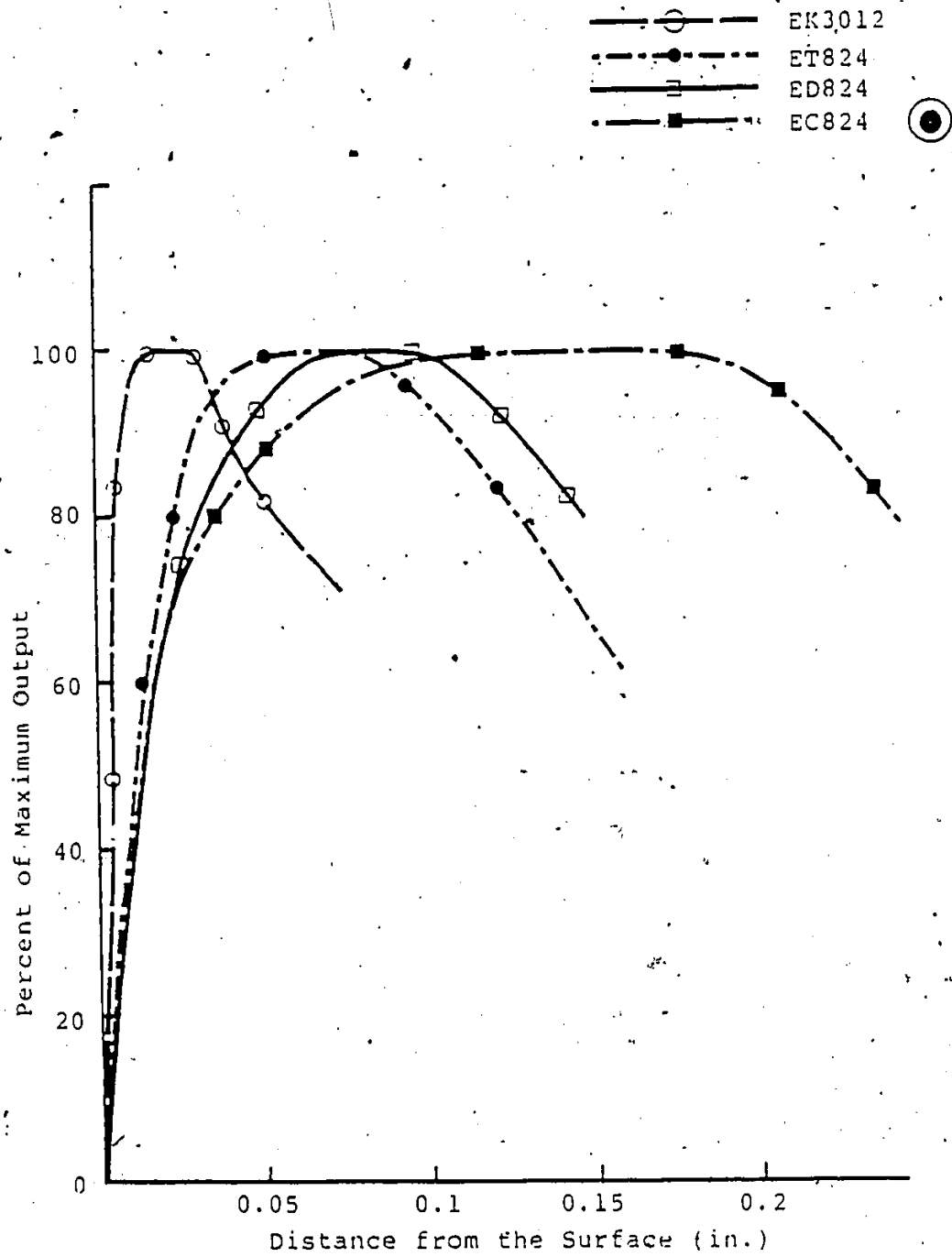


Figure 5.3: RESPONSE CHARACTERISTIC CURVE FOR EK3012, ET824, ED824 & EC824

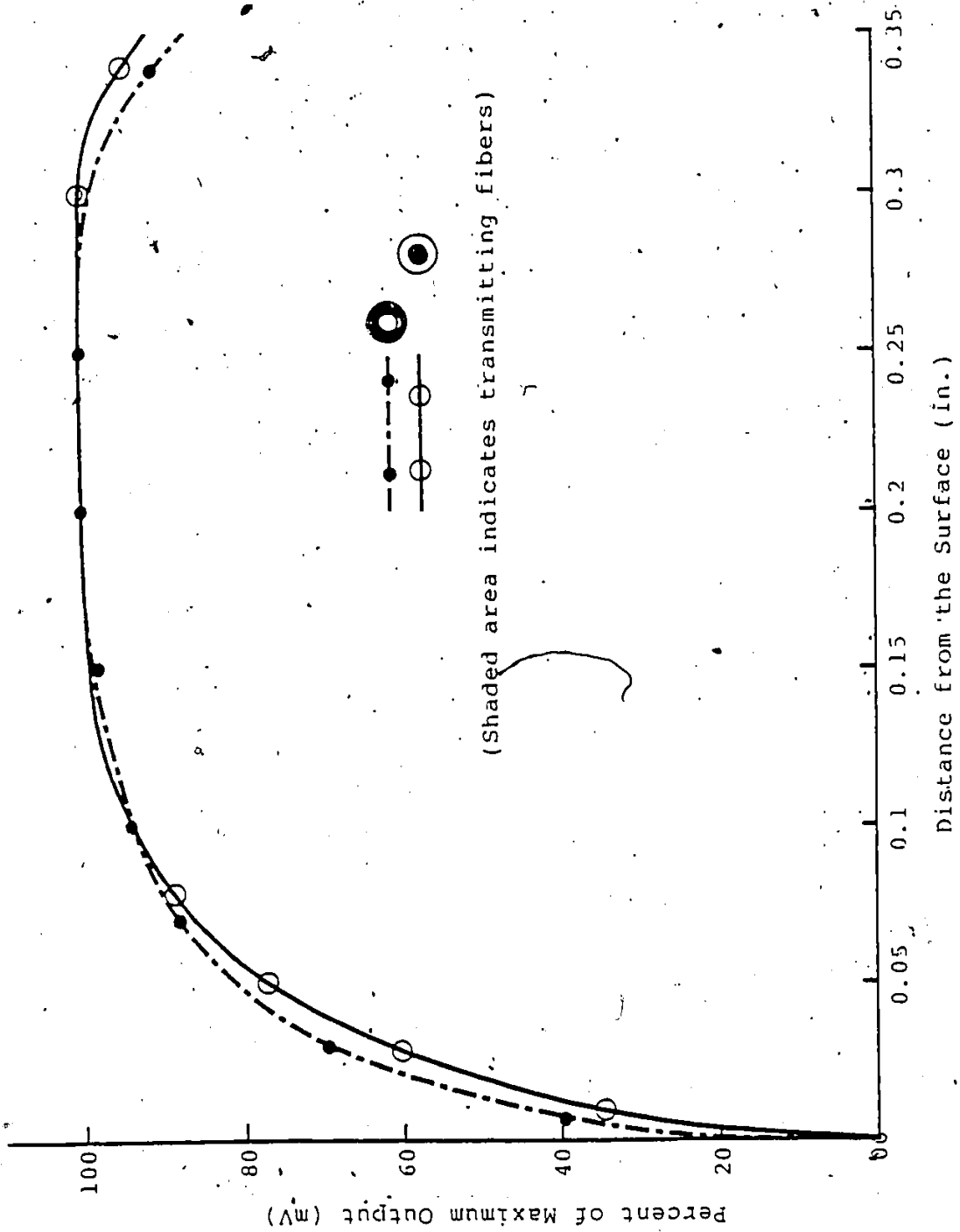


Figure 5.4: RESPONSE CHARACTERISTIC CURVES FOR EC424.

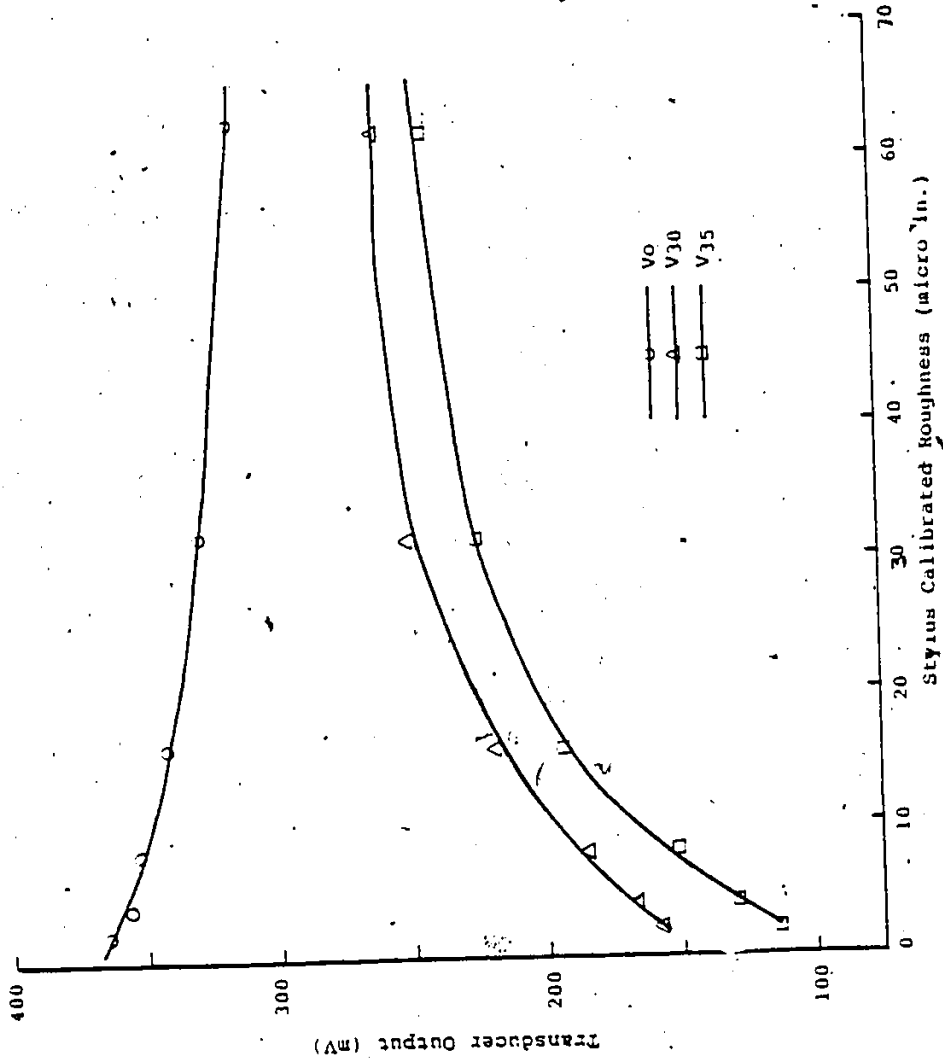


Figure 5.5: TRANSDUCER (ET824) OUTPUT VS. ROUGHNESS FOR DIFFERENT DETECTING ANGLES

9

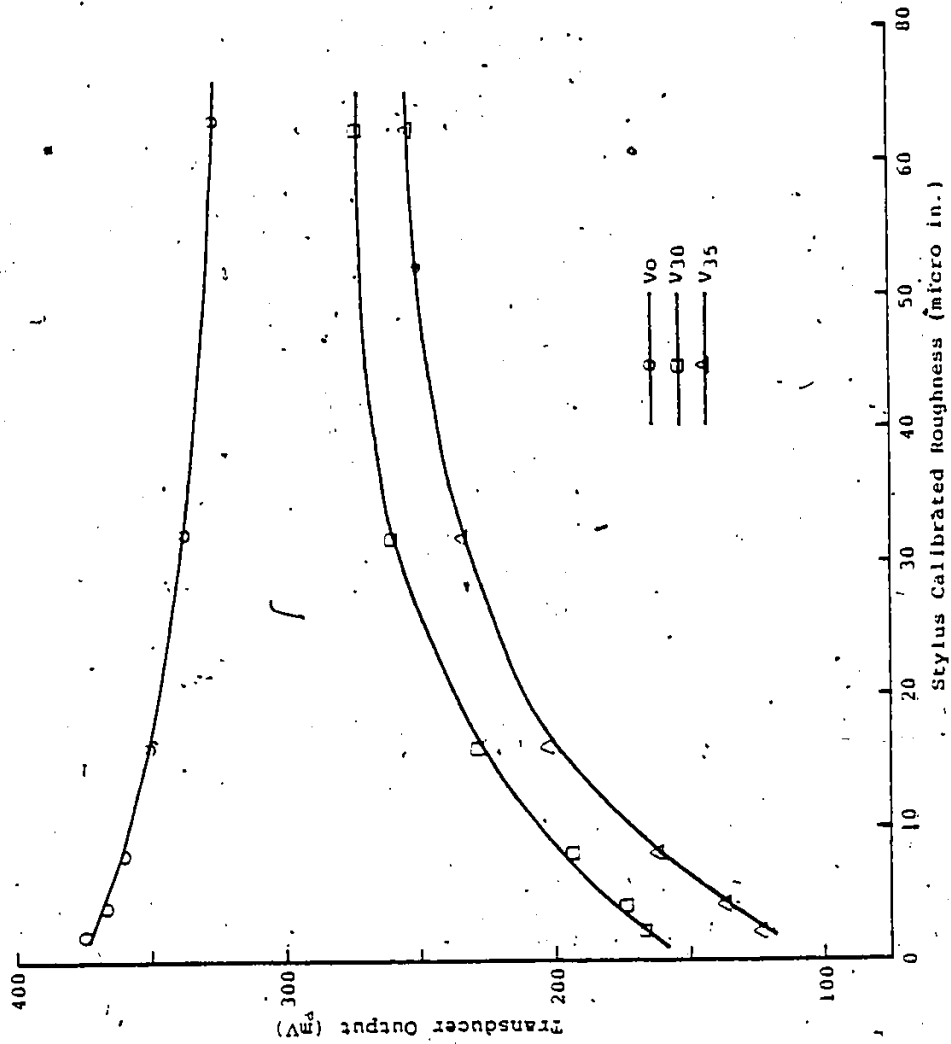
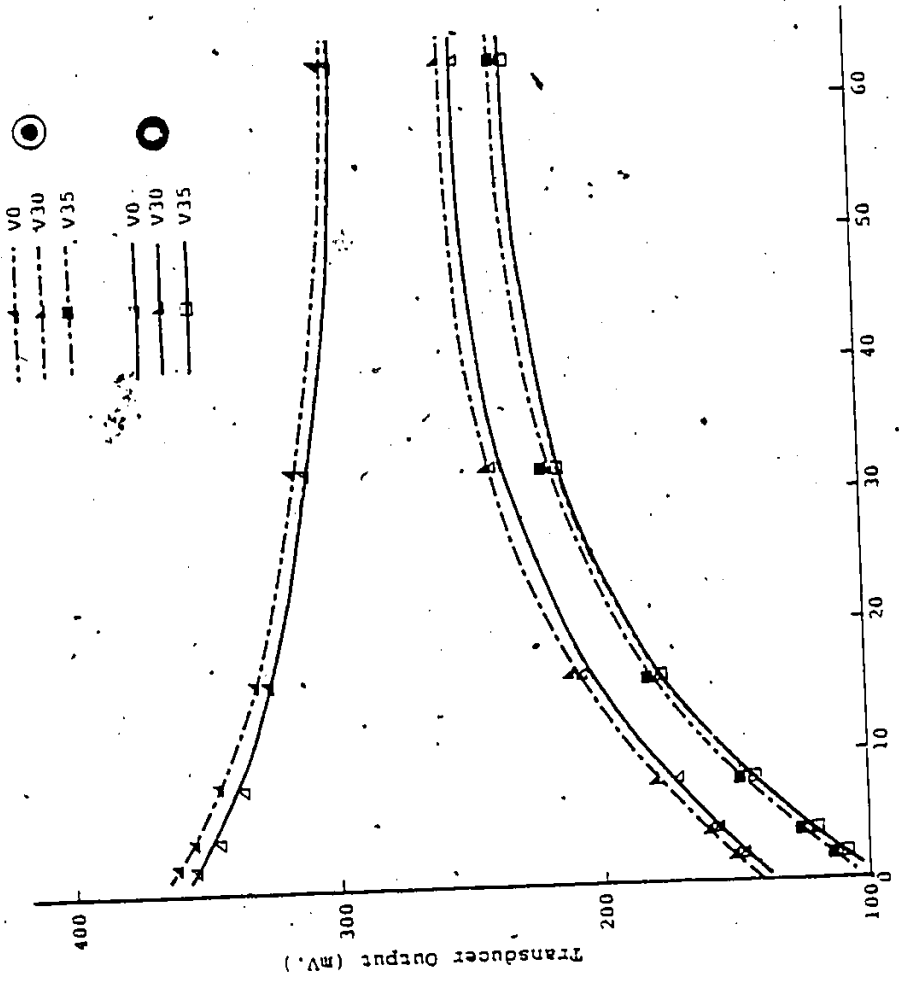


Figure 5.6: TRANSDUCER(ED824) OUTPUT VS. ROUGHNESS FOR DIFFERENT DETECTING ANGLES



Stylus-Calibrated Roughness (micro in.)
 TRANSDUCER (EC824) OUTPUT VS. ROUGHNESS FOR
 DIFFERENT DETECTING ANGLES

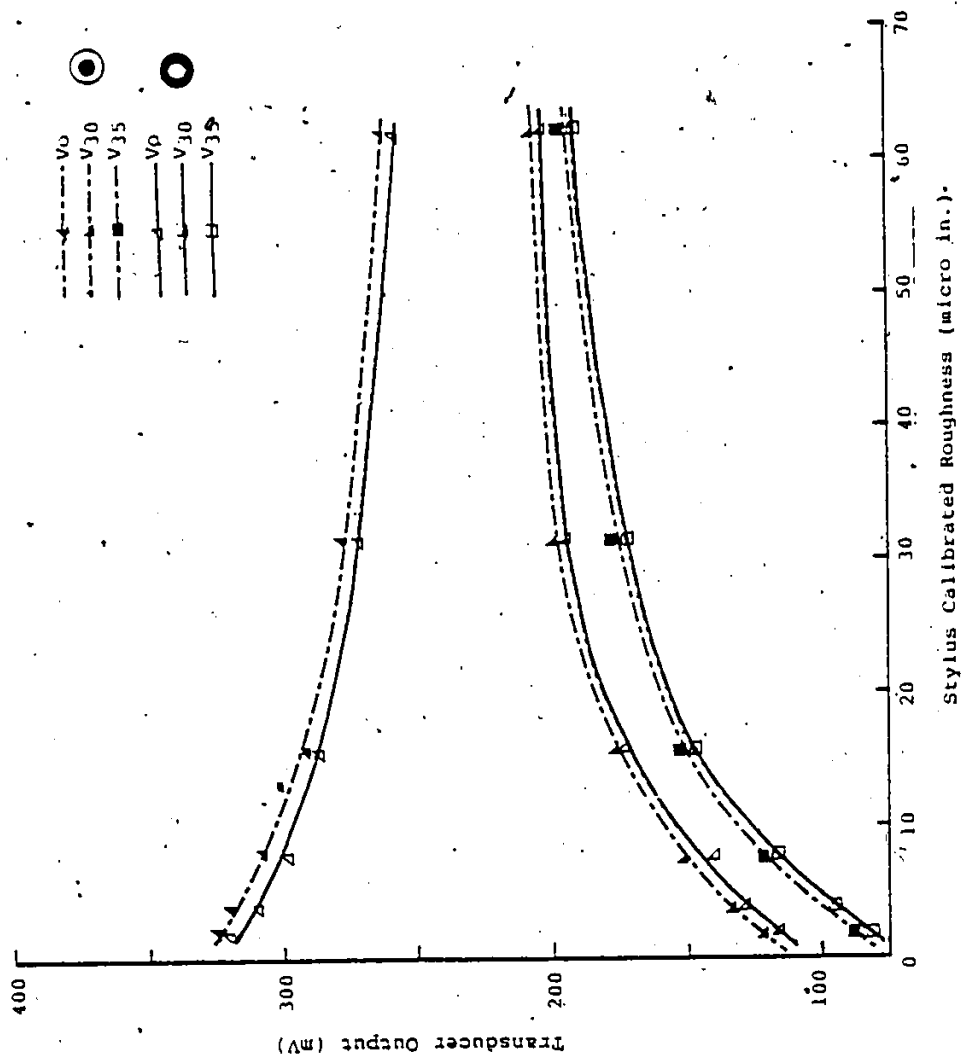


Figure 5.8: TRANSDUCER (EC424) OUTPUT VS. ROUGHNESS, FOR DIFFERENT DETECTING ANGLES

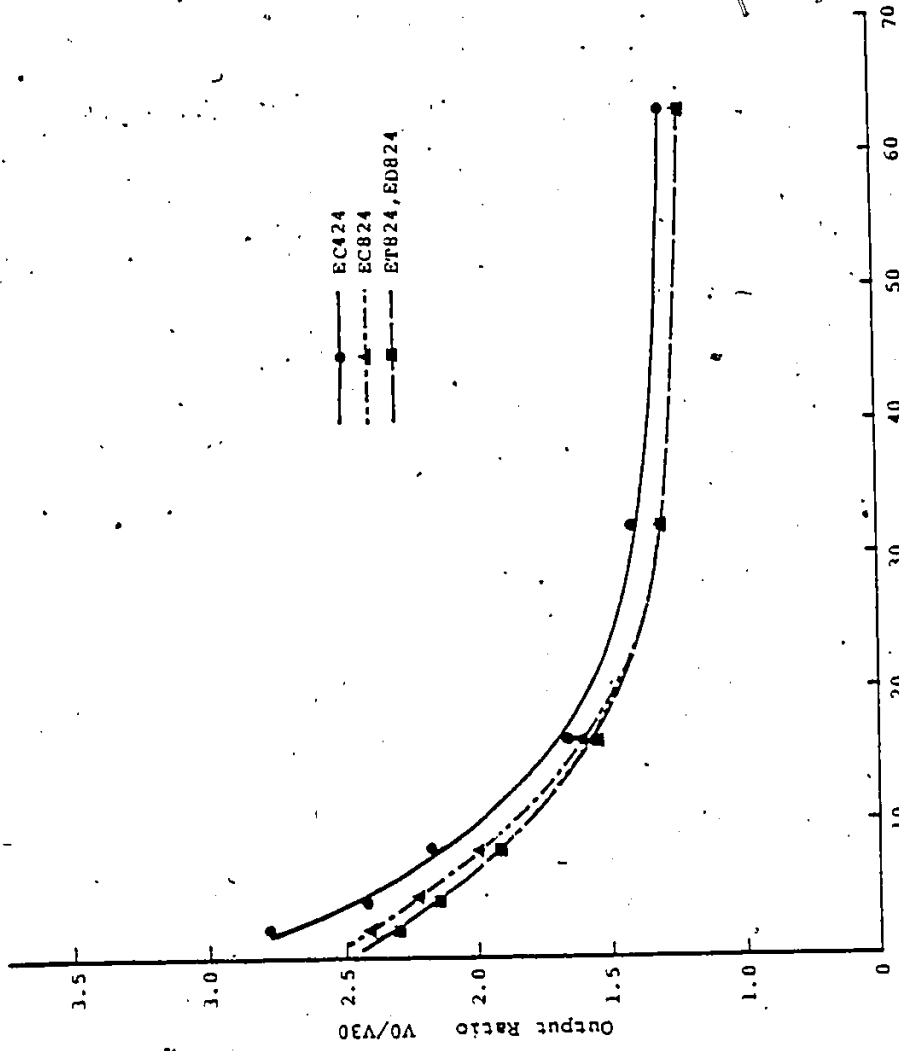


Figure 5.9: OUTPUT RATIO V0/V30 Vs. ROUGHNESS FOR EC424, EC824, ET824 & ED824

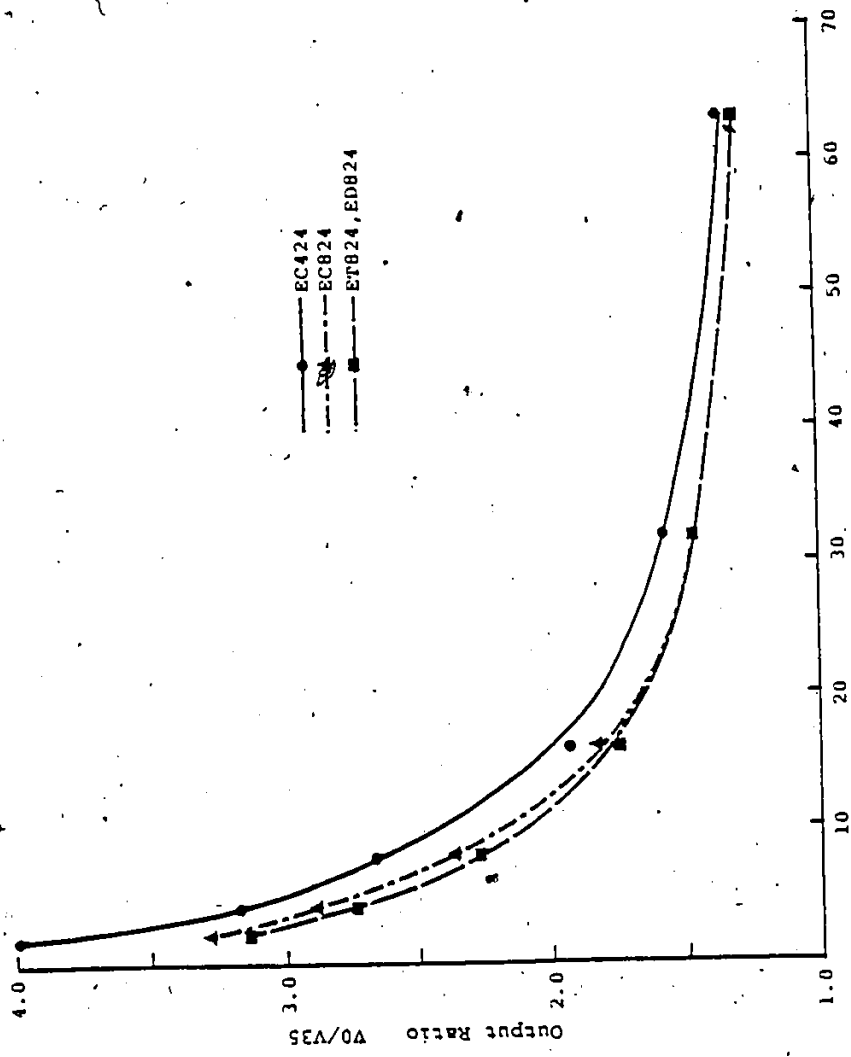


Figure 5.10: OUTPUT RATIO V0/V35 Vs. ROUGHNESS FOR EC424, EC824, ET824 & ED824

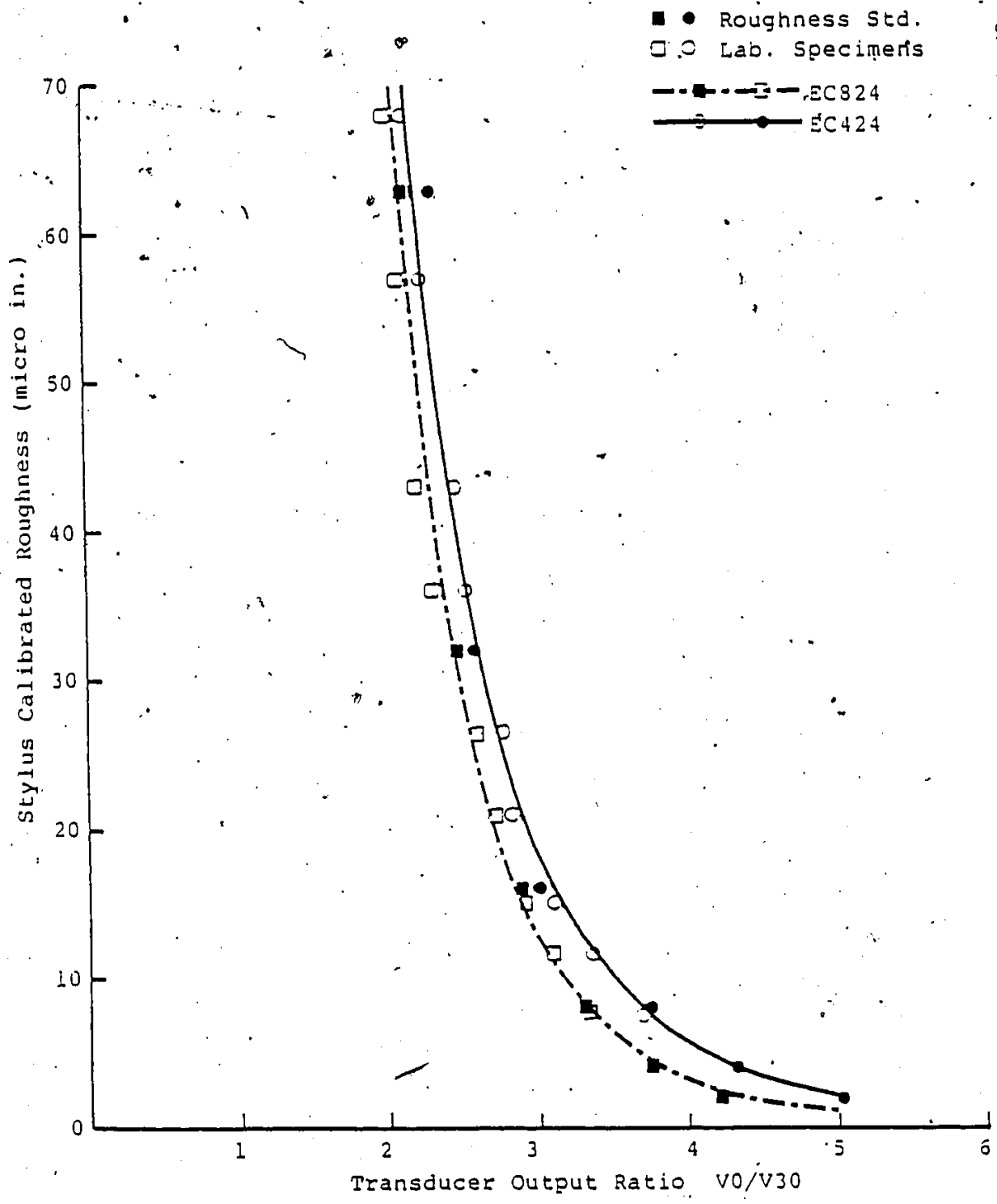


Figure 5.11: RELATION BETWEEN SURFACE ROUGHNESS AND THE TRANSDUCER OUTPUT RATIO V_0/V_{30} , FOR EC424 & EC824

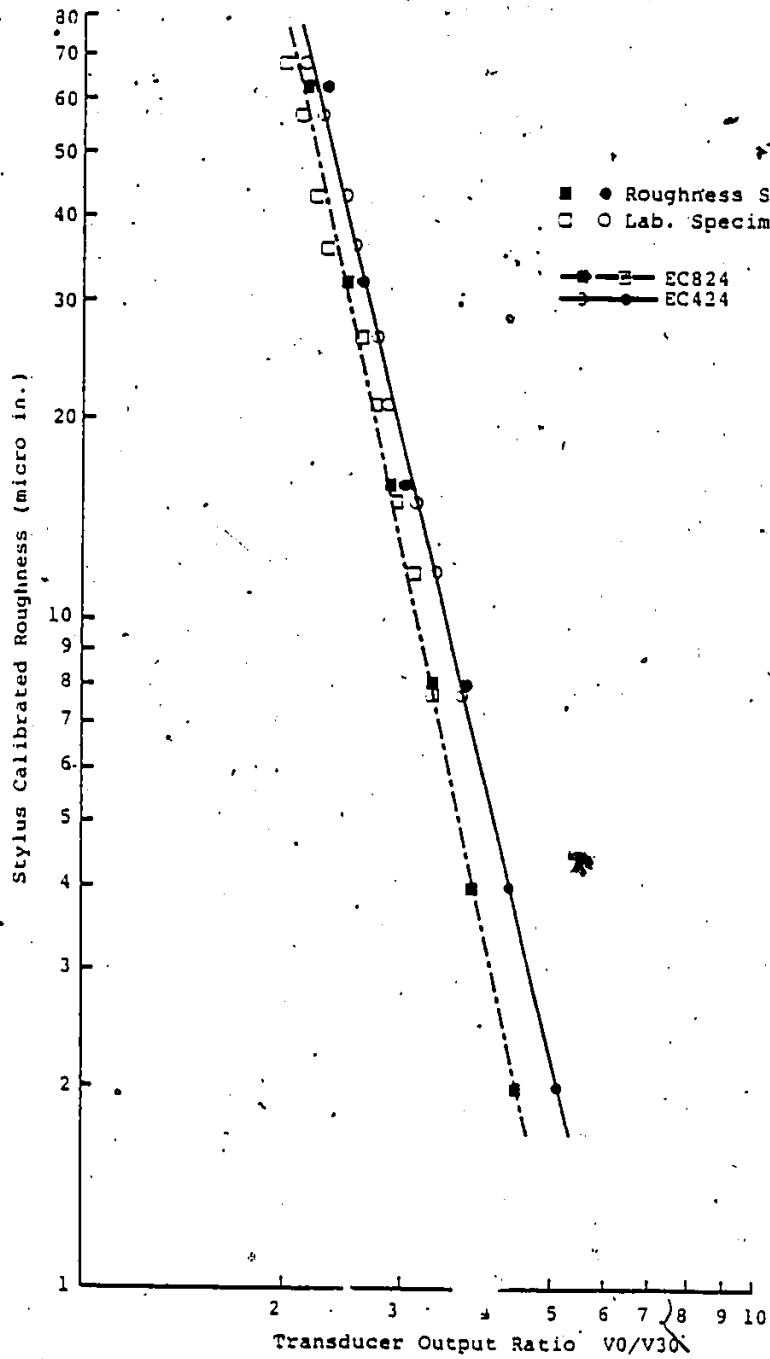


Figure 5.12: LOGARITHMIC RELATION BETWEEN SURFACE ROUGHNESS AND THE TRANSDUCER OUTPUT RATIO V_0/V_{30} , FOR EC424 & EC824

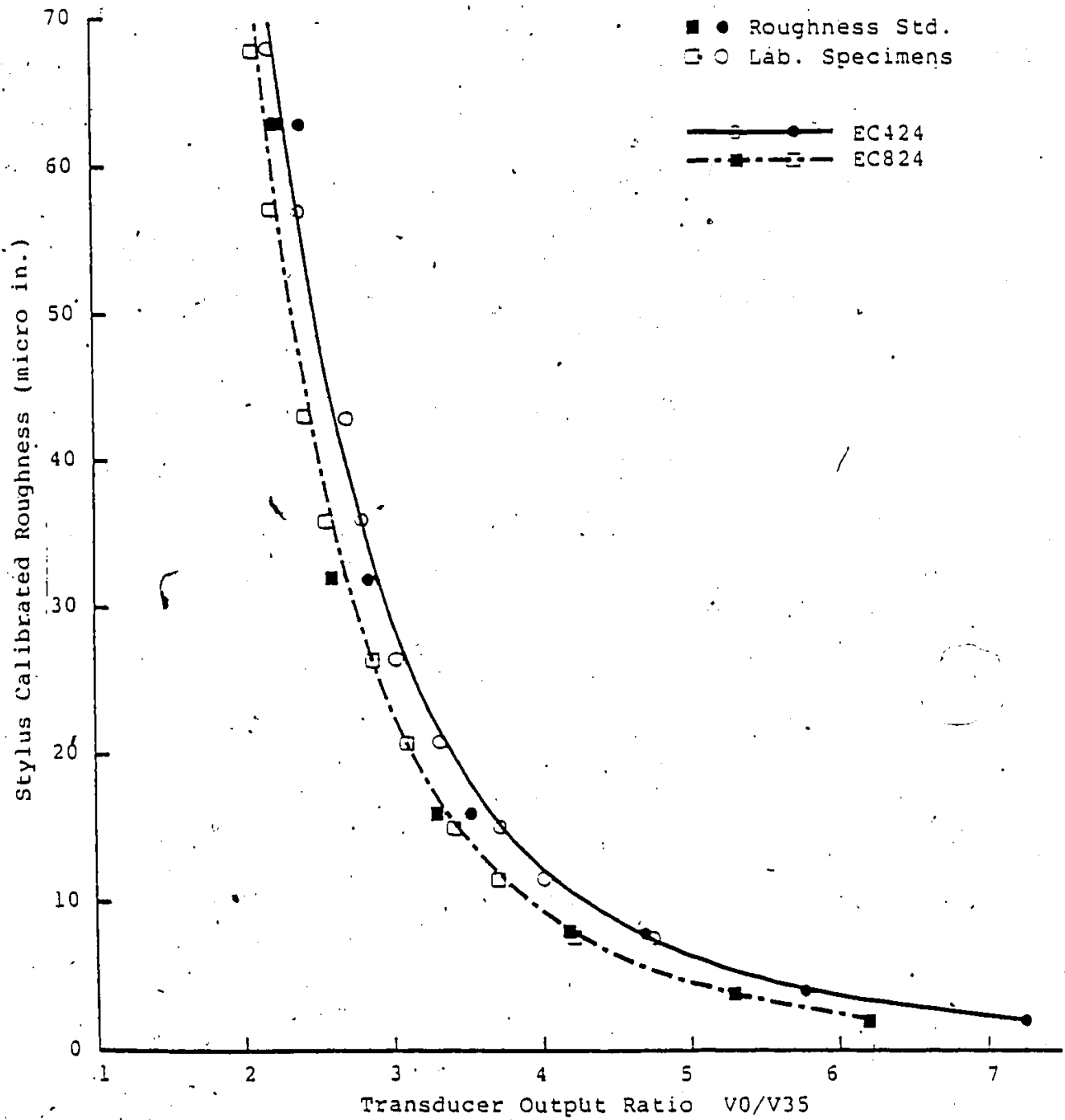


Figure 5.13: RELATION BETWEEN SURFACE ROUGHNESS AND THE TRANSDUCER OUTPUT RATIO V_0/V_{35} , FOR EC424 & EC824

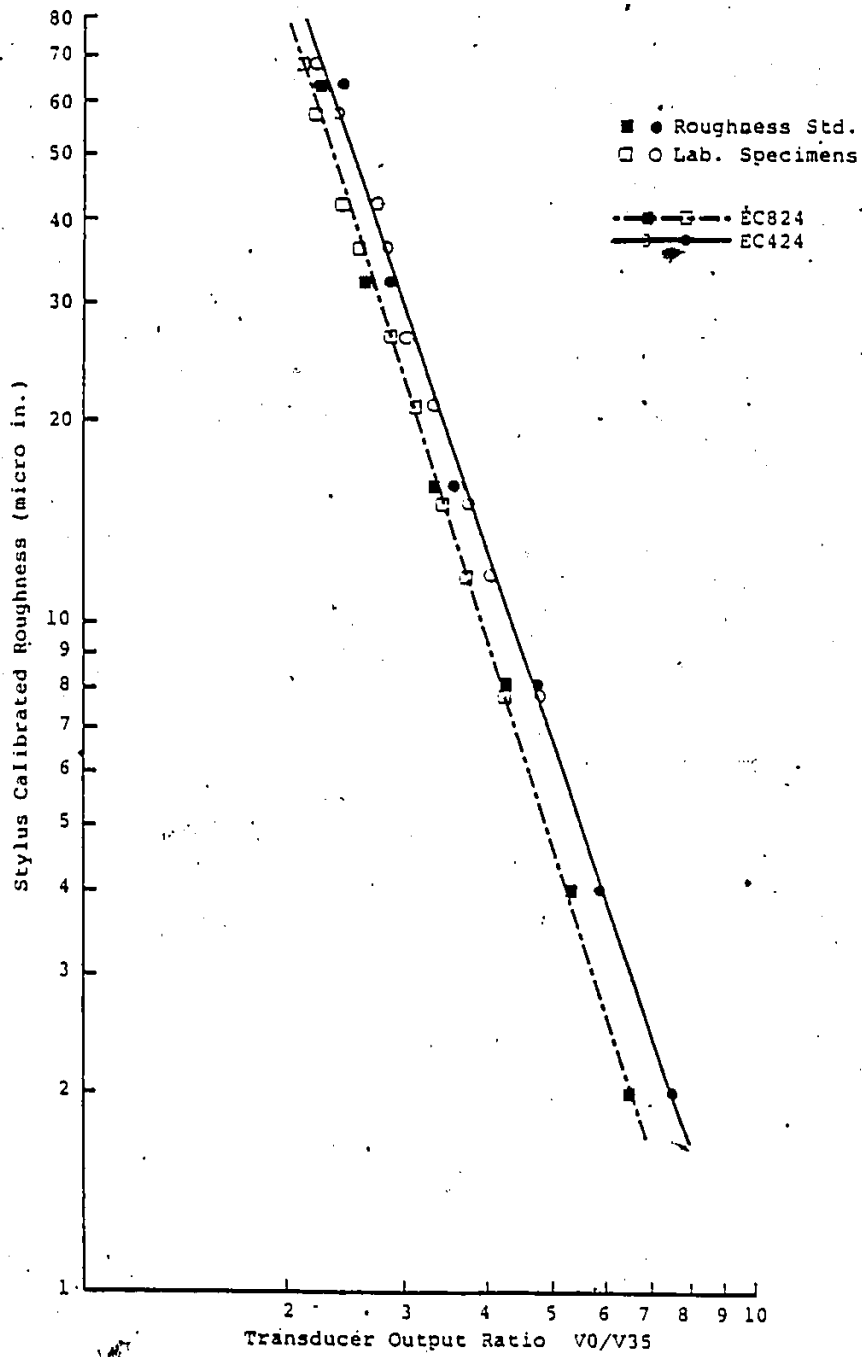
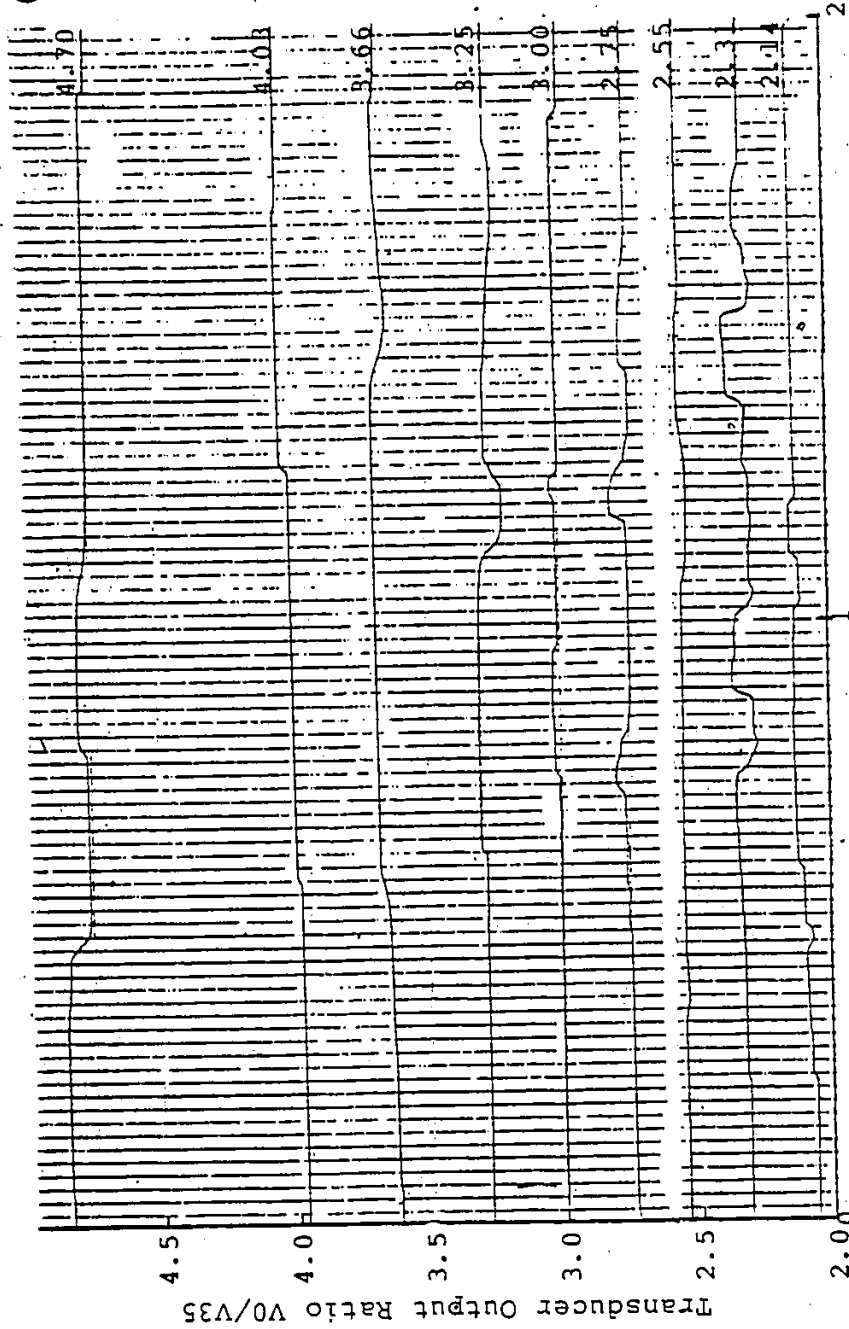


Figure 5.14: LOGARITHMIC RELATION BETWEEN SURFACE ROUGHNESS AND THE TRANSDUCER OUTPUT RATIO V_0/V_{35} , FOR EC424 & EC824

μ in. Ra.
 (Stylus Calib.)
 7.86



Scanning Distance (in.)

Figure 5.15: OUTPUT RATIO V0/V35 FROM A SCAN OF SURFACES BY

TRANSDUCER EC 424

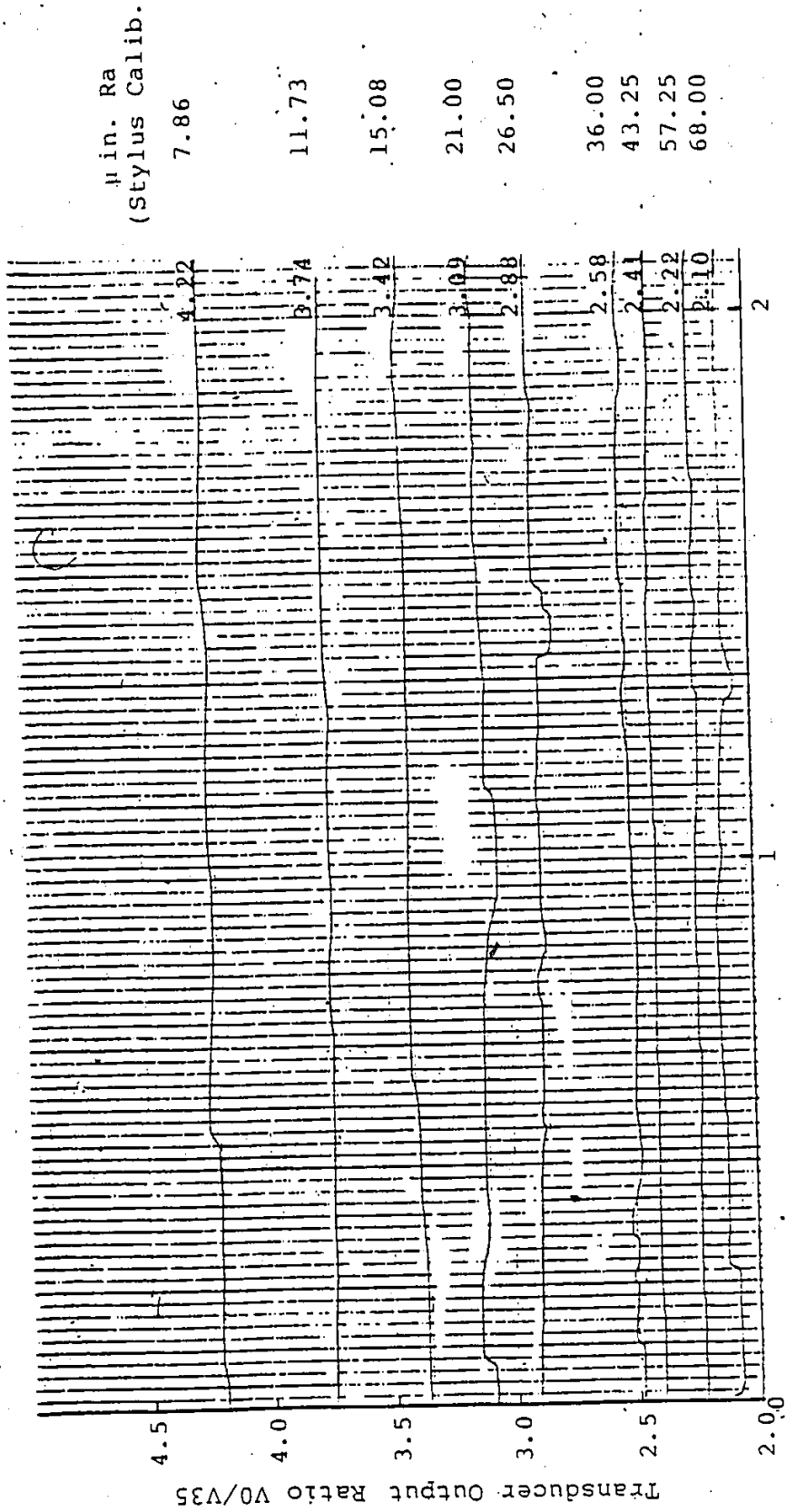


Figure 5.16: OUTPUT RATIO V0/V35 FROM A SCAN OF SURFACES BY TRANSDUCER EC824

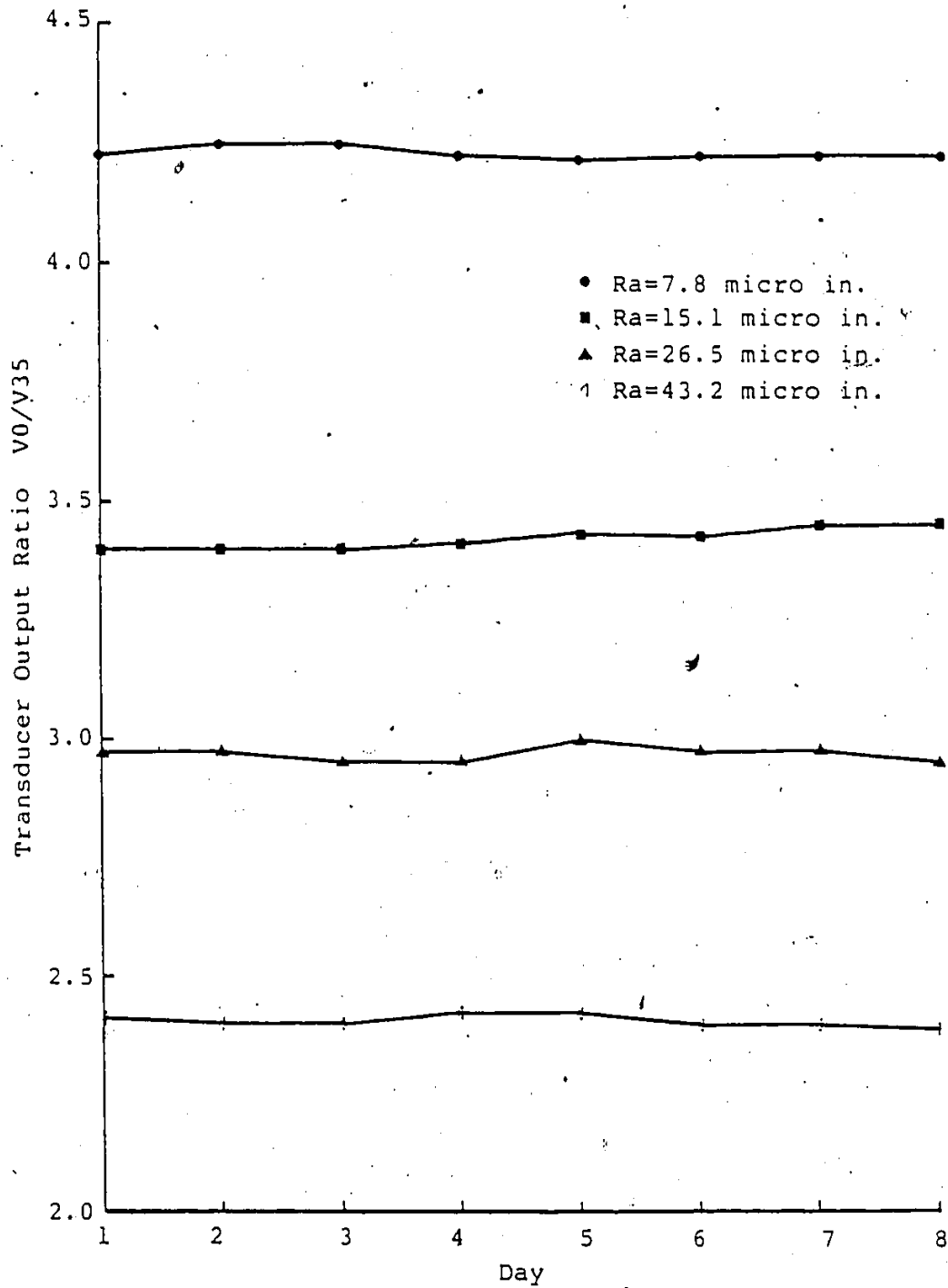


Figure 5.17: VARIATIONS IN OUTPUT RATIO V_0/V_{35} WITH TIME,
FOR TRANSDUCER EC824

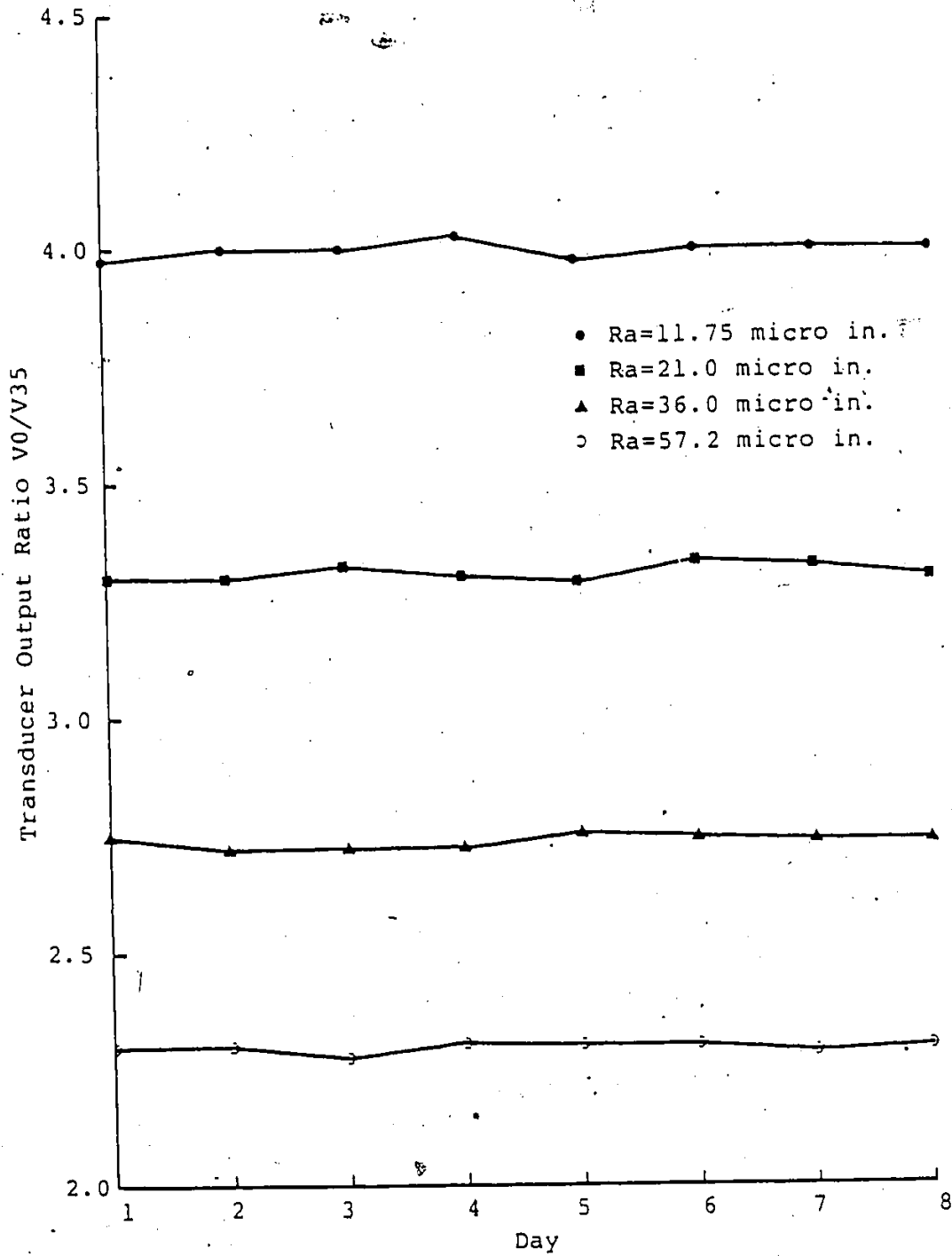


Figure 5.18: VARIATIONS IN OUTPUT RATIO V_0/V_{35} WITH TIME, FOR TRANSDUCER EC424

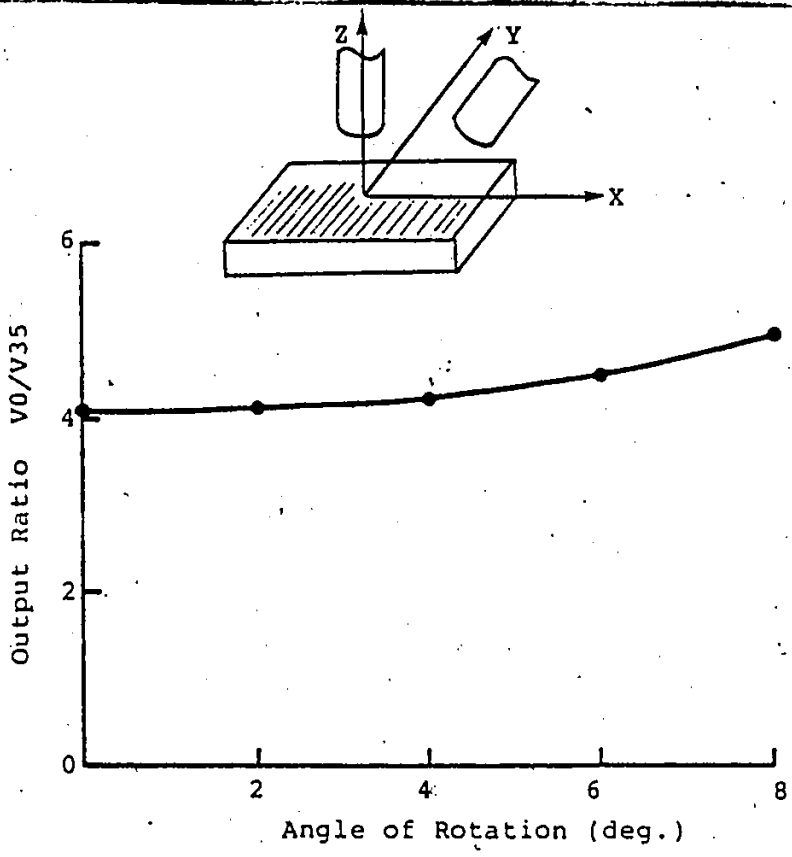


Figure 5.19: EFFECT OF POSITIVE OR NEGATIVE ROTATION ABOUT Z-AXIS, ON V_0/V_{35}

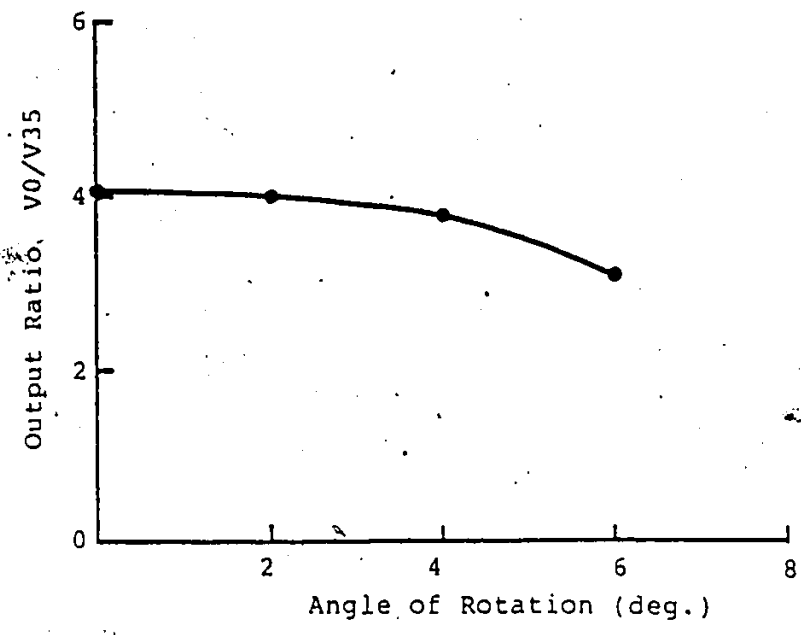


Figure 5.20: EFFECT OF POSITIVE OR NEGATIVE ROTATION ABOUT X-AXIS, ON V_0/V_{35}

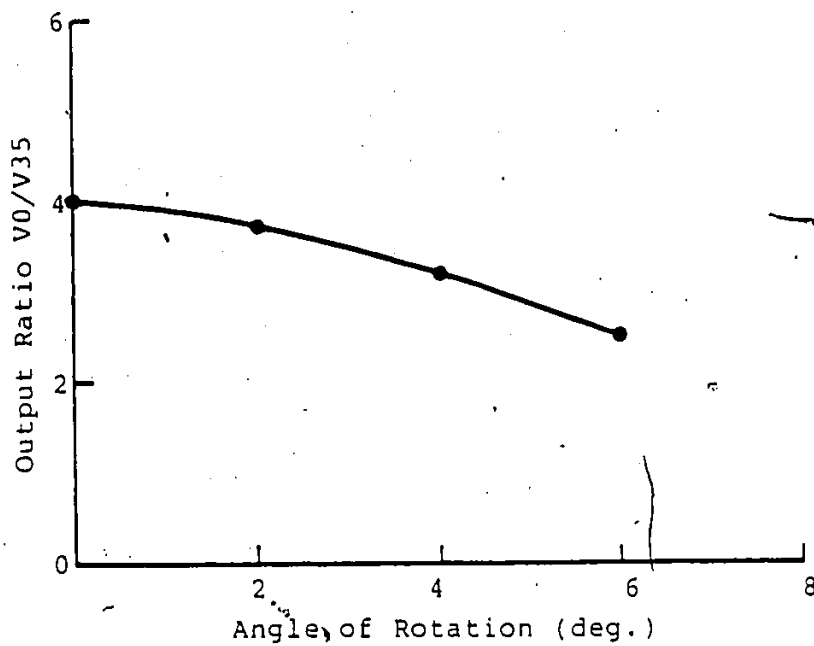


Figure 5.21: EFFECT OF POSITIVE ROTATION ABOUT Y-AXIS ON V0/V35

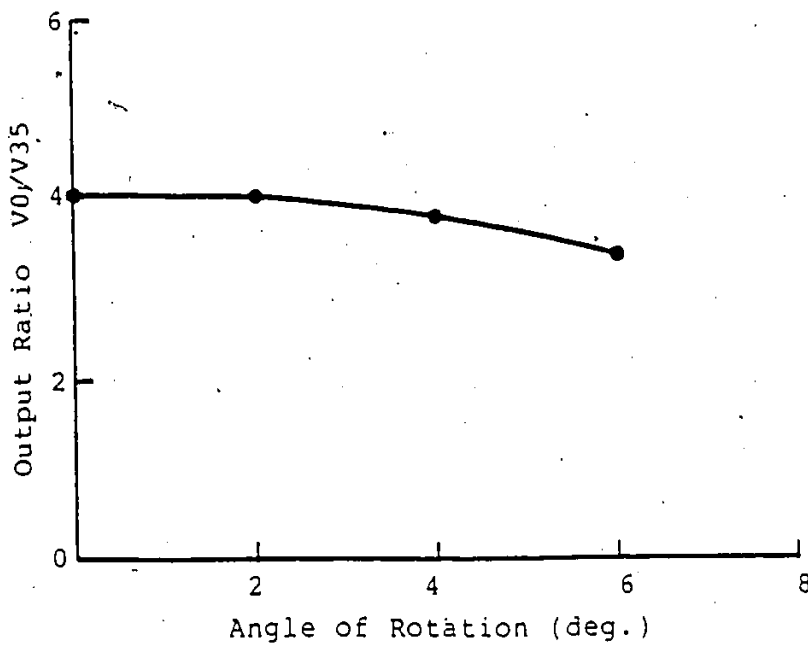






Figure 5.22: EFFECT OF NEGATIVE ROTATION ABOUT Y-AXIS ON V0/V35.

TABLE 5.1

Working Range of the Transducers

Transducer Type	Stand-off (in.)	Range (in.)
EK3012	0.0225	± 0.0025
ET824	0.0625	± 0.0125
ED824	0.0800	± 0.0150
EC824 	0.1400	± 0.0200
EC824 	0.1475	± 0.0275
EC424 	0.2350	± 0.0350
EC424 	0.2500	± 0.0500

The shaded area in the coaxial transducer indicates the transmitting fibers.

TABLE 5.2

Correlation Equations for Transducers EC424 &

EC824

Transducer Type	Correlation Parameters	Correlation Equations	Standard Error of Estimate	Coeff. of Correlation
EC824	Ra, V0/V30	$Ra = 1930.6 (V0/V30) - 4.622$	0.133	0.992
	Ra, V0/V35	$Ra = 736.9 (V0/V35) - 3.170$	0.069	0.998
EC424	Ra, V0/V30	$Ra = 1626.6 (V0/V30) - 4.130$	0.099	0.991
	Ra, V0/V35	$Ra = 728.7 (V0/V35) - 2.954$	0.094	0.996

TABLE 5.3

Comparison Between Roughness Measured by
Profilometer and EC824

AA Roughness (Profilometer) (micro inches) (1)	Avg. V0/V35 (Signal Processor)	Estimated AA Roughness from V0/V35 (micro inches) (2)	Percentage Difference Between (1) & (2)
7.80	4.22	7.67	1.58
11.75	3.72	11.45	2.56
15.10	3.40	15.23	-0.84
21.00	3.09	20.62	1.82
26.50	2.88	25.77	2.75
36.00	2.58	36.52	-1.45
43.20	2.41	45.33	-4.94
57.20	2.22	58.81	-2.82
68.00	2.10	70.14	-3.15

TABLE 5.4

Comparison Between Roughness Measured by
 Profilometer and EC424

AA Roughness (Profilometer) (micro inches) (1)	Avg. V0/V35 (Signal Processor)	Estimated AA Roughness from V0/V35 (micro inches) (2)	Percentage Difference Between (1) & (2)
7.80	4.70	7.54	3.40
11.75	4.00	12.14	-3.28
15.10	3.66	15.78	-4.50
21.00	3.30	21.42	-2.00
26.50	3.04	27.30	-3.07
36.00	2.74	37.10	-3.00
43.20	2.55	45.88	-6.20
57.20	2.31	61.44	-7.40
68.00	2.14	77.00	-13.24

Chapter VI

CONCLUSIONS

Based on the results of this investigation the following conclusions are made:

1. It is possible to use a laser and fiber-optics to measure surface roughness over a significant range. The ratio of the reflected light intensity as measured with a pair of transmitting/receiving fiber-optics of similar specifications and set at detecting angles of 0 and 35 degrees to the normal can be effectively used to characterize the average roughness of a 'ground' surface.

The relationship between the ratio of the outputs to the stylus calibrated surface roughness may be expressed by the equation;

$$Ra \cdot X^B = A$$

Where, Ra is the stylus calibrated AA roughness in micro in.

X is the output ratio V0/V35, and;

A & B are constants determined by calibration.

For the two sets of transducers used in this present work, the values of these constants are;

$$A = 728.7$$

$$B = 2.954$$

and

$$A = 736.9$$

$$B = 3.170$$

The output ratio V_0/V_{35} is a normalized parameter which, for an illumination of a particular wavelength, essentially depends on the surface roughness alone and will be unaffected by other variables like illumination intensity, surface reflection etc.

2. A coaxial fiber-optic transducer is best suited for the purpose of roughness measurement. Although a smaller coaxial transducer was found to be more accurate, a larger coaxial transducer, because of its higher output level, longer working distance and better sensitivity is preferable. In addition, the larger transducer is more robust and sturdy and hence will be more acceptable for industrial applications.
3. A typical drawing specification requires that a stylus instrument determine the average roughness R_a , over a length of at least 0.15" by averaging the roughness in 5 consecutive lengths of 0.03". The stylus scan time for this is approximately 2 seconds.

For this fiber-optic solution, the foot print of the illumination (for the transducer EC424) is approximately 0.18" long, hence one reading

essentially averages over this length. The time to take this reading is limited only by the detectors, amplifiers and incident intensity. Since the latter would normally govern, it is estimated that the time for this measurement would be in the order of one millisecond. A high power laser could reduce this time to microseconds if it were necessary.

4. It appears from figures 5.13 & 5.14 that it should be possible to measure roughness ≤ 70 micro in. Ra by this method. However, for roughness beyond 40 micro in. the change in V_0/V_{35} is small, so it is unlikely that this technique can, effectively and accurately, be used for measuring roughness of more than 40 micro in. Ra. This range of measurement, however, is much larger than that possible by the method suggested by Lin, Shea and Hoang[17]. The roughness measurements within this range are expected to be within 5% of the stylus measurements. Moreover, the measurement by this method is stable with time and repeatable within acceptable limits.
5. The results of this investigation indicate that a practical system could be produced quite cheaply to quickly ascertain the acceptability of the machined surfaces in a production line. Since the output from the fiber-optic system reduces as the surface roughness increases, a minimum acceptable output can

be determined by calibrating the system with similar surfaces of known roughness. If any surface under inspection, provides an output less than acceptable it could then be rejected or removed from the line for further investigations.

The entire length of the surface could be scanned by the transducers resulting in a longer inspection time and the requirement of a more elaborate system. In most cases, however, a single reading over a critical area should be sufficient for on line quality control purposes. A typical use of this procedure could be for on line roughness measurement of crankshaft journals and pins.

Figure 6.1 shows the possible position of the fiber-optic transducers over a crankpin. The highest reading (see Fig. 5.20), as the journal surface rotates past the transducer, represents the roughness of this surface. The transducers can similarly be positioned over a main journal to record its roughness.

6. The sensitivity of the measurement with respect to the surface orientation is the main drawback of this procedure. A maximum variation of 0.1" in the transducer position and a surface rotation of only 2° is permissible. This requires the use of a suitable fixture for the proper positioning of the surface

(This is also true for a stylus instrument).
However, the advantages offered by the optical method
more than compensate and make it a practical
alternative to profilometric techniques in current
use.

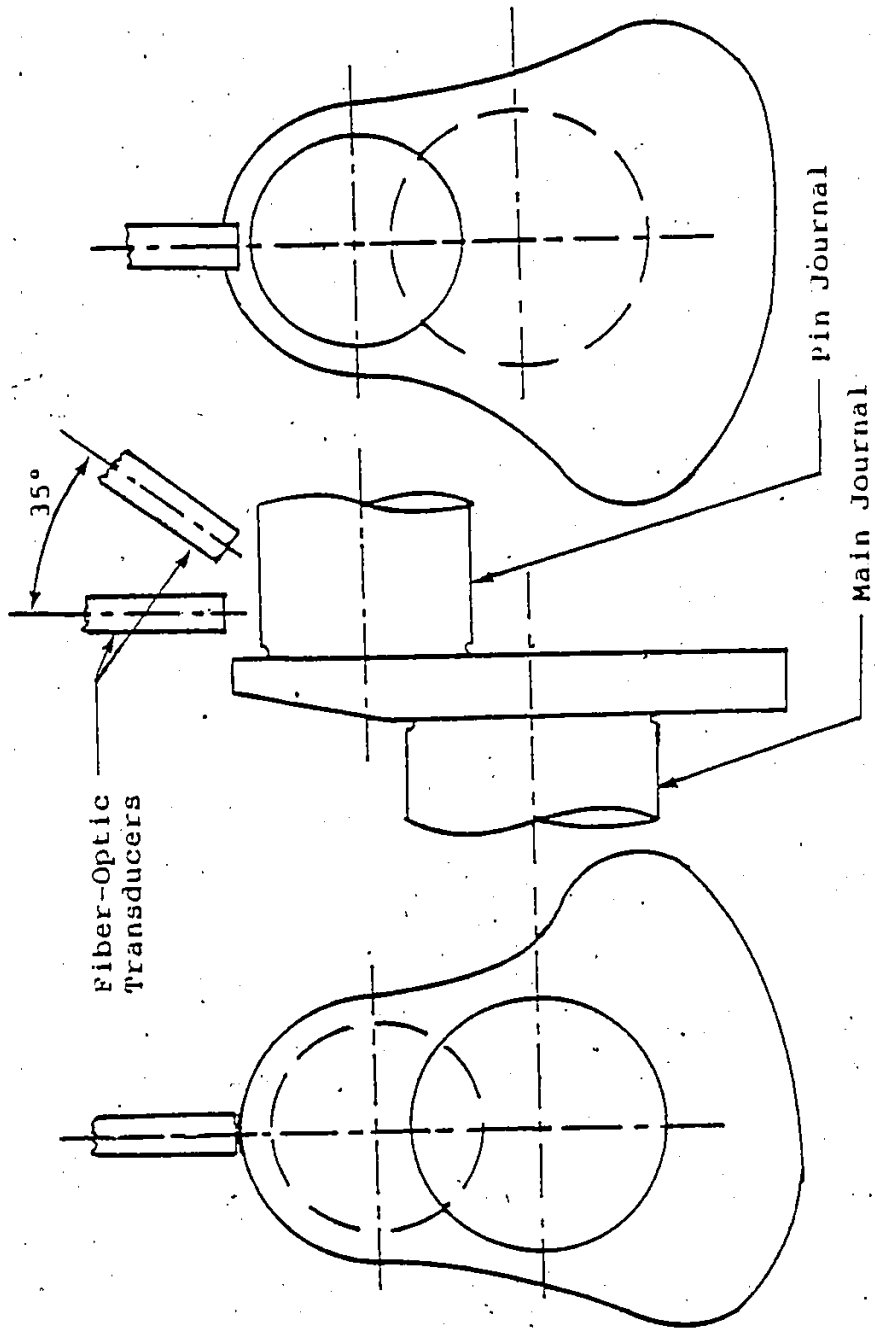


Figure 6.1: POSITION OF THE FIBER-OPTIC TRANSDUCERS TO MEASURE THE SURFACE ROUGHNESS OF A CRANKSHAFT JOURNAL

Chapter VII

RECOMMENDATIONS

It is recommended that the following investigations be undertaken to extend the research program described herein;

1. As predicted by the theoretical relation, the output ratio from the transducer does not depend upon the coefficient of reflection of the work surface, hence it is expected that this technique can be used to measure the roughness regardless of surface material. However to verify this it is suggested that a similar investigation be carried out for surfaces of... different materials, for example; steels, aluminium, brass, zinc, magnesium, plastic, painted surfaces, wood finishes, paper, gelatin or other surfaces which cannot be contacted using a stylus instrument.
2. The present study should also be extended to surfaces generated by different machining process such as milling, turning etc.
3. It has been shown during an earlier research work[31] that light reflected in a direction parallel to machining marks does not correlate well with the surface roughness as measured by a profilometer in a direction perpendicular to the lay. The concentric

fiber-optic used in this work collects some of this undesirable reflection. If these reflections were avoided it is expected that the resulting outputs will have a better correlation with the surface roughness. The use of a rectangular aperture to block the light reflected in the direction parallel to lay, or a specially designed fiber-optic is recommended for future investigations.

4. It was shown in section 3.2 that the light reflected from a surface depends both on the surface roughness as well as the wavelength of the illumination. The effect of surface roughness on this output becomes increasingly important as the wavelength becomes longer. An excellent explanation of this phenomenon is given by Bennett & Porteus[7] as follows:
"Consider a nominally plane surface made up of many small facets randomly oriented in various directions. If the dimensions of the facets are large compared with the wavelength of light, the reflectance of a surface in a given direction is determined entirely by geometrical optics and is a function only of the inclination of the facets. As the wavelength becomes longer, diffraction effects become important, and the reflectance is a function of both the inclination and the size of the facets. As the wavelength becomes still longer, so that the dimensions of the facets

become very small by comparison, the reflectance of the surface will be determined almost entirely by diffraction effects. The surface roughness will then be the only important parameter."

It is, therefore, suggested that this investigation be carried out using light of longer wavelength with a view to improve the range of measurement. For example an infrared laser with wavelength of 40 micro in. or 400 micro in. could be used. Indeed, the use of a 400 micro in. wavelength may prove interesting since the diameter of the stylus in a stylus instrument is of the order of this magnitude. Infrared detectors would of course be required.

5. The possibility of correlating the fiber-optic output with other roughness parameters like maximum peak to valley roughness R_t , ten points height R_z etc., should also be explored in a future work.
6. This method was based on the assumption that the surfaces under investigation are thoroughly cleaned before a measurement is taken. In most industrial environments, however, the machined parts are usually covered with a film of oil or other coolant fluids. The effect of these factors, on the correlation results also needs to be investigated in a future program.

7. The results of this investigation indicated that the reflected output, averaged over a small illuminated surface area, has a better correlation with the stylus calibrated surface roughness. This suggests that if the foot print of the illumination is reduced to the size of a common stylus tip (400 to 500 micro in.) by using a microscope objective it might be possible to correlate the output from each point of the surface with the corresponding output from a stylus instrument. This procedure will necessarily require the use of only one fiber-optic to obtain the output from a single illuminated surface point. A specially designed fiber optic will probably be needed to obtain a normalized output.

The output from such a system could also be fed into a general purpose micro computer which can be programmed to correlate this output with any of the roughness parameters like Ra, Rt, Rz, etc.

A successful investigation of this nature could result in the development of an optical profilometer.

LIST OF REFERENCES

1. Surface Texture. American National Standard Institution, ANSI B46.1-1978, New York, 1978
2. Surface Roughness. International Organization For Standards, ISO/R468 - 1966, Switzerland, 1966
3. Drews, William, -E. What's New In Surface Metrology, Production, July 1979, pp. 91-95
4. Teague, Clayton, E. Surface Finish Measurements: An Overview, Society Of Manufacturing Engineers, Technical Paper No. IQ75-137, 1975
5. Beckmann, P. and Spizzichino, A. The Scattering Of Electromagnetic Waves from Rough Surfaces, Macmillan , New York, 1963
6. Davies, H. The Reflection Of Electromagnetic Waves from a Rough Surface, Proc. Instn. Electrical Engineers, Vol. 101, 1954, pp. 209-214
7. Bennett, H.E. and Pořteus, J.O. Relation Between Surface Roughness and Specular Reflectance at normal Incidence, Journal of the Optical Society of America, Vol. 51, No. 2, Feb. 1961, pp. 123-129
8. Torrance, K.E. Monochromatic Directional Distribution of Reflected Thermal Radiation from Roughened Dielectric Surfaces, M.S. Thesis, University of Minnesota, 1964.
9. Depew, C.A. and Weir, R.D. Surface Roughness Determination by the Measurement of Reflectance, Applied Optics, Vol. 10, No. 4, April 1971, pp. 969-970
10. Birkebak, R.C. Monochromatic Directional Distribution of Reflected Thermal Radiation from Roughened Surfaces, Ph.D. Dissertation, University of Minnesota, 1962.
11. Birkebak, R.C. Optical and Mechanical RMS Surface Roughness Comparison, Applied Optics, Vol. 10, No. 8, Aug. 1971, pp. 1970
12. Hensler, D.H. Light Scattering From Fused Polycrystalline Aluminum Oxide Surfaces, Applied Optics, Vol. 11, No. 11, Nov. 1972, pp. 2522-2528

13. Chandley, P.J. Surface Roughness Measurements from Coherent Light Scattering, Optical and Quantum Electronics, Vol. 8, No. 3, March 1976, pp.323-327
14. Beckmann, P. Scattering of Light from Rough Surfaces, Progress in Optics, Edited by E. Wolf, Vol. VI, John Willey and Sons Inc., New York, 1976, pp. 55-69
15. Pernick, B.J. Surface Roughness Measurements with an Optical Fourier Spectrum Analyzer, Applied Optics, Vol. 18, No. 6, March 1979, pp.796-801
16. Spurgeon, D. and Slatter, R.A.C. In-Process Indication of Surface Roughness using a Fibre-Optics Transducer, Proc. of the Fifteenth International Machine Tool Design And Research, Vol. 15, 1974, pp. 339-347
17. Lin, G.C. , Shea, T. and Hoang, K. Measurement of Surface Roughness with a Laser Beam, Australian Conference on Manufacturing Engineering, Aug. 1977, pp. 132-133
18. Fiber Optics Theory and Applications. Galileo Electro-Optics Corp. , Technical Memorandum No. 100, Sturbridge (Massachusetts)
19. Menadier, C. , Kissinger, C. and Adkins, H. The Fotonic Sensor, Mechanical Technologies Inc., Bulletin No. 15126, Latham (N.Y.)
20. Church, C. , Jenkinson, H.A. and Zava'a, J.M. Measurement of the Finish of Diamond-Turned Metal Surfaces by Differential Light Scattering, Optical Engineering, Vol. 16, No. 4, July-Aug. 1977, pp. 360-374
21. Fukusima, E. A Surface Roughness Tester for Factory Use, The Journal of the Society of Aeronautical Science of Japan, Vol. 8, 1941, pp. 253-264
22. Tani, Y. Measurement of Roughness of Finished Metal Surface by Means of Photo-Electric Transducer, Kikai, Vol. 6, 1931
23. Model 120 Stabilite Gas Laser Instruction Manual. Spectra Physics Inc. , Mountain View (Calif.)
24. Models 332/333/334/336 Instruction Manual. Spectra Physics Inc. , Mountain View (Calif.)
25. Planar Diffused Silicon Pin Photodiodes. United Detector Technology Inc. , Data Sheet 9F002, Santa Monica (Calif.)

26. Differential Input Instrumentation Amplifier Model 3622. Burr-Brown Research Corp. , Data Sheet PDS-261, Tuscon (Arizona)
27. Analog Divider Model 4291. Burr-Brown Research Corp. , Data Sheet PDS-336, Tuscon (Arizona)
28. Oriel Multifunction Signal Processor Model 7600 Instructional Manual. Oriel Corporation, Stamford (Conn.)
29. Class Fiber Optics. Dolan-Jenner Industries Inc. , Bulletins 737, 738 and 812, Woburn (MA)
30. Surftest III Operation Manual. Mitutoyo Manufacturing Co., Ltd., Tokyo.
31. Pumpell, A. Electro Optical Determination of Surface Roughness, Senior Project Report, Mech. Engineering-University of Windsor, Windsor, 1981
32. Neville, A.M. and Kennedy, J.E. Basic Statistical Methods for Engineers and Scientists International Textbook Company, Scranton (Pennsylvania), 1964

Appendix A

LINEARITY RESPONSE CURVES FOR THE PHOTODETECTORS

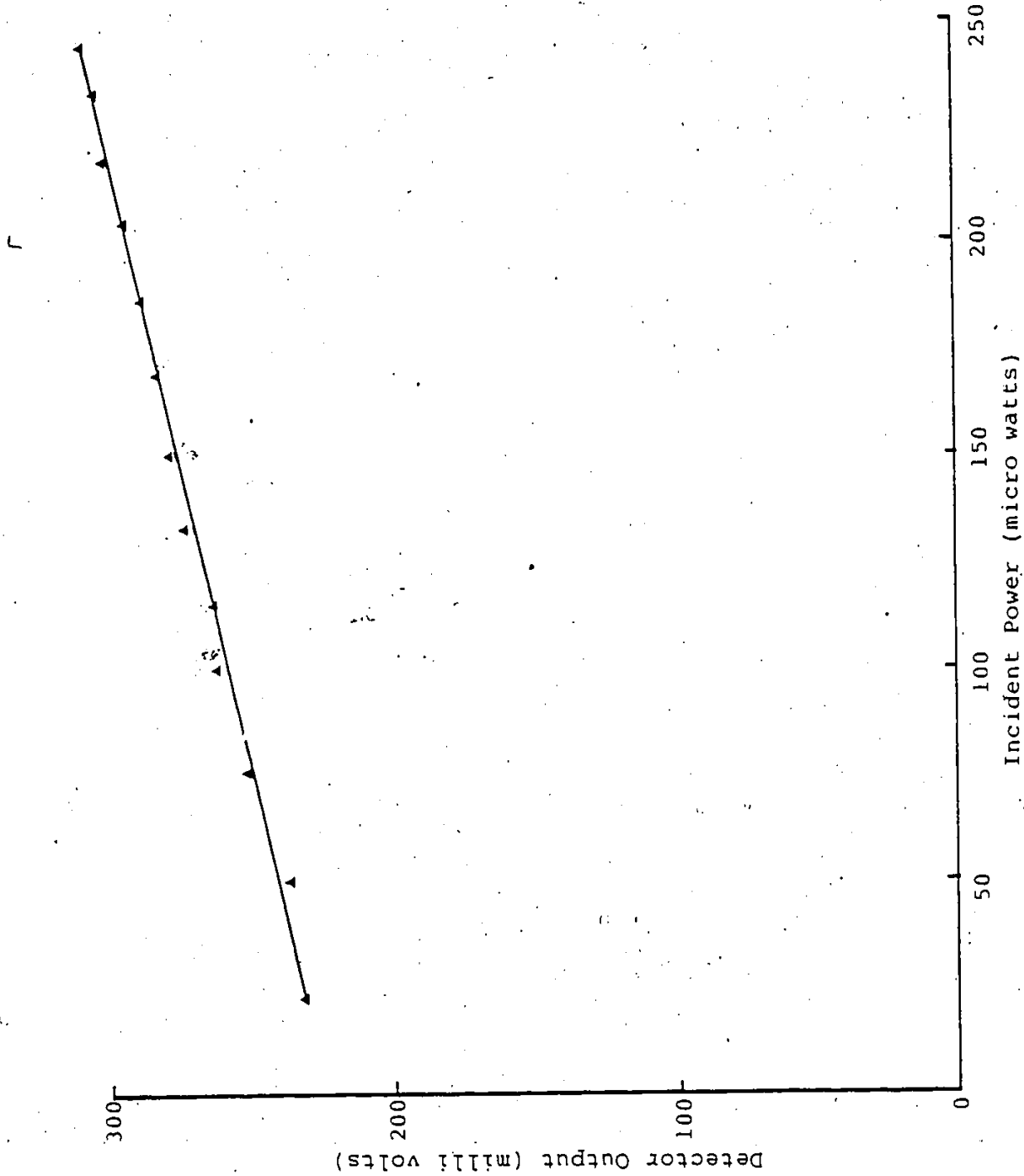


Figure A.1: LINEARITY RESPONSE CURVE FOR PHOTODETECTOR No. 1



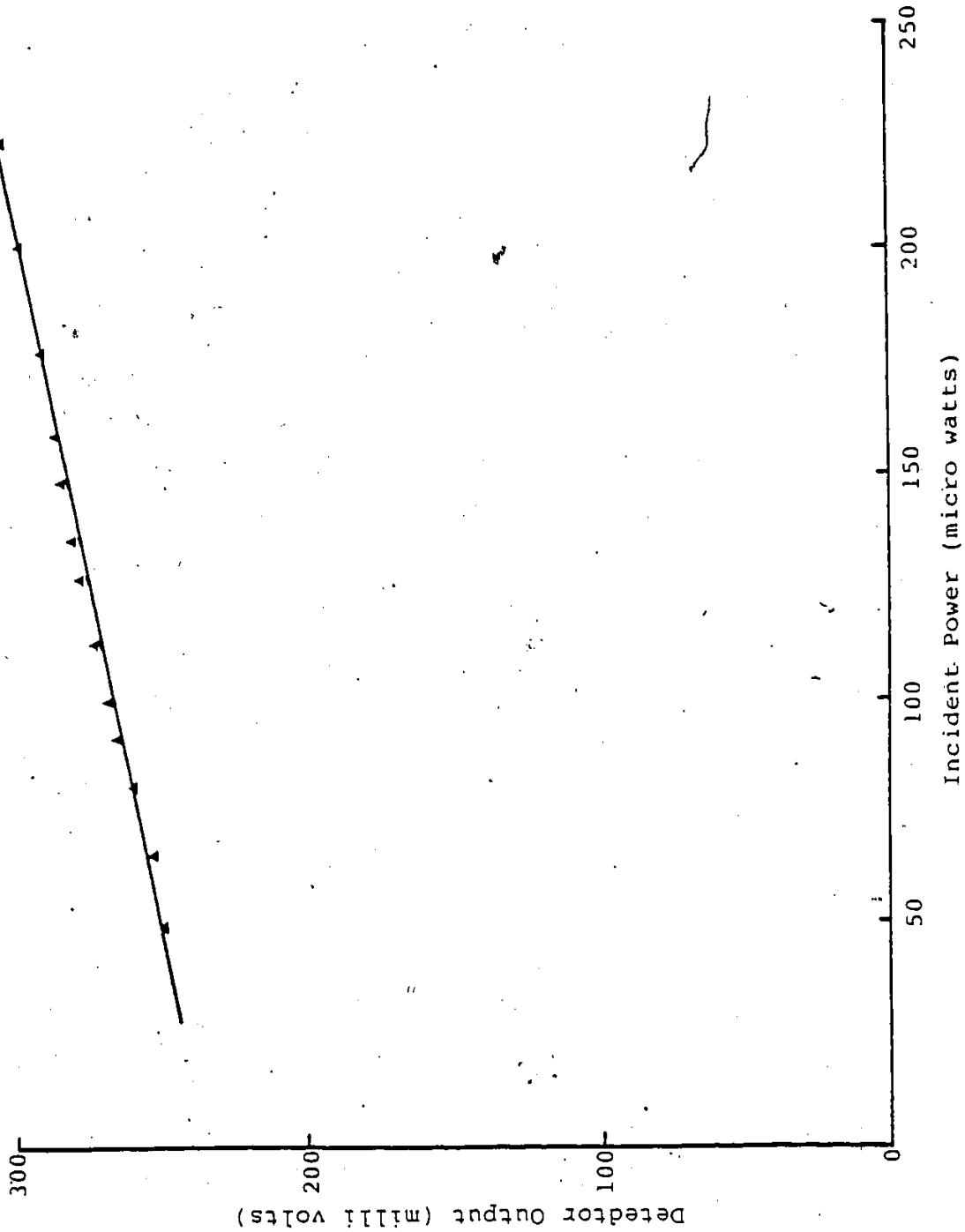


Figure A.2: LINEARITY RESPONSE CURVE FOR PHOTODETECTOR NO. 2

Appendix B

CALIBRATION CURVES FOR THE OPERATIONAL AMPLIFIER

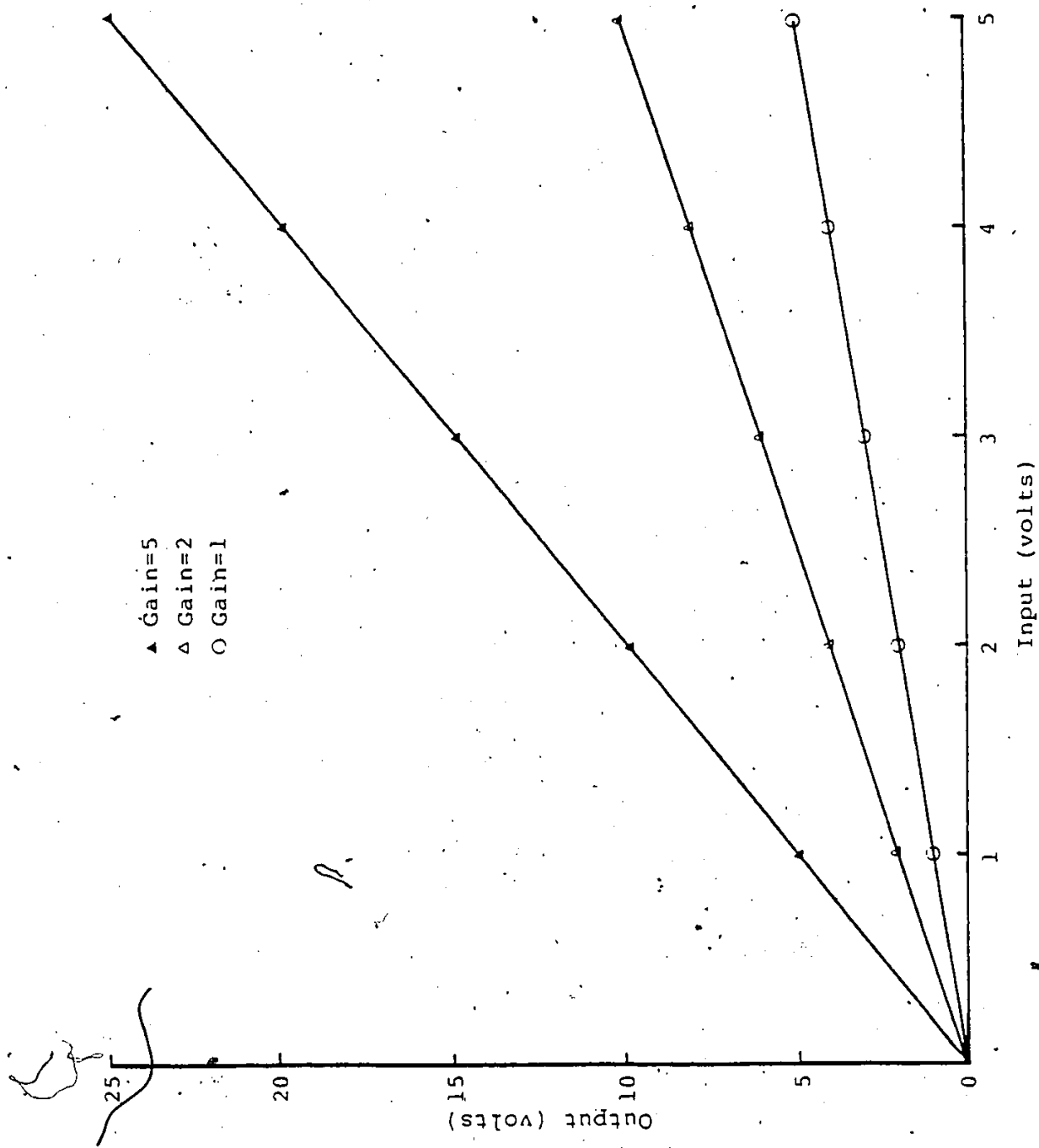


Figure B.1: CALIBRATION CURVE FOR THE AMPLIFIER CHANNEL A

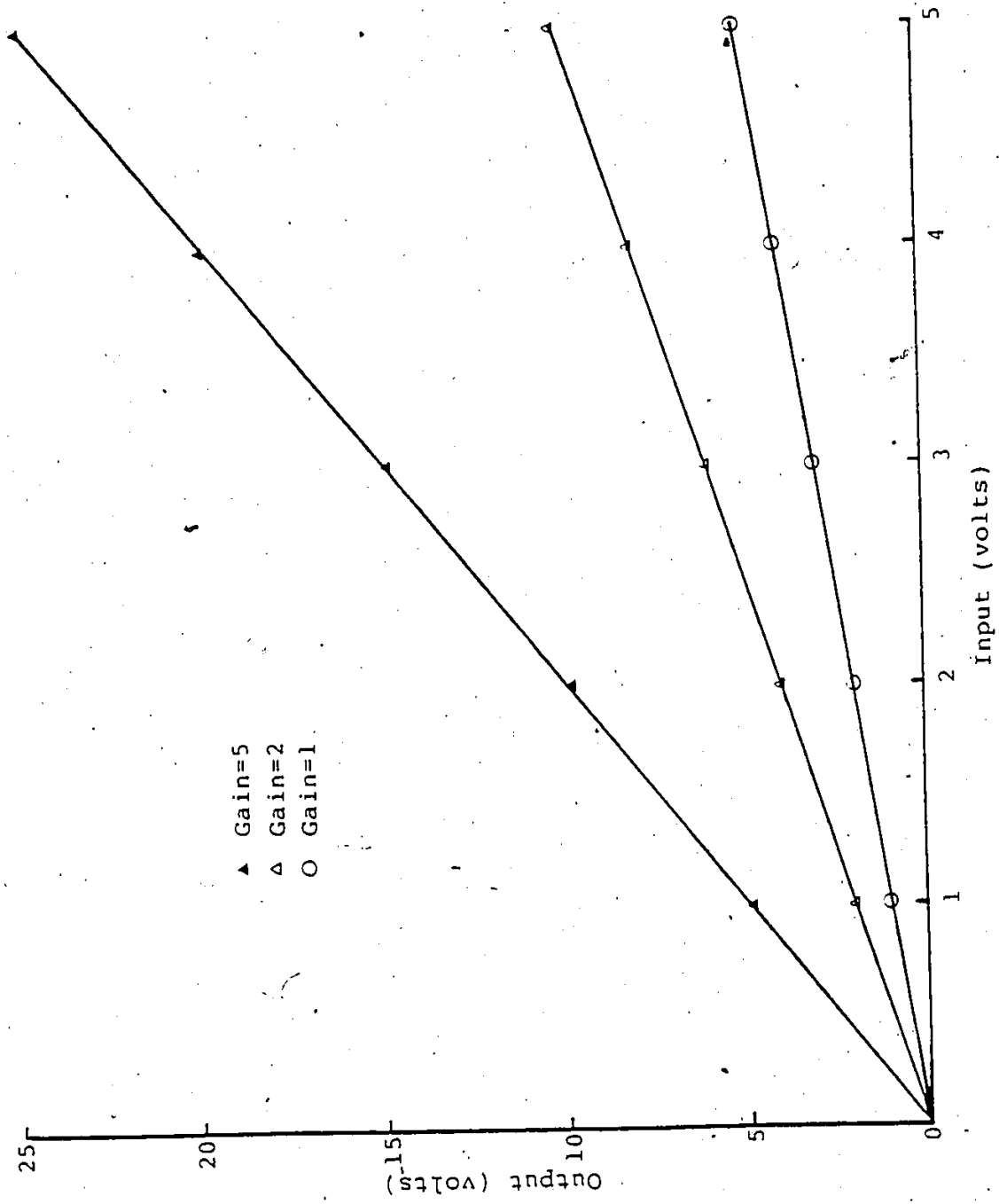


Figure B.2: CALIBRATION CURVE FOR THE AMPLIFIER CHANNEL B

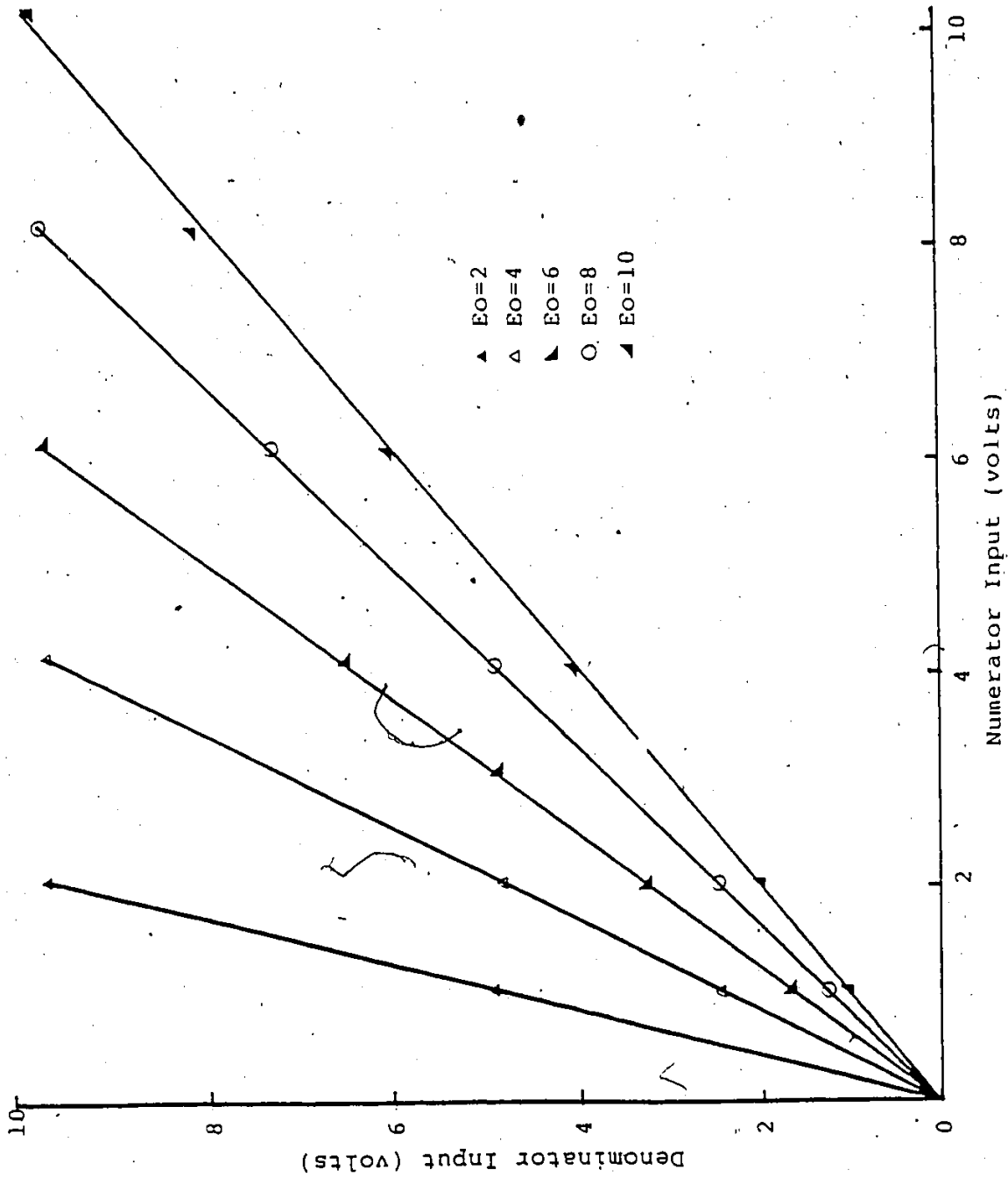


Figure B.3: CALIBRATION CURVE FOR THE ANALOG DIVIDER

Appendix C

PROFILOMETRIC AND OPTICAL MEASUREMENT READINGS
FOR LAB. SPECIMENS

TABLE C.1

Stylus Calibrated (Mitutoyo Surf-test III) Surface
Roughness of Laboratory Machined Specimens

Specimen No.	Surface Roughness (μ in.)						Ra	Std. dev.
	1	2	3	4	5	6	(μ in.)	(μ in.)
1	7.4	8.2	7.9	7.6	8.1	8.0	7.86	0.31
2	11.7	11.5	11.0	12.0	12.0	12.2	11.73	0.44
3	15.0	15.0	14.5	14.5	16.0	15.5	15.08	0.58
4	22.0	20.5	21.0	22.5	20.5	19.5	21.00	1.09
5	28.5	25.0	27.5	26.5	25.5	26.0	26.50	1.30
6	36.5	35.0	38.5	35.0	35.5	35.5	36.00	1.34
7	42.0	42.5	44.0	43.0	43.5	44.0	43.25	0.82
8	56.5	59.5	58.0	56.0	57.5	56.0	57.25	1.37
9	67.0	68.0	67.5	68.5	70.0	67.0	68.00	1.14

TABLE C.2

Output Ratio V_0/V_{30} for Transducer EC-824

Specimen No.	V_0/V_{30}										Avg. V_0/V_{30}	Std. dev.
	1	2	3	4	5	6	7	8	9	10		
1	3.36	3.40	3.25	3.28	3.30	3.32	3.26	3.30	3.28	3.29	3.30	0.05
2	3.08	3.15	3.06	3.11	3.11	3.13	3.14	3.07	3.06	3.10	3.10	0.03
3	2.88	2.96	2.98	2.92	2.89	2.93	2.88	2.91	2.92	2.94	2.92	0.03
4	2.75	2.73	2.80	2.69	2.74	2.60	2.78	2.66	2.76	2.76	2.73	0.06
5	2.62	2.59	2.60	2.59	2.55	2.61	2.63	2.60	2.58	2.57	2.59	0.02
6	2.31	2.27	2.35	2.25	2.28	2.30	2.38	2.29	2.27	2.31	2.30	0.04
7	2.18	2.21	2.25	2.22	2.21	2.20	2.19	2.27	2.20	2.19	2.21	0.03
8	2.04	2.07	2.09	2.10	2.05	2.08	2.14	2.08	2.11	2.07	2.08	0.03
9	2.00	2.03	1.99	2.05	2.01	2.00	2.06	1.98	2.01	2.01	2.01	0.03

TABLE C.3

Output Ratio V0/V35 for Transducer EC-824

Specimen No.	V0/V35										Avg. V0/V35	Std. dev.
	1	2	3	4	5	6	7	8	9	10		
1	4.18	4.23	4.20	4.24	4.20	4.16	4.19	4.23	4.22	4.18	4.20	0.03
2	3.73	3.76	3.69	3.70	3.72	3.74	3.73	3.68	3.72	3.73	3.72	0.02
3	3.43	3.39	3.42	3.41	3.43	3.40	3.35	3.42	3.38	3.39	3.40	0.03
4	3.11	3.08	3.14	3.10	3.12	3.10	3.11	3.09	3.16	3.08	3.11	0.03
5	2.82	2.86	2.85	2.92	2.91	2.91	2.88	2.93	2.84	2.87	2.88	0.04
6	2.56	2.53	2.50	2.55	2.65	2.59	2.51	2.50	2.56	2.54	2.55	0.05
7	2.42	2.43	2.37	2.39	2.43	2.47	2.42	2.45	2.44	2.43	2.43	0.03
8	2.26	2.21	2.18	2.20	2.20	2.27	2.19	2.22	2.18	2.19	2.21	0.03
9	2.10	2.16	2.11	2.09	2.18	2.15	2.14	2.16	2.13	2.17	2.14	0.03

TABLE C.4

Output Ratio V0/V30 for Transducer EC-424

Specimen No.	V0/V30										Avg. V0/V30	Std. dev.
	1	2	3	4	5	6	7	8	9	10		
1	3.70	3.64	3.68	3.74	3.65	3.66	3.70	3.71	3.72	3.65	3.69	0.04
2	3.40	3.43	3.30	3.32	3.38	3.31	3.33	3.35	3.36	3.37	3.35	0.04
3	3.08	3.12	3.15	3.06	3.09	3.10	3.09	3.06	3.11	3.10	3.10	0.03
4	2.92	2.75	2.71	2.89	2.95	2.70	2.71	2.73	2.75	2.82	2.80	0.09
5	2.71	2.74	2.78	2.76	2.75	2.74	2.75	2.78	2.71	2.76	2.75	0.02
6	2.50	2.49	2.61	2.48	2.55	2.57	2.43	2.48	2.49	2.49	2.51	0.05
7	2.43	2.46	2.50	2.41	2.45	2.48	2.46	2.44	2.45	2.44	2.45	0.03
8	2.21	2.25	2.28	2.19	2.23	2.30	2.27	2.25	2.26	2.25	2.25	0.03
9	2.09	2.15	2.18	2.08	2.11	2.10	2.09	2.10	2.13	2.08	2.11	0.03

TABLE C.5

Output Ratio V0/V35 for Transducer EC-424

Specimen No.	V0/V35										Avg. V0/V35	Std. dev.
	1	2	3	4	5	6	7	8	9	10		
1	4.79	4.82	4.71	4.75	4.70	4.83	4.77	4.71	4.72	4.73	4.75	0.05
2	4.07	4.00	3.98	4.00	4.10	3.95	3.98	3.99	4.02	4.00	4.01	0.04
3	3.73	3.72	3.72	3.78	3.68	3.65	3.70	3.71	3.72	3.74	3.72	0.03
4	3.31	3.30	3.35	3.29	3.36	3.30	3.33	3.28	3.29	3.28	3.31	0.03
5	2.98	2.95	3.02	3.07	2.99	2.98	2.98	2.96	3.00	2.92	2.98	0.04
6	2.76 2.68	2.68	2.81	2.66	2.85	2.86	2.79	2.80	2.83	2.83	2.79	0.07
7	2.68	2.60	2.59	2.63	2.69	2.68	2.61	2.61	2.59	2.55	2.62	0.05
8	2.35	2.38	2.45	2.41	2.33	2.39	2.31	2.35	2.33	2.38	2.37	0.04
9	2.22	2.19	2.20	2.15	2.10	2.08	2.23	2.14	2.18	2.20	2.17	0.05

VITA AUCTORIS

- 1952 Born in Bareilly (India) on October 15.
- 1974 Received the degree of Bachelor of Engineering from the department of Mechanical Engineering, University of Roorkee, Roorkee, India.
- 1974 Joined the Tata Engineering and Locomotive Co. Ltd. @ Poona, India, and worked there as a Manufacturing Engineer till 1979.
- 1982 Currently a candidate for the degree of Master of Applied Science in Mechanical Engineering at the University of Windsor, Windsor, Ontario, Canada.